Karlsruher Institut für Technologie

SegemAR
Servicio Geológico Minero Argentino

ITBA
Instituto Tecnológico de Buenos Aires

THESIS WORK

Master of Science in Energy and Environment

Instituto Tecnológico de Buenos Aires - Karlsruhe Institute of Technology

FEASIBILITY STUDY FOR A MEDIUM-ENTHALPY GEOTHERMAL POWER PLANT IN ROSARIO DE LA FRONTERA, SALTA, ARGENTINA

Niklas Brender
Mechanical Engineer (KIT)

Tutor
Lic. geol. Alejandro Conde (SegemAR)
Dr. Dietmar Kuhn (KIT)

Examiners
Dra. Silvia Barredo
Dra. Ing. Cecilia Smoglie (ITBA)
Prof. Dr. Ing. Martin Gabi (KIT)

Buenos Aires
24/08/2018

Declaration of Authorship

I declare that I have developed and written the enclosed Master Thesis completely by myself, and have not used sources or means without declaration in the text. Any thoughts from others or literal quotations are clearly marked. The Master Thesis was not used in the same or in a similar version to achieve an academic grading or is being published elsewhere.

Buenos Aires, 24. August, 2018

_____

Niklas Brender

Abstract

In this study the surrounding of Rosario de la Frontera was investigated for its suitability for geothermal energy production. The area is located in north-western Argentina, in the province of Salta, which is at the foothills of the Andean retro-wedge and in the northern part of the Sierra de la Candelaria anticline. In this region there are 13 hot springs with temperatures between 24.1 °C to 90.5 °C, which have been used for commercial purposes since 1880 and geological investigations were carried out early on, suggesting a large hydrothermal reservoir at a maximum depth of 3000 meters. In 2012 the presence of two aquifers at different depths was detected with the help of audiomagnetotelluric investigations and recent studies indicate these depths to 150 meters and 2400 meters respectively. Samples and calculations show temperatures between 100 °C to 130 °C and a permeability of 49 - 81.2 mD for the deep aquifer.

Based on these data, the focus was placed on the performance calculation of an Organic Rankine Cycle (ORC) power plant. Thereby, a power plant adapted to the boundary conditions in Rosario de la Frontera can deliver net outputs between 388.9 kW to 893.9 kW for well head temperatures ranging from 95 °C to 125 °C. In contrast, the achievable net outputs of two example turnkey systems are in the range of 137 kW - 491 kW.

Further economic calculations determine the electricity generation costs at a value of 26.3 - 47.9 US cents per kWh for a custom made solution and between 35.6 to 118.5 US cents/kWh for the two turnkey systems. However, if the thermal water mass flow can be doubled, for example by hydraulic shearing, the levelized costs of energy for all systems and temperature ranges can be reduced by 30 - 40 %. Nevertheless, these costs are still higher than those of other technologies, which illustrates the relevance of possible subsidy programs for this kind of geothermal energy.

Resumen

En este estudio se examinó la aptitud de los alrededores de Rosario de la Frontera para la producción de energía geotérmica. La zona está ubicada en el noroeste de Argentina, en la provincia de Salta, al pie de la cordillera de los Andes, la misma yace al norte del anticlinal de la Sierra de la Candelaria. En esta región se encuentran 13 fuentes de aguas termales con temperaturas entre 24.1 °C a 90.5 °C, han sido utilizadas desde 1880 con fines comerciales. Con el paso del tiempo se han ido realizando varias investigaciones geológicas, lo que sugiere la existencia de un gran reservorio hidrotérmico a una máxima profundidad de 3000 metros. En el año 2012 se pudo detectar la presencia de dos acuíferos a diferentes profundidades, uno a 150 metros y el otro a 2400 metros, con la ayuda de investigaciones audiomagnetotelúricas. Las muestras y los cálculos indican temperaturas entre 100 °C y 130 °C con una permeabilidad de 49 - 81.2 mD para el acuífero profundo.
En base de estos datos, se hizo énfasis en el cálculo del rendimiento de una central eléctrica de Ciclo Orgánico Rankine (ORC). Es por esto que una central eléctrica adaptada a las condiciones en Rosario de la Frontera con temperaturas de agua termal dentro de un rango entre 95 °C y 125 °C genera potencias netas entre 388,9 kW y 893,9 kW. En cambio en los sistemas de llave en mano las potencias netas generadas rondan entre 137 kW y 491 kW.
De los cálculos económicos realizados se determinan los costos de generación de electricidad en un valor de 26,3 a 47,9 US centavos por kWh en el caso de una central eléctrica adaptada, si se lo compara con los sistemas de llave en mano que el valor ronda entre 35,6 a 118,5 US centavos/kWh. Resulta oportuno destacar, que los costos nivelados de energía pueden ser reducidos en un 30 - 40 % sin importar los sistemas y rangos de temperatura si el flujo del agua termal puede ser duplicado, por ejemplo a través de estimulación hidráulica. Empero, estos costos son aún más altos que los de otras tecnologías, lo que ilustra la importancia de los programas de subsidios para este tipo de energía geotérmica.

Contents

Nomenclature

Abbreviations

AGEERA	Asociación de Generadores de Energía Eléctrica de la República Argentina, engl.: Association of Electricity Producers of the Argentinine Republic
ARS	Argentine Peso
CAMMESA	Compañía Administradora del Mercado Mayorista Eléctrico, engl.: Wholesale Electricity Market Management Company
CF	Capacity Factor
CFC	Chlorofluorocarbon
CGA	Cámara Geotérmica Argentina, engl.: Argentine Geothermal Chamber
CP	Critical Point
CHP	Combined Heat and Power
COP	Conference of the Parties
DFN	Discrete Fracture Network
EGS	Enhanced/Engineered Geothermal System
ENARSA	Energía Argentina S.A.
ENRE	Ente Nacional Regulador de la Electricidad, engl.: National Electricity Regulatory Agency
engl.	English
fig.	Figure
FM	Formation
FODER	Fondo para el Desarollo de Energías Renovables, engl.: Renewable Energy Development Fund
GeSi	Geothermal Simulation
GEF	Global Environment Fund
GENREN	Generación Eléctrica a partir de Fuentes Renovables, engl.: Electricity Generation from Renewable Sources

ger.	German
GHP	Ground-source Heat Pump
GUI	Graphical User Interface
GWP	Global Warming Potential
HC	Hydrocarbon
HCFC	Hydrochlorofluorocarbon
HDR	Hot Dry Rock
HFC	Hydrofluorocarbon
HFO	Hydrofluoroolefin
HO	Hydroolefin
IAEA	International Atomic Energy Agency
IBRD	International Bank for Reconstruction and Development
IPCC	Intergovernmental Panel on Climate Change
IRR	Internal Rate of Return
LCOE	Levelized Cost of Energy
LWD	Logging While Drilling
Ma	Million years ago
mD	milli Darcy
MINEM	Ministerio de Energía y Minería, engl.: Ministry of Energy and Mines
Mio.	Million
MWD	Measurement While Drilling
NIST	National Institute of Standards and Technology
NPV	Net Present Value
NTA	Nitrilotriacetic acid
NW	North West
OCA	Organic Clay Acid
ODP	Ozone Depletion Potential
O&M	Operation and Maintenance
ORC	Organic Rankine Cycle
PERMER	Proyecto de Energías Renovables en Mercados Rurales, engl.: Renewable Energy Project in Rural Markets
PFC	Perfluorocarbon

PM	Precio Monómico
PME	Precio Monómico Estacional
PPA	Power Purchase Agreement
REFPROP	Reference Fluid Thermodynamic and Transport Properties Database
RMA	Regular Mud Acid
rpm	Rotations per minute
S.A.	Sociedad Anónima, engl.: Public Limited Company or Incorporated (Inc.)
sect.	Section
TDS	Total Dissolved Solids
TPES	Total Primary Energy Supply

Symbols	**Description**	**Unit**
c_p	Heat capacity	[kJ/kgK]
D	Thickness of the aquifer	[m]
E	Generated electricity	[kWh]
F	Fuel cost	[US$], [ARS]
g	Gravitational constant	[m/s^2]
H	Enthalpy	[J]
h	Specific enthalpy	[J/kg]
I	Investment cost	[US$], [ARS]
K	Permeability	[mD], [m^2]
k_f	Hydraulic conductivity	[m/s]
M	Maintenance cost	[US$], [ARS]
m	Mass	[kg]
$\dot{m}$	Mass flow	[kg/s]
n	Lifetime	[years]
P	Power	[W]
p	Pressure	[Pa]
Q	Heat	[J]
$\dot{Q}$	Heat flow	[J/s], [W]
q	Specific heat	[J/kg]

r	Discount rate	[%]
s	Specific entropy	[J/kgK]
T	Temperature	[°C], [K]
T	Transmissivity	[m^2/s]
U	Internal energy	[J]
u	Specific internal energy	[J/kg]
V	Volume	[m^3]
w	Specific work	[J/kg]
η	Efficiency	[-]
μ	Dynamic viscosity	[Ns/m^2]
ρ	Density	[kg/m^3]

Indices

c	Carnot
con	Condenser
dis	discharged
e	electric
hx	Heat exchanger
i	year $[i]$
max	maximum
min	minimum
net	net power
nom	nominal
$pump$	Feed pump
sup	supplied
t	thermodynamic
th	thermal
$turb$	Turbine

List of Tables

List of Figures

1 Introduction

1.1 Motivation

The global primary energy demand has risen continuously over the past decades. Due to enormous population growth on the one hand and rising social prosperity on the other, it can be assumed that this development will at least continue for the time being. The way in which this demand is met today, but also the amount of natural resources needed for it, has taken on dimensions that the chemist and atmospheric researcher Paul Crutzen (2000) made the concept of the *Anthropocene* popular. This states that mankind has become one of the most important factors influencing almost all natural processes on earth.
Even though these influences are still largely unnoticed by the global population, people are becoming increasingly aware of them, especially as more and more institutions, above all the Intergovernmental Panel on Climate Change, are warning of the negative consequences and many countries now have ambitious goals to minimize their ecological footprint.
The main focus here is on reducing greenhouse gas emissions, which occure especially from the generation of energy from fossil fuels such as coal, oil and gas. Renewable energies should therefore not only be sustainable in terms of the used resources, but also have the goal of providing either completely emission free or emission neutral electricity and heat. Unfortunately, the most prominent representatives among renewable energies, namely wind and solar power as well as biomass plants come along with a number of disadvantages, such as highly fluctuating and therefore unreliable energy production, large surface requirement or the use of rare materials.
As a continuous and fuel independent energy source, geothermal energy can make an important contribution here. Of course, there are also hurdles to overcome, especially in the area of cost effectiveness, but geothermal energy with its base-load capability can nevertheless represent an important element in the power supply network of the future and with many decentralised systems it could guarantee a high level of supply security and help to reduce transmission losses. Furthermore, this technology offers a wide range of uses, from private use of heat to large scale industrial electricity production, so that it can be adapted to people's local needs.

1.2 Objective and structure of this thesis

Similar to wind and solar energy, there are also locations for geothermal energy that are more suitable due to their local conditions, and as a result, permit higher electricity production. Therefore, this study will investigate whether the results of previous geological investigations in Rosario de la Frontera are of interest for a commercial geothermal use.

For this purpose, the origin of heat within the earth and how it is distributed worldwide will be explained first (chapter 2). The main focus thereby is set on the situation in Argentina, to introduce its geothermal potential as well as to point out already advanced projects.
Based on this, the following chapter 3 describes the current state of the art technology to explore deep geothermal fields, with medium enthalpy reservoirs. In addition, possibilities for increasing performance through secondary heat sources are shown and examples of already installed binary power plants are presented.
Chapter 4 begins by describing the geological and geochemical situation of the reservoir in Rosario de la Frontera. With this data as a basis, the performance of a possible ORC power plant is calculated with the help of a simulation program (GeSi), which was implemented at the Institute of Nuclear and Energy Technology at KIT. Thereby, various parameters are varied to assess their impact on performance. These include, for example, the temperature of the thermal water, which represents a great uncertainty at the present time, but also the influence of fluctuating ambient temperatures and thus changes in the cooling capacity of the power plant are investigated.
Consequently, in chapter 5, an economic analysis is carried out for the various solutions. Whereby the legal framework is explained first and also reference is made to different subsidy programs. Secondly, based on the expected investment costs and the current economic situation of the Argentine energy market, the electricity generation costs are determined.
Finally in chapter 6, the assumptions made in the two previous sections are recapitulated and their respective effects on the presented results are evaluated.

2 Fundamentals of geothermal energy

2.1 Geothermal energy around the world and in Argentina

2.1.1 Structure and energy supply of the Earth

The Earth is shell-shaped (fig. 2.1) with a relatively thin earth's crust, followed by the mantle, the outer and finally the inner core. The average surface temperature is around 14 °C whereas in the inner core temperatures of around 5500 °C are expected [Litasov, Shatskiy, 2015]. Approximately 99 % of the earth are hotter than 1000 °C but due to the great depth mostly unavailable for technical usage. Not only the temperature rise with depth, but also the density and pressure increase, so that in the inner core pressures of up to 360 GPa are expected. The inner core with its radius of roughly 1220 km consits of a solid iron-nickel alloy. The outer core with a thickness of approximately 2250 km however is with 4000 °C and lower pressures molten iron. Convection in the outer core and interaction of earth's rotation give rise to the magnetic field of the earth.The strict line between core and mantel can be drawn due to a rapid decrease of density caused by the change from iron to lighter elements [Stober, Bucher, 2014, sect. 1.2].

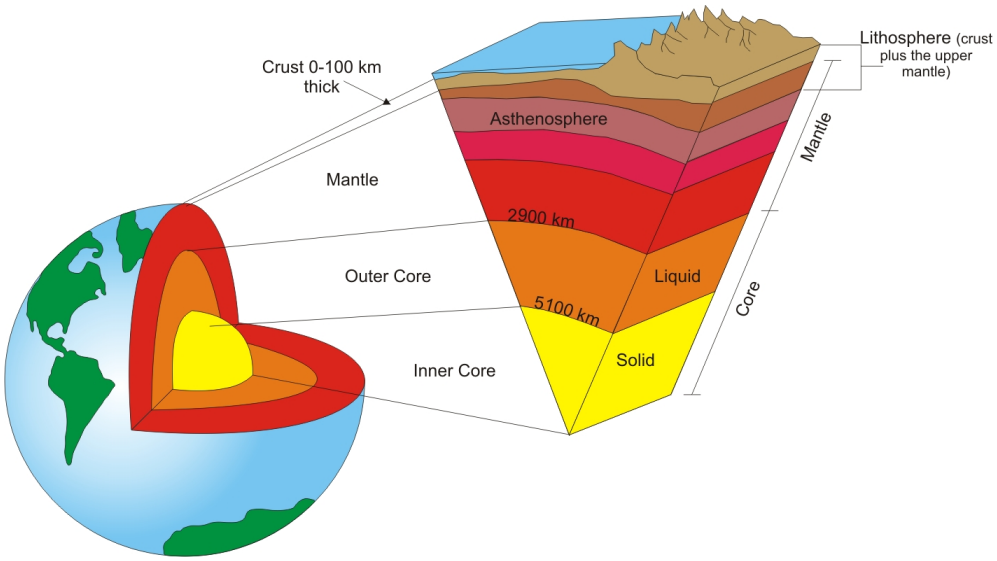

Figure 2.1: Structure of the Earth [Hildyard, 2010]

The crystallization heat caused by the slow cooling process of the core, produce sufficient energy to heat up the earth's mantle [Hirose et al., 2017]. This leads to a difference in density which cause a convective flow movement of the solid but (on a geological timescale) ductile material over millions of years (fig. 2.2). Thereby hot material rises from the core-mantle boundary up to higher areas, whereas cooler material sinks down. This part of the mantle is known as asthenosphere. The lithosphere lays above that and includes the uppermost part of the mantle as well as the earth's crust. Its magnitute vary from few kilometres at mid-ocean ridges up to 200 km on the continents. Although the lithosphere itself can be regarded as rigid it "floats" on the ductile asthenosphere and is subject to a constant movement by the convective flows within the asthenosphere. The dynamic of the lithosphere is known as plate tectonics and can be assigned to three categories [Frisch et al., 2011, sect. 1]:

- **Converging plates** where two plates either collide and form mountain ranges such as the Himalaya, or an oceanic plate slides down another plate (subduction) which leads to an oceanic trench as well as volcanic mountain ranges like the Andes.
- **Diverging plates** result in rift events or mid-ocean ridges where ascending magma cools down and forms new oceanic crust.
- **Relative movements** transverse to the plate boundaries.

All of those movements have in common that they are a source of earthquakes and in many cases also of volcanic activity.

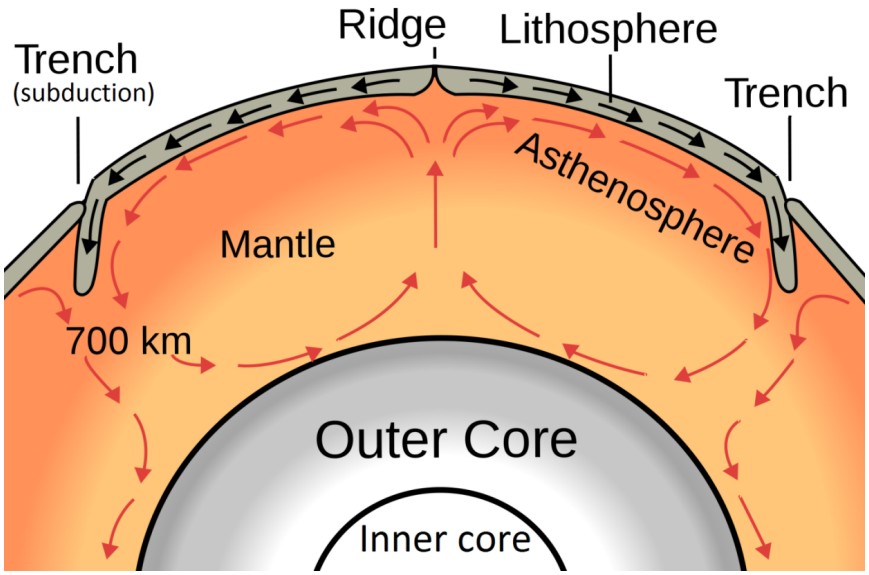

Figure 2.2: Model of convection within Earth's mantle [OTB,]

In the nowadays most explored depths up to 6000 m the average geothermal gradient is 3 °C per 100 m. This temperature increase is not distributed equally over the world, especially where continental plates drift together or volcanic activities occure, much higher temperatures in shallow depths can be found, as in Larderello (Italy) for example, with temperatures between 150 °C to 270 °C in about 1000 m depth [Razzano, Cei, 2015].
Due to the great temperature difference between the earth's core and the surface there is a continuous power output from the earth. This terrestrial heat flow is approximately 0.065 W/m^2 and leads in the long term to a cooling of the earth. But from the heat flow measured at the surface only around 30 $\%$ are coming from the earth's core. Over 70 $\%$ of it are "generated" within the earth's crust. The high percentage of the earth's crust heat production is a result of radioactive decay of the natural isotopes uranium [^{238}U, ^{235}U], thorium [^{232}Th] and potassium [^{40}K]. The heat generated in the earth's interior is estimated at 27.5·10^{12} W, whereas about 44.2·10^{12} W is radiated from the surface [Bauer et al., 2014, sect. 1.2]. That the net heat loss, as estimated by [Clauser, 2009], is only 1.4·10^{12} W and the earth therefore does not cool down quickly, is mainly attributed to the absorption of solar radiation. Calculations have shown that the temperature in the core within the last three billion years is only decreased by 300 °C to 350 °C, therefore the geothermal energy can be regarded as inexhaustible.

2.1.2 Status of geothermal energy around the world

In 2015 the worldwide energy production from geothermal resources used to be 251 TWh. Of this, 176 TWh were heat utillizations, the remainder was electricity. Compared to the world total primary energy supply (TPES) this share is tiny. There, wind-, solar-, tide- and geothermal-energy combined make up only 1.5 $\%$ of the TPES of 158,714 TWh [IEA, 2017]. Table 2.1 lists the top five countries for direct-usage and electricity production out of geothermal energy. Whereas geothermal energy is used for heating purposes in roughly 80 countries, less than 30 countries worldwide use this resource to generate electricity. Reasons for the discrepancy may be on the one hand the fact that high enthalpy reservoirs, preferred for electricity production, only occur in a few areas, and on the other hand the high investment costs associated with the exploration and exploitation of conventional geothermal resources.
The first traditional applications of geothermal energy were direct utilizations in order to heat public baths or laundry purposes and can be dated back to the time of the Roman Empire. Nowadays the application possibilities of direct-use are manifold and can be found in various industries. Those might be agriculture applications (greenhouse heating), aquaculture applications (fish ponds), industrial processes (lumber drying) and heating or cooling applications for buildings with ground-source heat pumps (GHP) [CanGEA, 2014].
Compared to these possibilities, electricity production is an indirect way of using geothermal energy. Thereby the geothermal energy in form of heat is converted into electrical energy

via steam turbines. When the water leaves a geothermal power plant, it is typically still hot enough for the most direct-use applications. Such a combined-heat-and-power (CHP) application is characterized by a large temperature spread and thus a high efficiency. A so called geothermal cascade, where thermal water is used serveral times and users are sequentially likend according to their decreasing heat demand, could include for example a power plant, a district heating network and greenhouses [Bauer et al., 2017, sect. 5.3].
In addition to the wide range of possible uses, geothermal energy is also characterized by high capacity factors (mostly above 90 $\%$). In this way, geothermal power plants could make an important contribution to the base load supply and at the same time they do not suffer from the disadvantages of conventional coal- or nuclear power plants, such as high CO_2 emissions or radioactive waste [Younger, 2015, p. XII].

Table 2.1: Top countries of geothermal direct-usage 2015 and electricity production 2015 / 2016. [Bertani, 2015], [IEA, 2018], [Lund, Boyd, 2015]

Direct-usage			Electricity production		
Country	Capacity [MW_{th}]	Production [TWh]	Country	Capacity [MW_e]	Production [TWh]
China	17,870	48.43	USA	3,800	17.41
USA	17,416	21.07	Philippines	1,870	9.64
Sweden	5,600	14.42	Indonesia	1,340	9.60
Turkey	2,937	12.74	New Zealand	1,068	7.64
Germany	2,848	5.42	Mexico	982.3	5.93

2.1.3 Geothermal situation in Argentina

As explained in section 2.1.1, regions in which a subduction of continental plates is present, and therefore form a volcanic area, are predestined for geothermal energy thanks to high temperatures. The so called *pacific ring of fire* surrounds the pacific in an u-shape from west, north and east and is a direct result of subduction between different continental plates. The entire area, which includes the Andes, has a remarkable high volcanic activity as well as frequent earthquakes [Armijo et al., 2015], [Neukirchen, 2011].

From the map in figure 2.3 there can be pointed out three main areas of geothermal projects in Argentina:

- The Andes range with volvanic systems in the west,
- El Salado basin in the province of Buenos Aires and
- Chacoparanense basin including the provinces Santiago del Estero, Chaco, Formosa, Santa Fe, Entre Ríos, Corrientes and Missiones, as well as parts of Paraguay, Uruguay and Brazil.

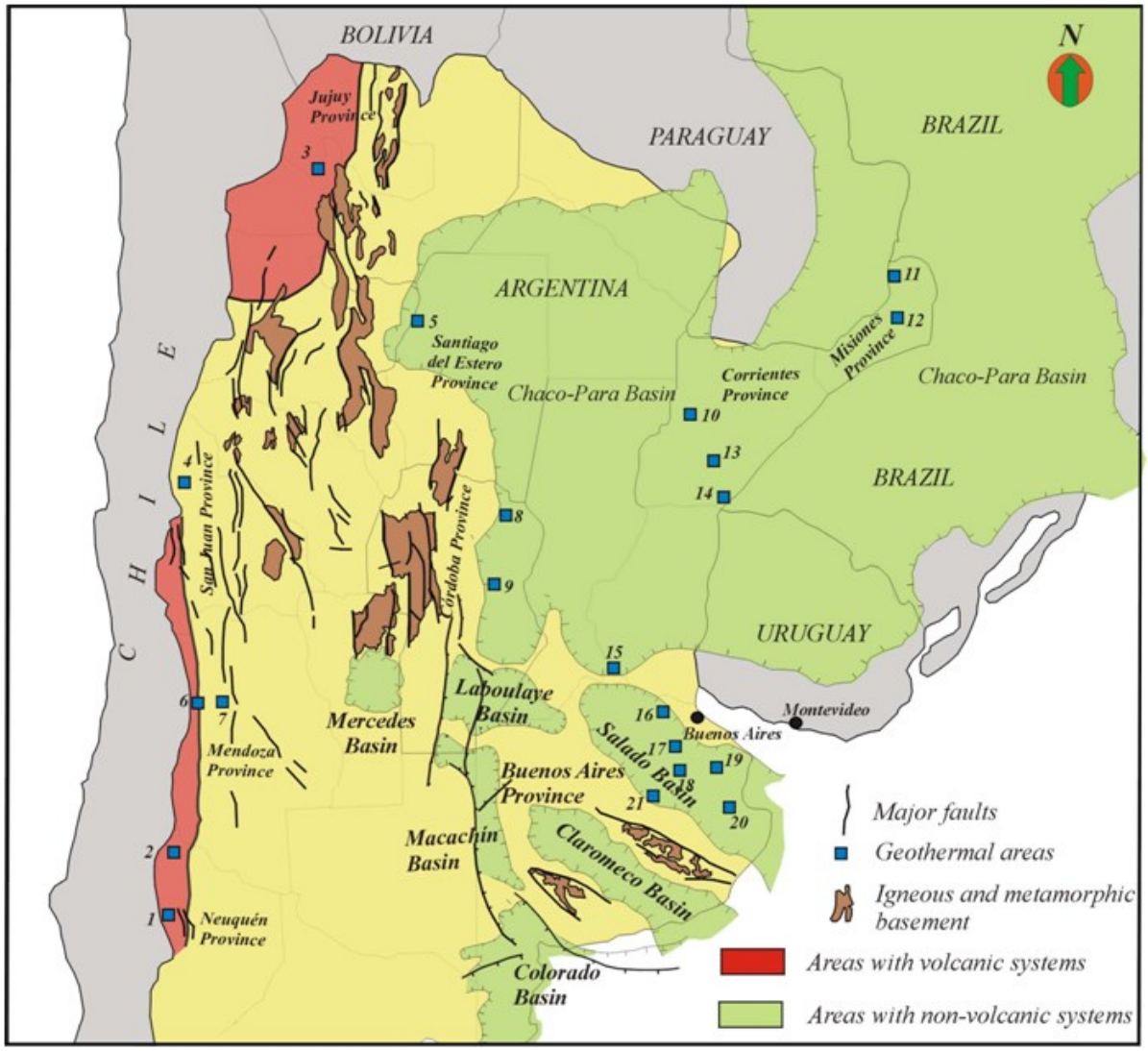

Figure 2.3: Distribution of geothermal projects in Argentina:
1 Copahue, 2 Domuyo, 3 Tuzgle, 4 Los Despoblados, 5 Termas de Río Hondo, 6 Peteroa, 7 Los Molles, 8 Mar Chíquita, 9 Chazón, 10 San Roque, 11 Wanda, 12 2 de Mayo, 13 Curuzú Cuatiá, 14 Monte Casero, 15 Ramallo, 16 Tigre, 17 Navarro, 18 Las Flores, 19 Chascomus, 20 Dolores, 21 Tapalqué [Pesce, 2015]

The high-enthalpy projects are within the Andes range, with exception of Termas de Río Hondo, at the border between Santiago del Estero and Tucumán, where a strong heat anomaly is found with a geothermal gradient between 3.5 to 4 times above average.
Almost all projects in the Chacoparanense and El Salado basins provide low-enthalpy sources. Most of them are still in the development stage but the already drilled wells (Talpalqué, Dolores, Curuzú Cuatiá and Monte Casero) show temperatures between 31 °C to 42 °C, depths between 441 m to 1060 m and flow rates of 25 l/s to 95 l/s respectively [Pesce, 2015].

In 2017 the National Ministry of Energy and Mining (MINEM) of Argentina expressed interest in the development of geothermal energy projects. Sebastián Kind, undersecretary of the MIMEM highlighted the geothermal potential and also the Argentine Geothermal Chamber (CGA) was formed in order to boost the sector.
The electric-geothermal potential of Argentina is subject to some uncertainties, but the values given in different sources are within the same order. According to Giorgio Stangalino, president of the CGA, the nationwide potential is up to 1500 MW_e [Gubinelli, 2017], which fits into the range of 490 MW_e to 2010 MW_e given in [Bona, Coviello, 2016]. However it should be mentioned that the upper limit is estimated under the subject of only applying state of the art technology. Whereas [Chiodini et al., 2014] estimate, in the volcanic area of Domuyo (Province Neuquén) alone is a thermal energy release of around 1100 MW_{th}, which would make it a very important geothermal field in the world, comparable to Mutnovsky (Russia) and Wairakei (New Zealand).

The provinces in which there are geothermal projects in different stages of study are: Catamarca, Jujuy, La Rioja, Mendoza, Neuquén, Salta, San Juan and Tucumán. Of these, four have geothermal projects which are already in the stage of feasability studies with the following results [Gubinelli, 2017]:

- Province Jujuy, vulcano Tuzgle, estimated capacity 20 to 30 MW_e.
- Province Neuquén, vulcano Copahue, confirmed capacity 30 MW_e.
- Province Salta, geothermal project Falla Tocomar, estimated capacity 20 to 30 MW_e.
- Province San Juan, geothermal project Los Despoblados, estimated capacity 15 to 20 MW_e.

Despite these positive prospects little advance has been made in recent years as the example of Copahue shows, where the first geothermal power plant was a 670 kW pilot project. Drillings were made in the 1970s and 1980s, containing four wells between 954 m to 1414 m and temperatures in a range of 220 °C to 250 °C [ADI-NQN, 2014]. Regardless of the promising results and good logistical conditions, the plant only operated between 1988 to 1997. Attempts by the government of Neuquén since 2009 to promote and reactivate the project have so far been unsuccessful, most recently with the withdrawal of the Canadian company

Geothermal One in 2013 [Pesce, 2015].
With the change of government in 2015, the new president Mauricio Macri introduced ambitious targets and plans a 20 % share of renewable energies by 2025. Those targets come along with the new Ministry of Energy and Mining as well as the renewable energy plan RenovAr, both established in 2016 [Heinonen et al., 2016, p. 51]. Although the first rounds of the RenovAr program focus on energies such as wind, solar and biogas there is hope that it will also attract investment for geothermal projects. This could be the step from the current status to the development of geothermal energy in Argentina.

2.2 Concepts of geothermal usage

For areas without special geothermal conditions it is necessary to drill deep wells as the temperature increases with depth. In Germany for example most wells for geothermal power plants are between 3000 m to 5000 m. In contrast to this deep geothermal energy, there are near-surface systems such as geothermal probes or groundwater wells with depths mostly less than 100 m [Stober, Bucher, 2014, sect. 4].
The different depths make a subdivision useful whereby the transition from shallow to deep geothermal energy is smooth and usally in the range of 150 m to 400 m and 20 °C to 25 °C. These low temperatures normally require a level increase (for example by heat-pumps) to make the energy usable, whereas with deep geothermal systems the energy can be used directly. However, for the considered situation in Rosario de la Frontera, near-surface systems are not relevant and therefore will not be discussed further in the following.

2.2.1 Hydrothermal resources

As one type of deep geothermal energy, hydrothermal resources characterize natural aquifers. Furthermore, these aquifers can be divided into those with high and those with low enthalpy. High enthalpy systems allow the use of Flash or Dry-Steam processes, whereas low enthalpy systems require an additional cycle such as the Organic Rankine Cycle (ORC) or the Kalina process (see section 3.2 for a more detailled description).
[Younger, 2015, p. XIV] gives a proposal for the catigorization of geothermal resources according to their pressure, temperature and enthalpy, as shown in figure 2.4. The enthalpy is a property of a thermodynamic system and is equal to the internal energy of the system plus the product of its pressure and volume. It is defined as:

$$H = U + pV \tag{2.1}$$

where H is the enthalpy, U the internal energy, p the pressure and V the volume of the system. As state variable the enthalpy is a basic for efficiency calculations of steam processes (see equation 3.4).

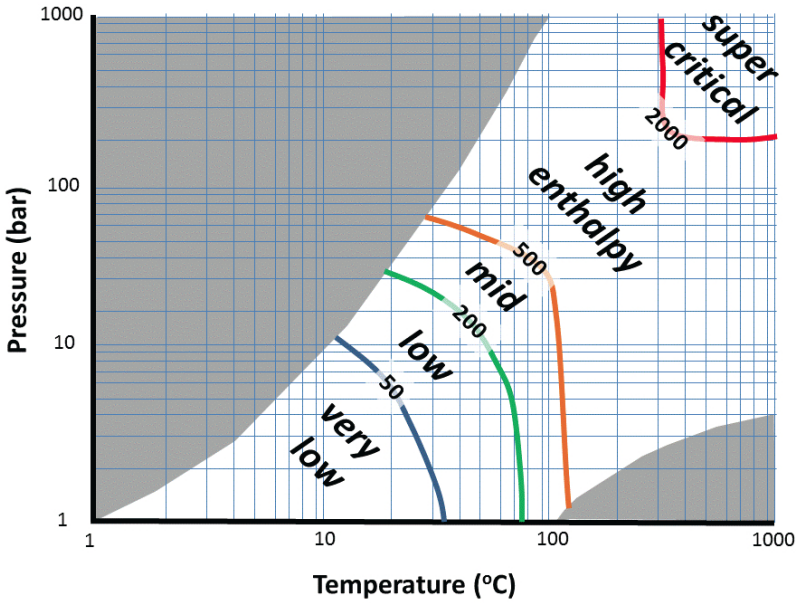

Figure 2.4: Categorization of geothermal resources. The number on the lines are approximate values of enthalpy in kJ/kg [Younger, 2015]

Not only temperature and pressure of an aquifer determine its economic efficiency, but also its transmissivity. This is a measure of an aquifer's ability to transport fluids and is expressed in m^2/s [Feldrappe et al., 2008, p. 9]. Since the required pumping power increases with a low transmissivity, this must be taken into account when considering the efficiency of the system. Furthermore a sustainable water management also demands reinjection into the same aquifer, which also needs pumping capacity. In this context, additional stimulation of the reservoir to increase permeability may be useful.

2.2.2 Petrothermal resources

In the case of petrothermal resources, there are no aquifers from which thermal water can be pumped to the surface. Instead, water is pressed through an injection well into the depth and returned to the surface through a second well. The heat transport of the underground rock can be devided into a conductive and a convective component. Both forms always occure together, but which type of heat transfer dominates depends on the geological situation. In contrast to hydrothermal deposits, where convective heat transfer dominates due to the

natural circulation of the aquifer, petrothermal systems usually are dominated by a conductive heat transfer through the rock. Whereby when water is pumped through the hot rock, it acts as a natural heat exchanger [Bauer et al., 2014, sect. 6.1].
First used in Frenton Hill (New Mexico, USA) in the 1970s, the exploration of petrothermal systems used to be called Hot-Dry-Rock (HDR). Nowadays the term Enhanced or Engineered Geothermal System (EGS) is more common because it has been shown that dry-rocks in the actual sense do not exist, but instead all cracks are filled to a certain degree with fluids [Stober, Bucher, 2014, sect. 9].

2.2.3 Stimulation options

Stimulation, optional for hydrothermal resources to increase the permeability, is indispensable for petrothermal use. Thereby three different types of stimulation can be distinguished, namely hydraulic shearing, chemical stimulation and proppant fracturing [Bauer et al., 2014, sect. 6.3].

Hydaulic shearing

Hydraulic shearing (sometimes known as pure shear stimulation) [Sutra et al., 2017] is by far the most used stimulation method in Central Europe. Hereby water without additives is pumped into the ground under high pressure, which induces fault movements along fracture surfaces. Therefore the water pressure must be above the rock pressure (For example: Soultz-sous-Forêts (France) well head pressure: 180 bar; Harris (USA) well head pressure: 538 bar [NREL, 2011]) in order to create a stress field. If the water pressure is subsequently reduced, the fracture width will also reduce, but the surfaces no longer “fit” together as a result of the previous displacement movement, resulting in cavities which improves the permeability of existing fissure systems. This effect is called self-propping [Stober, Bucher, 2014, sect. 9.3].
The effectiveness of the hydraulic shearing is particularly dependent on the angle of the fissures in relation to the main stress direction. In addition, minor seismic activity is an elementary component of this stimulation method due to the necessary tectonic stress [Xie et al., 2014].

Chemical stimulation

Hereby chemicals are added to the pressurized water. These dissolve mineral residues in the fracture system and therefore shall reduce the required pressure. This can lead on the one hand to a reduced seismic activity at the surface and on the other hand to better stimulation

results within the reservoir. Depending on the geological conditions and other environmental aspects, various chemicals can be used, whereas the most common are [Bauer et al., 2014, sect. 6.4.2]:

- **Hydrochloric acid** [HCl], a corrosive solution with irritant effect and particularly suitable for limestone, as these react with each other:

$$2\,HCl\ +\ CaCO_3\ \rightarrow\ CO_2\ +\ CaCl_2\ +\ H_2O$$

  The reaction products are harmless to health with the exception of calcium chloride [$CaCl_2$], which further reacts by contact with water to antarcitite [$CaCl_2 \cdot 6H_2O$], a natural hexahydrate. As the dissolving reaction does not occur, this option has no effect on other rocks such as granite or sandstone.

- **Organic Clay Acid** (OCA) can be an alternative if the rock does not react to a single acid, for example [HCl]. It is a mixture of different acids whose exact composition depends on the rock and the temperature. However, the central component is usually hydrogen fluoride [HF], which is toxic and water contaminating. OCA is often used for rocks containing clay, as this is stabilised and undesirable reactions with other substances are thus avoided.

- **Regular Mud Acid** (RMA) is a compound of hydrochloric acid and hydrogen fluoride. Ammonium bifluoride [NH_4HF] is necessary for its formation and it is well suited for dissolving silicate material. However, contact with calcium chloride should be avoided, as otherwise insoluble calcium fluoride [CaF_2] is formed which closes the pore spaces. In general, RMA should not be used for rocks with a lime content of more than 20 $\%$. As with OCA, contact with near-surface groundwater should be avoided, as otherwise harmful environmental effects may occur.

- **Nitrilotriacetic acid** (NTA) is a poorly water-soluble solid, usually in the form of a white, crystalline powder. It is used as a chelating agent and is 95 $\%$ biodegradable. In combination with ions of calcium [Ca^{2+}], potassium [K^{+}] or magnesium [Mg^{2+}] it forms stable water-soluble complexes and thus helps to dissolve these minerals more easily from the rock. However, it is classified as a water hazard and is carcinogenic in high doses.

Proppant or hydraulic fracturing

Is a process which is known from the petroleum and gas industry and serves the exploration of deposits without natural fissure systems. A mixture of proppants, high-viscosity gels and chemicals are pressed into the ground, where cracks are formed and sometimes also parts

of the rock are dissolved. Characteristic for this method is the final rinsing process, in which an attempt is made to bring all fluid back to the surface as a so known flowback. With the exception of the proppants (mostly quartz- / bauxite sand or aluminium oxide) and other thickening agents as these are intended to hold the fractures open after the hydraulic pressure is removed from the well [Sutra et al., 2017]. However, this method is often regarded as unsuitable for geothermal applications due to different reasons. On the one side are technical problems like proppant dissolution [Childers et al., 2017] or the concern that the large flow of water could leach out the proppants [Bauer et al., 2014, sect. 6.4.3]. On the other side is a considerable cost factor, as larger cracks would require larger amounts of proppants.

Differentiation to fracking

Although stimulation for geothermal applications originates in the hydrocarbon industry, there are some differences to the fracking methods used there, especially regarding the field of chemical stimulation and hydraulic shearing [Bauer et al., 2014, sect. 6.5.3], [Sutra et al., 2017].

- Fracking of unconventional reservoirs usually targets reservoir depths between 1000 and 2000 m and is intended to create a large number of new cracks and pathways there. The rock is mostly characterized by claystone or slate with a high content of organic ingredients.
  The Frac Fluid consists mostly of gel fracs and proppants and occasionally biocides. In addition, the process creates a flow back, which means a return flow of this fluid to the surface, which must be specially disposed due to the chemicals it contains.
- Stimulation for geothermal applications is mainly within a depth of 3000 to 5000 m and therefore has a higher distance to groundwater levels. Furthermore it mostly perforates limestone, sandstone or quartzite with the aim not to create new cracks, but to activate existing fissure systems. Both hydraulic shearing and chemical stimulation do not require a flow back, as the used stimulation fluid can remain in the subsequent thermal water circuit. Therefore a special disposal of the stimulation fluid is not necessary.

3 Exploitation technology

3.1 Drilling technology

Drilling platforms for geothermal drilling have their origin mainly in the oil and gas industry. However, the mostly higher temperatures, more aggressive components in the thermal water and a required service life of the well of usually more than 30 years, pose special challenges for the used technologies and materials. For these reasons and due to the larger diameters needed by higher volume flows, the drilling costs are usually higher. Another point is the fact that drilling for geothermal plants mostly takes place in the vicinity of residential areas and thus places high demands on emission values (air / noise) and groundwater protection [Stober, Bucher, 2014, sect. 11].

Figure 3.1 shows a schematic representation of a typical drilling rig with rotary drive. Thereby the drill pipe is driven from the rotary table via a driving rod (the so called *Kelly*). Besides this method, there can be a top drive, where the drive unit is located between the hook and drill pipe, as well as turbine drilling, whereby not the entire drill pipe is driven, but the bit is connected to a turbine which is directly located behind the bit and itself driven via the downwardly pressed drilling mud (Moineau principle) [Stober, Bucher, 2014, sect. 11].
The drilling head can be either a roller cone bit or a diamond bit (to obtain drill cores) but also special directional drill bits are usually used, always dependent on the task to be performed. The necessary contact force on the rock comes from the dead weight of the drill pipe itself, at least from its lower part, and is regulated via the hook. This means that only the lowest meters of the drill pipe are subjected to pressure and the rest to tension. Directly behind the bit *drill collars* with larger wall thicknesses are used to prevent the rod from buckling in the pressure loaded area [Reich, 2015, sect. 7.3]. Finally there are some important parameters for the rotary procedure such as [Bauer et al., 2014, sect. 8.3]:

- Maximum hook load, limits the maximum depth as the drill pipe gets heavier, normally in the order of 150 - 350 t (with exceptions in the size range of 750 t [ITAG, 2013]).
- Rotations per minute, mostly between 50 - 200 rpm.
- Weight on Bit, for roller bits 5 to 15 kN/cm, for diamond bits around 15 kN/cm bore hole diameter.

- Hydraulic and mechanical performance, the former being significantly higher (factor 20 - 30).
- The rate of penetration, meaning the feed speed of the drill pipe, which is determined by the speed, the contact pressure, the underground situation and further parameters.

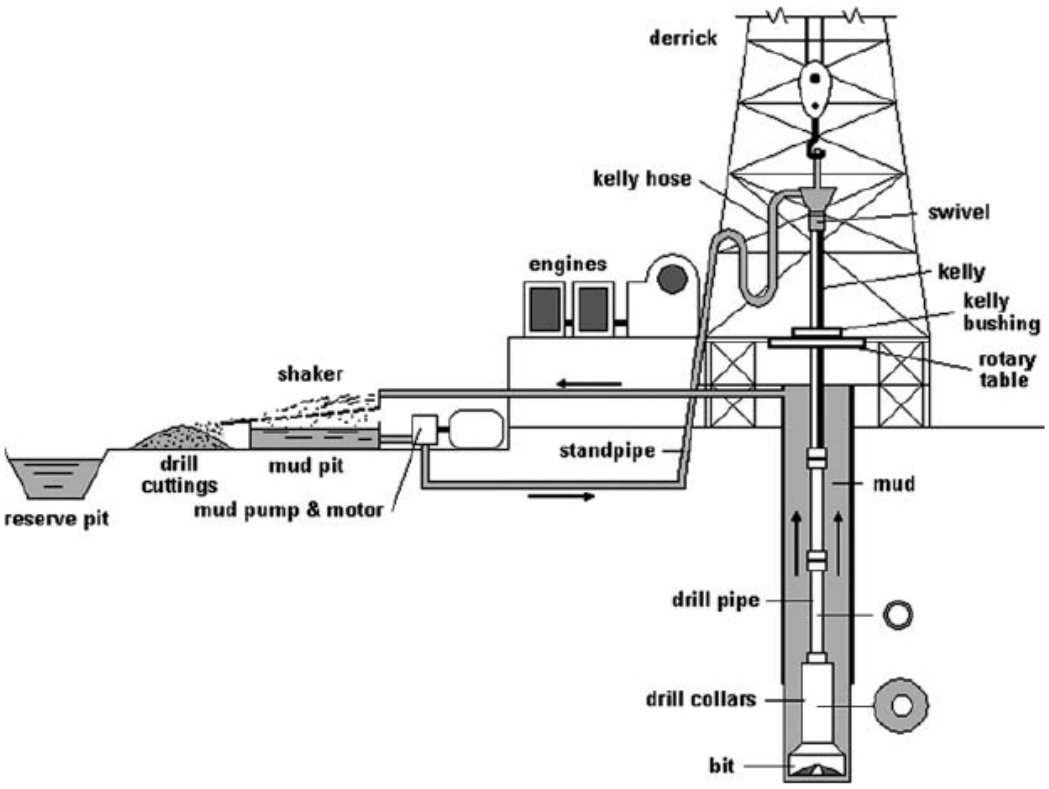

Figure 3.1: Scheme of a typical drilling rig [DiPippo, 2015]

To drill a well, the corresponding drill site must first be created. Average sizes are 5,000 to 12,000 m^2, whereby not only the space required for the drilling rig must be considered, but also the storage area of the pipes, tanks for the drilling mud, drive motors and other equipment. Furthermore, water and power supply (approximately 3 - 5 MW) must be ensured and a drainage and waste concept must be worked out [Stober, Bucher, 2014, sect. 11].
The actual drilling is carried out in phases, with each new phase ending with the piping and cementation and each subsequent phase being continued with a smaller bit diameter (fig. 3.2). The cementation is done in order to create a coherent connection between the rock and the piping. Hereby the cement is led down inside the pipe and fills the cavity between the rock and the pipework from below. Drilling mud still in the borehole or cavity thereby floats up and is thus transported to the surface.

The required initial diameter is determined by the number of phases and the final diameter. The latter, in turn, is calculated by the desired volume flow and the associated pressure losses. If there is stable rock in the last section, piping can be dispensed, which is called *open hole*, otherwise a *closed hole* is needed [Bauer et al., 2014, sect. 8.8.12].

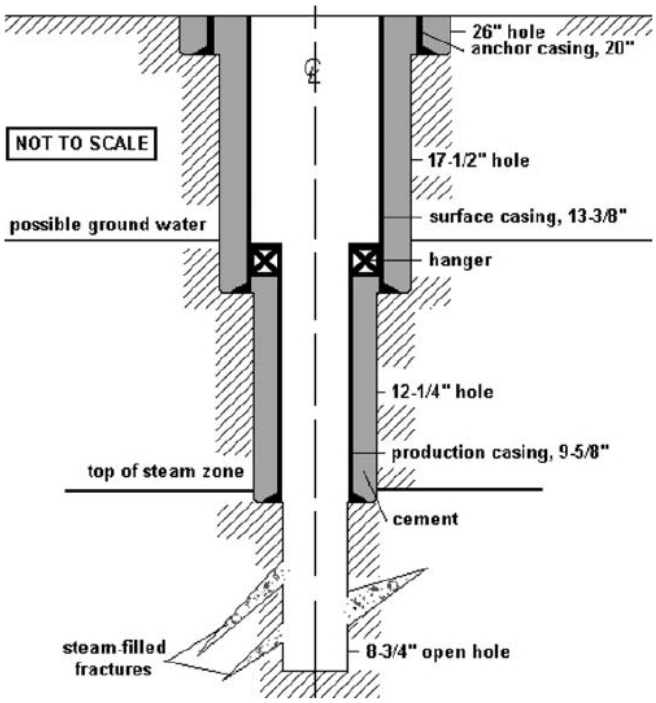

Figure 3.2: Scheme of a well completion with three phases [DiPippo, 2015]

Many wells are nowadays made as directional bores, whereby the course is not simply vertical but can be controlled in any direction. This also makes it possible to produce horizontal sections, as is often used in the oil and gas industry to increase the yield of a relatively thin layer. There are different variants of how a change of direction during drilling can be realized. Firstly, a bend can be made between the drill bit and the drive unit of the aforementioned turbine drilling, where the drill pipe, can, but does not have to be rotated. This bend measures approximately 2 ° and results in drilling a curve when the pipe is stationary. However, if the complete drilling pipe is driven, the bend also rotates and a straight bore is produced.
In the case of very steeply inclined bores, however, the problem occurs that as soon as the drilling pipe is stopped in order to be able to change direction, the pipe comes into contact with the borehole wall and makes advance difficult due to the high static friction. To avoid this problem, another variant can be used, where a rotatably mounted sleeve is placed behind the drill bit. This contains three ribs that can be pressed hydraulically against the borehole wall. When all three ribs are extended evenly, the sleeve and thus the drill head are centered and a straight bore is made. However, if eccentrical positioning is achieved, the bit is deflected in

a new direction.
Regardless of whether it is a directional bore or a purely vertical bore, it must always be ensured that the current bore path still matches with the planned one or if the rock type is as expected. Therefore a number of measuring methods and instruments are used but in general, a distinction can be made between the measurement while drilling (MWD) systems and the logging while drilling (LWD) systems.
MWD systems are used to determine the position using built-in compasses and position sensors. LWD sensors, on the other hand, make it possible to make statements about the type of rock and its porosity with the aid of conductivity measurements, gamma and/or neutron beams [Reich, 2015, sect. 12.1, 12.2].

3.2 Geothermal power plants

In conventional power plants water is used as working fluid and heated up till 600 °C into dry steam, and also high-enthalpy geothermal resources, which provide temperatures above 200 °C or 250 °C, use the steam of water directly for driving the turbines. These cycles, which use water as working fluid, are known as Clausius-Rankine Cycle.
In a dry-steam geothermal power plant saturated or slightly superheated steam with temperatures of 200 °C or more is used directly from the reservoir to drive the turbines. However, such favourable conditions like in Larderello (Italy) or The Geysers (USA) are very rare and those systems make up only a fraction of the global geothermal supply. Much more frequently, so called flash systems can be found in which a two phase mixture is present under high temperature. At the surface, the steam content is regulated by a pressure drop and separated from the remaining water by a separator. The steam fraction is then fed into the turbine and, after condensation, together with the previously separated water, led back into the reservoir [Bauer et al., 2014, sect. 22.1].
For lower temperatures though, this would mean that the steam pressure needs to be reduced significantly, in some cases even below the environmental pressure in order to turn the two phase mixture into steam and use it directly as the working fluid. Therefore a secondary cycle is installed, using alternative working fluids, with lower evaporation temperatures, which can be classified into the organic working fluids for the organic rankine cycle (ORC) or a mixture between mostly ammonia and water for the Kalina cycle. In these so called binary cycle power plants, the thermal water transfers its heat to the working fluid via heat exchangers before being conducted back into the ground, forming the primary cycle. The working fluid in the secondary cycle, evaporates and is used to drive a turbine [Zahoransky, 2015, sect. 15.5].

3.2.1 Thermodynamic cycle

A thermodynamic cycle describes a linked sequence of thermodynamic processes which contain a transfer of heat and work in and out of a system, so that start and end state of the system are identical. Therefore such a cycle can be described as follows [Vetter, 2011, sect. 2.2.1]:

$$\oint du = \oint dw + \oint dq = 0 \tag{3.1}$$

For a heat engine, such as a thermal power plant, that means the supplied energy dq in form of heat is transformed to mechanical energy dw and the internal energy du remains constant. In a closed system the sum of anergy and exergy remains constant. Exergy describes the part of energy of a system that can be transformed into work, while anergy is the energy a system contains while it is in equilibrium with its surrounding. To close the thermodynamic cycle, the anergy, as the part of the heat which can not be transformed, must be removed from the system. Figure 3.3 shows the Carnot-process as example of an ideal cycle without losses.

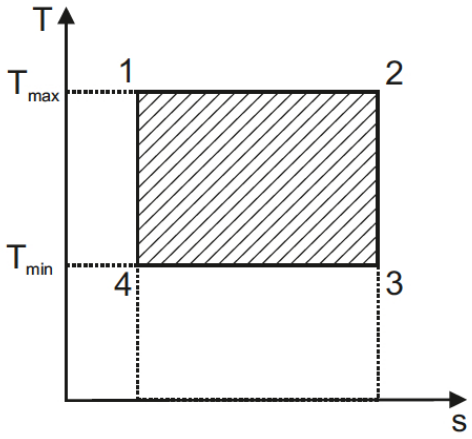

Figure 3.3: Carnot-process in the T,s - diagram [Vetter, 2011]

Here T describes the Temperature in [K], where s stands for the specific entropy in [kJ/kgK], and the four changes of state during the process are:

- 1 → 2: Isothermal expansion, supply of heat.
- 2 → 3: Isentropic expansion, discharge of work.
- 3 → 4: Isothermal compression, discharge of heat.
- 4 → 1: Isentropic compression, supply of work

The surrounded surface in the T,s - diagram describes the difference between the supplied and discharged specific heat q. From that the thermal efficiency can be calculated:

$$T_{max}\Delta s = q_{sup}$$
$$T_{min}\Delta s = q_{dis}$$

$$\eta_t = \frac{q_{sup} - |q_{dis}|}{q_{sup}} \tag{3.2}$$

Due to the heat exchange at constant temperature, the efficiency of the Carnot ideal cycle only depends on the ratio between low and high heat source temperatures. This is the theoretical upper limit of any cyclical thermal machine and it cannot be reached in practice. Its efficiency is expressed as:

$$\eta_c = 1 - \frac{|q_{dis}|}{q_{sup}} = 1 - \frac{T_{min}}{T_{max}} \tag{3.3}$$

3.2.2 Organic Rankine Cycle

Selection of a working fluid within an organic rankine cycle depends on its thermo-physical properties as well as the temperature of the thermal water. Therefore the working fluid should meet some criteria such as a critical point suitable for the temperature range of the thermal water, low specific volume, high thermal conductivity as well as non toxic or flamable. Furthermore, regarding environmental issues, it should have a low global warming potential (GWP) and a low ozone depletion potential (ODP) [Nusiaputra, 2017, sect. 2.1].
Depending on the fluids pressure while vaporized, the process is either subcritical (below the critical point, fluid passes through the two phase region) or supercritical.
This needs to be regarded while choosing the working fluid, as [Vetter, 2011, p.60] comes to the conclusion that a suitable choice of the working fluid, and with it a change from a sub- to a supercritical process, can lead to a power increase up to 36 $\%$ under certain conditions.
Another important characteristic of the working fluid is the gradient of its dew line. Water with a negative dew line is a non-retrograde fluid, whereas many organic fluids, such as Butane or Isopentane are retrograde, thus have a positive dew line. In the case of non-retrograde fluids, superheating must take place in order to prevent the development of droplets at the turbine outlet. Due to the positive gradient of retrograde fluids, relaxation into the two-phase area is not possible and therefore no superheating is necessary. However, the steam cannot be cooled down to condensation temperature during expansion and thus a larger part of the supplied heat remains unused. Therefore, additional internal heat exchangers, so called recuperators, are often used for retrograde fluids, whereby some of the waste heat can be

used to preheat the fluid.

The left image of figure 3.4 gives a simple system layout of an ORC power plant. In the T,s - diagram on the right are displayed the two phase areas of the non-retrograde fluid Dimethylether with a supercritical process as well as the retrograde fluid Butane with a subcritical process. Thereby the state changes by passing the individual components are as follows [Vetter, 2014, sect. 2.1.1]:

- 1 → 2: Isentropic compression, supply of work by the feed pump.
- 2 → 3: Isobaric supply of heat, within the heat exchanger.
- 3 → 4: Isentropic expansion, discharge of work in the turbine.
- 4 → 1: Isobaric discharge of heat, through the condenser.

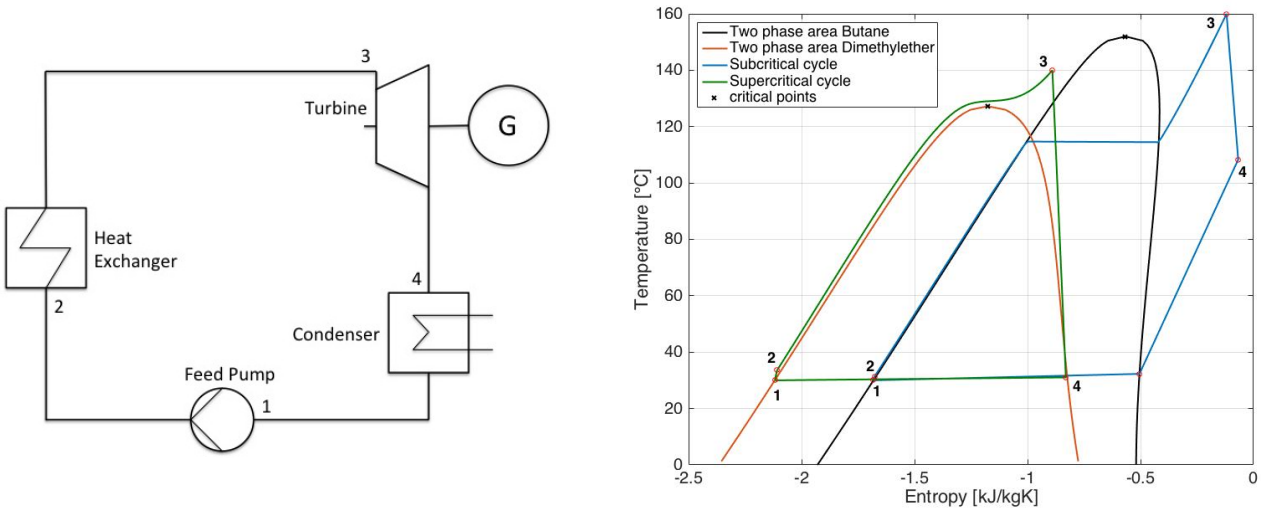

Figure 3.4: System layout of an ORC plant (left) and T,s - diagram of Butane and Dimethylether (right)

The specific enthalpies of the individual states can be determined from steam tables or via approximate equations. The specific energy content of the respective components is obtained via enthalpy differences [Zahoransky, 2015, sect. 4.1.1]:

- Feed pump: $w_{pump} = \Delta h_{pump} = h_2 - h_1$
- Heat exchanger: $q_{sup} = \Delta h_{hx} = h_3 - h_2$
- Turbine: $w_{turb} = \Delta h_{turb} = h_3 - h_4$
- Condenser: $q_{dis} = \Delta h_{con} = h_4 - h_1$

As with equation 3.2, the thermal efficiency can be calculated accordingly:

$$\eta_t = \frac{|q_{sup}| - |q_{dis}|}{|q_{sup}|} = \frac{(h_3 - h_2) - (h_4 - h_1)}{h_3 - h_2} \tag{3.4}$$

3.2.3 Kalina Cycle

While the organic rankine cycle operates with an organic fluid, the russian scientist Alexander Kalina suggested in the 1970s to use a binary mixture. A binary fluid does not evaporate isothermally, but increases its temperature during the evaporation process because the composition of the mixture changes [Zahoransky, 2015, sect. 15.5.2]. This results in lower temperature differences between working fluid and thermal water, allowing to extract more heat from the latter. The same applies to condensation, which is also not isothermal as shown in figure 3.5.

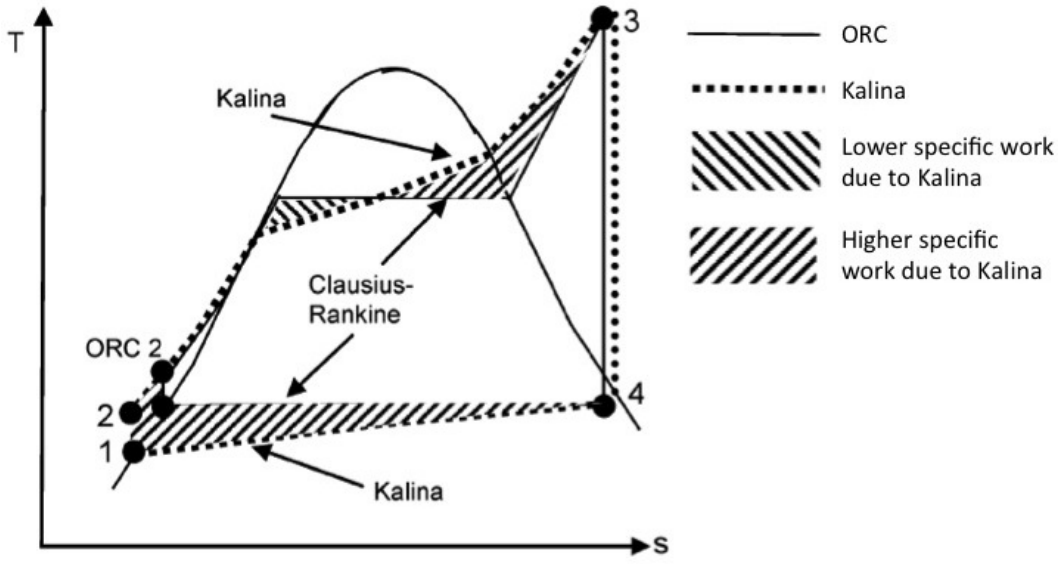

Figure 3.5: Comparison between ORC and Kalina process [Zahoransky, 2015]

The lower temperatures at the end of condensation and at the start of evaporation increase the specific work and thus the efficiency. The Kalina process, which is mainly operated as an ammonia-water mixture, is therefore particularly suitable for low temperature sources, such as low enthalpy geothermal fields and offers some advantages [Zahoransky, 2015, sect. 15.5.2]:

- Lower temperature differences in the heat exchanger and the condenser which leads to higher efficiency.
- Better cooling with lower minimum temperatures leads to a higher specific work.
- The thermal water can further be cooled down and therefore the supplied heat can be used more efficiently which also results in higher work.

Contrary to these advantages however, it must be noted that ammonia has a strong basic effect in both phases. It can burn the skin and respiratory tract and is considered a powerful metabolic poison. In addition, it forms an explosive mixture in air. Therefore, maintenance and operation of Kalina plants are complex in terms of safety. Currently, only a few Kalina plants are in operation, mainly as pilot or test plants with low capacity. Although the ammonia water mixture is well investigated, the composition of the binary fluid represents a further optimization parameter.
Finally, it should be mentioned that an optimized multi-pressure ORC, which means a process operating with several evaporation pressures, could achieve similarly good efficiencies. However, this increases the technical expenditure and thus the investment costs.

3.3 Optional heat sources

As already mentioned, the number of geothermal resources with high enthalpy and thus with high temperatures is very limited. As the thermodynamic efficiency increases with higher temperatures, the idea of supporting low temperature geothermal reservoirs with external heat sources suggests itself. There are basically two possibilities to operate such a hybrid power plant [Sanner, 2005]:

- A geothermally operated ORC process with superheating from an external heat source,
- A power plant operated with another heat source and a preheating of the working fluid by geothermal energy.

In this chapter shall be given two examples of how these options could look like with other renewable energies, which also could be of interest for the plant in Rosario de la Frontera.

3.3.1 Solar energy

Among the renewable energies, solar energy is the most abundant resource and can be operated economically almost anywhere in the world thanks to relatively low investment costs. The most commonly used solar thermal collector for commercial purposes is the parabolic

through, which focus the sunlight with a parabolic mirror on a focal line. There, a tube is positioned which contains a heat transfer fluid and can reach temperatures between 150 °C and 400 °C, depending on the concentration factor. Serveral studies propose the hybrid solar-geothermal use for almost all kind of geothermal cycles such as single flash, double flash and binary plants [Bonyadi et al., 2017], [Cardemil et al., 2016], [Ghasemi et al., 2014], [Sanner, 2005].
In [Ghasemi et al., 2014], they develop a model to expand an existing ORC geothermal power plant with a parabolic through. The solar system provides 17.6 MW of thermal energy at nominal conditions (direct nomal insolation = 1000 W/m^2, ambient temperature = 15 °C, maximum fluid temperature = 182 °C).
Solar and geothermal energy are operating parallel, the working fluid is split into two streams, one heated by the thermal water and the other by the heat transfer fluid of the parabolic through. For this constellation they come to the result of an 5.5 $\%$ boost of annual power generation.
Another option given by [Bonyadi et al., 2017], is to extend an existing ORC geothermal power plant with a topping steam cycle. Here the solar field is designed to reach temperatures of the heat transfer fluid of 395 °C, driving a standard Clausius Rankine cycle where the steam leaves the turbine at 170 °C. A coupling system links the ORC with the Clausius Rankine cycle. The cooled down thermal water after the heat exchanger of the ORC is used to cool down the steam of the Clausius Rankine cycle in the condenser and is then turned back to the heat exchanger of the ORC.
For a designed ORC with a geothermal brine flow rate of 100 kg/s and a solar field that can provide 50 kg/s at design conditions, he concludes an annual power output increase by 12.72 $\%$.

3.3.2 Biomass

Biomass is defined as substances of organic origin. These can be naturally growing or cultivated plants as well as animal or domestic waste. Biomass can be used in a wide variety of ways. Heat can be obtained from the direct combustion of wood, fuel such as bioethanol or biodiesel can be produced from crops and drive cars, or electricity can be generated from biogas, produced by the fermentation of biomass under the exclusion of oxygen. Alternatively, after the biogas has been processed, it can also be fed into existing natural gas networks [Quaschning, 2015, sect. 9.1].

There are also combination possibilities with geothermal energy, depending on the needs of the environment. Similar to the proposal of [Bonyadi et al., 2017], the waste heat from a gas power plant operated by biogas, could be used to raise the temperature of a geothermal ORC process. Due to higher exhaust temperatures of a gas turbine in comparison with a

steam turbine, the power output increase determined by [Bonyadi et al., 2017] could thereby be surpassed.
A second possibility would be to use biomass or biogas to fire a superheater in order to increase the operating temperture of the working fluid within the ORC. This option was investigaded by [Nakao et al., 2015] and showed an increase in power output of 889 kW and an increase in thermal efficiency of 2 % for a 3 MW geothermal power plant.
Alternatively the operation of a combined heat and power plant with biogas, parallel to a geothermal power plant could provide electricity and heat. If the resulting waste heat is used locally, the overall efficiency in relation to the used primary energy can increase sharply. However, this requires a well-developed district heating network.
Finally, biogas could also be fed into the local gas grid and thus be used for cooking and heating purposes inside the houses, while electricity is provided by the geothermal power plant.

3.4 Examples of low- to medium-enthalpy geothermal power plants

3.4.1 Low-enthalpy ORC in Chena

Chena is a city in a rural area of Alaska which supplied the most of its electricity from diesel generator sets, spending 365,000 US$ alone on fuel in 2005.Therefore it was decided to install a geothermal power plant based on an organic rankine cycle with 210 kW net output and R134a as working fluid [Aneke et al., 2011].
The bore well provides thermal water from 300 m depth with a temperature of 73 °C and a mass flow rate of 33 kg/s. The preheater and evaporater heat up the working fluid to 64 °C at a pressure of 16.9 bar, which then enters the turbine with a flow rate of 12 kg/s. At the turbine outlet, the steam has a temperature of 16.5 °C at 4.4 bar which is cooled down to 11.6 °C by the condenser, using 101 kg/s of cooling water with a temperature between 4.4 °C at the inlet and 9.9 °C at the outlet.
With this small-scale geothermal power project it was able to reduce electricity costs from 30 US cents/kWh to 5 US cents/kWh, also thanks to the provision of various direct use applications, through which electricity generation costs could be further reduced.

3.4.2 Medium-enthalpy ORC in Fang, Chiang Mai

Since there are one hundred eighteen thermal springs in Thailand, with surface temperatures ranging from 40 °C to 100 °C, systematic studies have been conducted since 1977 in order to

extract the geothermal energy to produce electricity. The first geothermal power plant was completed on December 1989, using a binary cycle. It is located at the Fang geothermal field in the Chiang Mai province of northern Thailand and generates 300 kW of electricity. The thermal water inlet temperature to the heat exchanger varies nowadays between 115 °C and 120 °C. The released water with an outlet temperature of around 80 °C is further used for a drying house in order to dry chili, tabacco, tea, and so on [Raksaskulwong, 2015].
The shallow well with only 100 m depth provides a flow rate of 22 l/s at originally 125 °C and drives the power plant. Other two wells were drilled up to 500 m at the same temperatures but with lower flow rates of 8 l/s respectively. Although the results were promising, the plan to expand the power plant was halted due to the lack of detailed information on the geothermal field [Amatyakul et al., 2016].

3.4.3 Kalina cycle in Húsavík

The geothermal power plant in Húsavík, in the north of Iceland, was first commissioned 2000. It is the first geothermal power plant operating with the Kalina cycle worldwide and generates more than 1.6 MW of electricity. The wells with depths between 400 m and 1000 m provide thermal water with a flow rate of 90 kg/s, a typical temperature of 121 °C and are located 20 km south of the town of Húsavík. The power plant supplies around 80 % of the electricity demand of the town with a population of 2500.
Additionally to the production of electricity, the local district heating system is fed by the still 80 °C hot thermal water after the heat exchanger. Other direct uses are greenhouse and swimming pool heating, as well as snow melting. The cooling water for the Kalina cycle comes from mountains and enters the condencer with 5 °C. Within the condenser it is heated up to 25 °C and then pumped to a trout fish farm.
The working fluid is an 82 % ammonia-water mixture at 5.4 bar. It is preheated in two recuperators to 68 °C before entering the evaporator. There it is heated up to 118 °C and is vaporized to a quality of 75 % vapor. The remaining water is seperated and the steam led to the turbine, which the steam exits at 60 °C [Mlcak, Mirolli, 2002].
After a turbine failure in 2008, the Australian Company Wasabi Energy Ltd. acquired the power plant and intended to refurbish it with the aim to resume power generation by 2012 [Wasabi, 2011].

4 Analysis of the geothermal field at Rosario de la Frontera

Rosario de La Frontera is a city located in the north-west of Argentina (25°47'55.14" S - 64°58'3.54" W), in the Province of Salta. The city itself has a population of 26,174 (2010) and was founded in 1874. In this area, thermal springs for commercial purposes were first exploited by Dr. Antonio Palau and on April 1, 1880 opened the thermal complex, which makes it the oldest in South America. It is located around 6 km southeast from the city center and is used by the Hotel Termas till today [INDEC, 2010], [Invernizzi et al., 2014].
In the vivinity of Hotel Termas are 13 hot springs, with surface temperatures ranging between 24.1 °C to 90.5 °C, which are fed by two main aquifers in 150 m and 2400 m depths [Chiodi et al., 2015]. [Barcelona et al., 2012] proved the precence of hot fluids in the Rosario de La Frontera geothermal area by audiomagnetotelluric investigation and [Invernizzi et al., 2014] estimated a hydrographic network and recharge area of 51.5 to 62.9 km^2 which feeds the reservoir of Pirgua Subgroup with an overall volume of 71.12 km^3, considering an average thickness of the Subgroup of 700 m and a reservoir surface at depth of 101.6 km^2. Thereby an effective volume of around 39 km^3 is expected, in which temperatures exceed 60 °C and therefore is interesting for geothermal applications. Furthermore they calculated the stored heat within the fluid to 222 TWh, for an assumed temperature of 90 °C.

4.1 Characterization of the thermal water resource

4.1.1 Geological conditions

In the area of NW-Argentina the Andean retro-wedge crop out in the subandean foreland which generally consist of anticlines formed during the cenozoic Andean shortening (66 Ma - present) caused by a compressive deformation migrating to the east. The retro-wege overlies the over-riding slab of the subduction zone which formed the Andean range. Furthermore the subandean foreland in NW-Argentina can be subdivided into different structural provinces due to along-strike differences in tectonic style, whereby Rosario de La Frontera is located within the area of the Santa Barbara System (fig. 4.1) [Maffucci et al. 2016].

The Sierra de La Candelaria anticline is north-south orientated, about 50 km long and up to 10 km wide (fig. 4.2). It lays south-east of Rosario de la Frontera and is dominated by a basement involved thrust system. The anticline is uplifted by a high-angle thrust fault along its eastern limb and in its central portion extensional faults offset the stratigraphic succession from east to west. The stepped fold pattern is characteristic for this area, caused by the Andean inversion of pre-existing normal faults associated to a regional rifting event in the Jurassic-Createceous era (145 - 66 Ma) [Invernizzi et al., 2014].

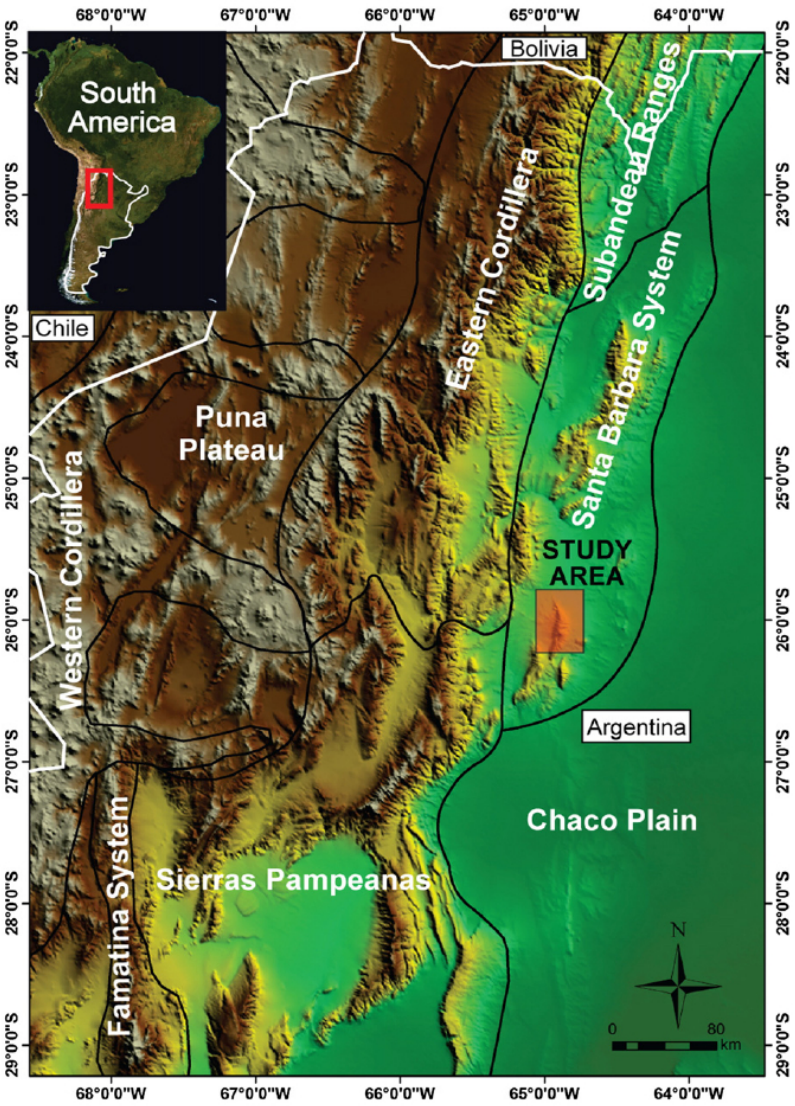

Figure 4.1: Structural provinces in NW-Argentina [Maffucci et al. 2016]

In the stratigraphic succession of the Sierra de La Candelaria anticline can be pointed out three main sedimentary sequences (fig. 4.2) [Cohen et al., 2017], [Invernizzi et al., 2014], [Maffucci et al. 2016]:

- The **Medina Formation** is the oldest unit, this Precambrian (4600 - 541 Ma) basement crops out of the core of the anticline.
- The **Salta Group** which overlays the Medina Formation and predominantly consist of red beds with limestone interbeds. It was formed in a Cretaceous (145 - 66 Ma) to Paleogene (66 - 23 Ma) era and can further be subdevided into three subgroups, namely from bottom to top:
  - The Pirgua Subgroup, which mainly consists of red breccias, conglomerates and sandstones and was conditioned by extentional faults during the formation of the Salta Basin.
  - The Balbuena Subgroup where deposits of the Pirgua Subgroup evolve and is mainly represented by limestones and shales. It is roughly 180 m thick and was formed during the latest Cretaceous to early Paleocene era (72 - 61 Ma).
  - The Santa Bárbara Subgroup, which, similiar to the Balbuena Subroup, is a post-rift event, deposited in lacustrine, shallow marine and continental environments of the Paleocene to early Eocene era (66 - 47 Ma) with a thickness of around 330 m.
- The **Payogastila Group**, including the Orán Group, formed in the middle Miocene (13 Ma) to Pleistocene (2.58 - 0.01 Ma) which crops out of the anticline in its northern sector and overlying the Salta Group, mostly represented by sandstones and massive quartzarenites with gypsum interlayers.

The Orán Group can further be subdevided into the Jujuy and Metán Subgroups, both formed during the Neogene era (23 - 2.58 Ma). The Metán Subgroup crops out at the northern sector of the Sierra de La Candelaria anticline and is regarded as the cap rock of the thermal aquifer, whereas the Medina Formation is considered as an impermeable basement.
For their calculations [Invernizzi et al., 2014] assume an average reservoir temperature of 90 °C, according to the suggested geothermal gradient of 40 °C/km by [Seggiaro et al., 1995]. [Chiodi et al., 2015] on the contrary, based on further geochemical investigations, come to the conclusion that the temperature in the reservoir is more likely in the range of 100 °C to 130 °C. In the same year, [Maffucci et al., 2015] carried out a systematic study on the fracture system in order to assess its dimensional and spatial properties. Based on previous investigations from [Barcelona et al., 2012], [Chiodi et al., 2012], [Invernizzi et al., 2014] and on 3D Discrete Fracture Network modelling (DFN), they suggest that the most favorable site for exploitation of geothermal fluids is located northwards from the outcrops of the Pirgua and Balbuena Subgroups along the Balboa anticline (fig. 4.3) where they expect a secondary permeability of 49 mD, which is more conservative than the 81.2 mD given by [Invernizzi et al., 2014], who also tested the sandstone with results of the total porosity of 7.2 % and a mean pore diameter of 0.3 micron.

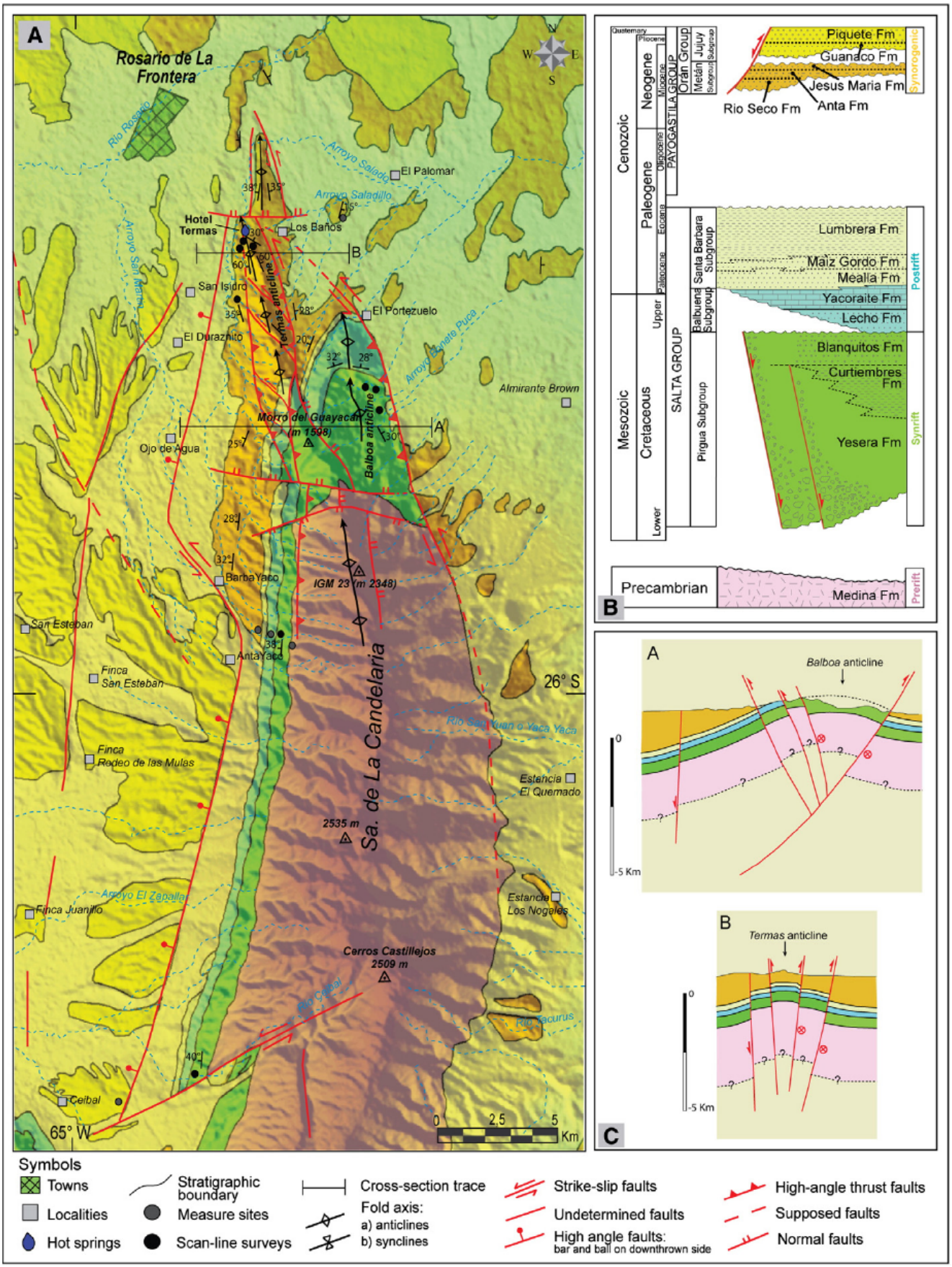

Figure 4.2: Geological map of the Rosario de La Frontera area [Maffucci et al., 2015]

The recharge of the geothermal system is mainly due to meteoric water, which infiltrates the ground in the area where the Pirgua Subgroup crops out. From there it is moving into deep with a northward direction as shown in figure 4.3. The residence time of the water within the reservoir is expected to be more than 50 years before it rises again to the surface in one of the hot springs [Invernizzi et al., 2014], [Maffucci et al., 2016].

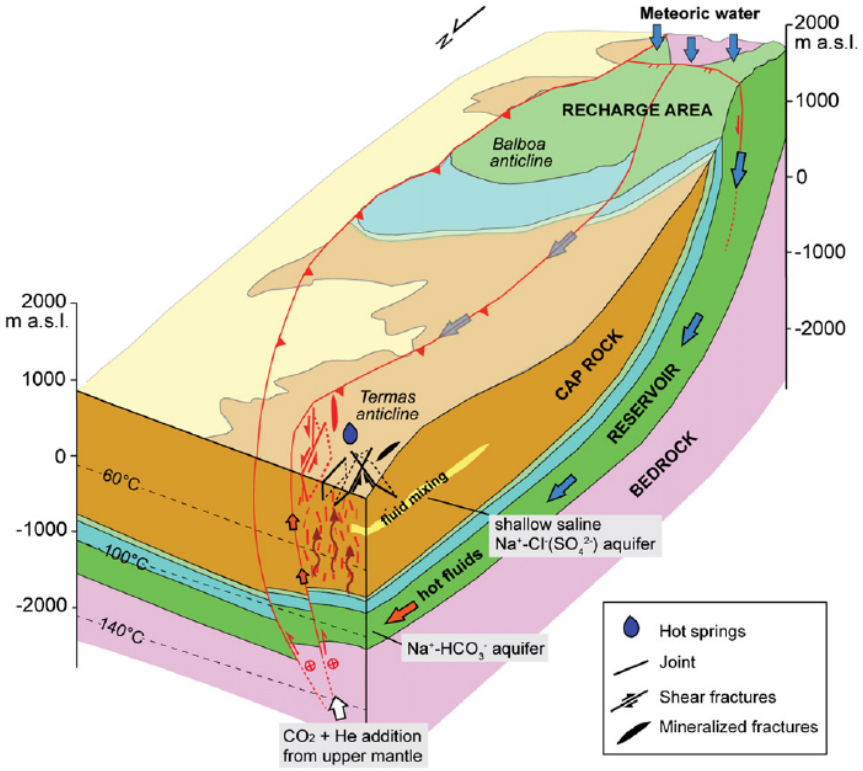

Figure 4.3: Conceptual 3D model of the undeground fluid movement [Maffucci et al., 2016]

4.1.2 Geochemical conditions

From the geochemical composition of the thermal water some conclusions can be drawn about the conditions within the reservoir [Stober, Bucher, 2014, sect. 14.2]. So can the amount of silica or the ratio between sodium and potassium be used to estimate the temperature of the reservoir due to so called geothermometers. Furthermore the electrical conductivity (salinity) is a product of the electrical conductivity of the cations and anions and gives a first information about the total dissolved solids (TDS). Another indicator is the pH value, which represents the negative logarithm of the hydrogen ion concentration, $pH = -log(H^+)$, where a $pH = 7.0$ indicates a neutral dissolution, which means that the concentrations of $[H^+]$ - and

$[OH^-]$ - ions are balanced. This neutral point decreases with increasing temperature and the pH value also influences the solubility of many substances, which can be used to calculate whether certain minerals are saturated or not.
An overview of the locations of the 13 hot springs around Hotel Termas is shown in figure 4.4 and the chemical composition as well as the temperature, pH value and the flow rate for each hot spring are listed in table 4.1. It should be mentioned, that the data available in the literature vary slighty from one another, so indicates [Invernizzi et al., 2014] a temperature range of 22.6 °C to 92.6 °C and a pH value of 6.65 to 8.43, whereas in [Chiodi et al., 2015] a range between 24.1 °C to 90.5 °C and 6.09 to 7.36 can be found, but as data from [Invernizzi et al., 2014] show, this values also vary throughout the year.
The amount of total dissolved solids in the majority of the hot springs is relatively low (TDS < 1050 mg/l) with a composition mostly of sodium $[Na^+]$ and chloride $[Cl^-]$ (alkali-chloride waters) with exeption of two sodium bicarbonate $[NaHCO_3]$ springs (RF07, RF12). The concentration of silica $[SiO_2]$ varys in a range of 47 mg/l to 124 mg/l, whereas values of bromide $[Br^-]$ and boron $[B]$ are below 2.08 mg/l and 0.51 mg/l respectively [Chiodi et al., 2015].
From the analysis of oxygen isotopes $[\delta^{18}O]$, which vary in a narrow range of - 7.1 ‰ to - 6.4 ‰, can be assumed that the water of the hot springs has a meteoric origin [Invernizzi et al., 2014], and due to comparison of four probes for its tritium content with data from the international atomic energy agency (IAEA) catalogue for Salta, it could be shown that the residence time of the water within the reservoir must last for more than 50 years.
Furthermore, [Chiodi et al., 2015] comes to the conclusion, that the alkali-chloride dominated water comes from the shallow aquifer system, whereas the sodium bicarbonate water represents the main hydrothermal reservoir.

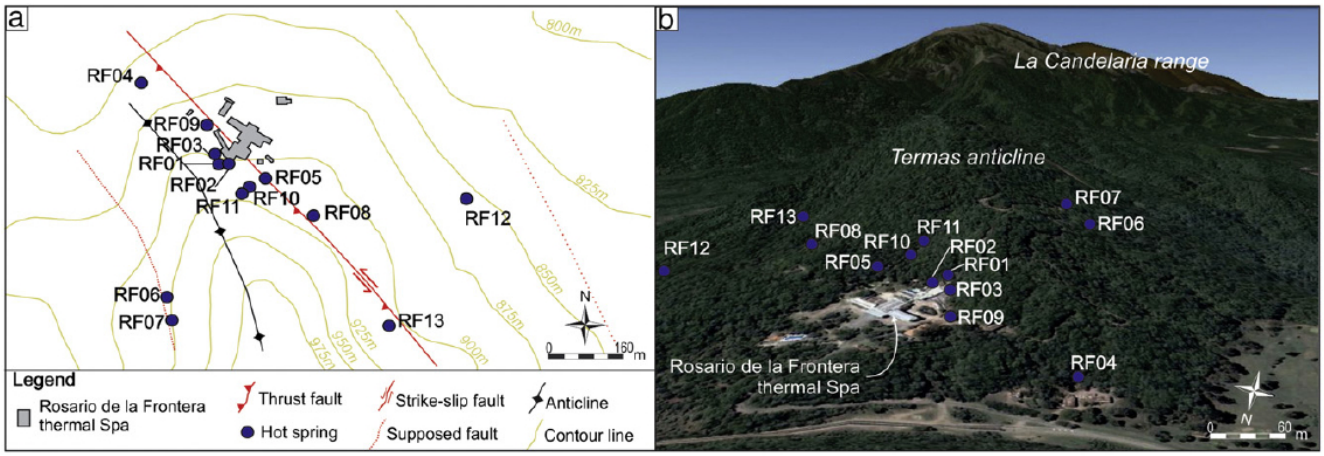

Figure 4.4: Locations of the hot springs around Hotel Termas [Chiodi et al., 2015]

Table 4.1: Chemical composition (in mg/l), temperature, pH value and flow rate of the hot springs around Hotel Termas [Chiodi et al., 2015], [Invernizzi et al., 2014]

	Temp. [°C]	pH	flow rate [l/h]	HCO_3^-	Cl^-	Br^-	NO_3^-	SO_4^{2-}	Ca^{2+}	Mg^{2+}	Na^+	K^+	B	SiO_2
RF01	74.0	6.75	540	169	313	0.1	0.6	128	11	0.5	305	4.3	0.12	92
RF02	81.2	6.88	350	156	682	0.2	0.5	190	10.6	0.5	587	7.4	0.18	88
RF03	71.4	7.06	800	201	16000	2.1	0.1	2100	326	20.1	11200	80.8	0.23	47
RF04	24.1	6.84	38	315	5340	2.0	6.1	3010	440	63.5	4290	17.4	0.33	54
RF05	52.7	6.42	270	198	137	0.2	1.2	146	32	1.5	188	2.7	0.21	94
RF06	64.8	6.09	950	149	270	0.2	1.4	104	5.1	0.1	288	4.0	0.39	89
RF07	58.2	6.73	1300	224	42	0.1	1.5	103	15	0.7	147	1.7	0.27	85
RF08	74.9	6.83	2500	219	122	0.1	1.0	143	22	0.9	193	2.3	0.15	87
RF09	24.2	7.36	460	279	2510	1.6	2.7	626	75	10.9	1900	17.4	0.45	51
RF10	90.5	6.12	400	171	276	0.2	0.2	187	3.9	0.2	321	5.7	0.28	102
RF11	90.4	6.39	1200	190	254	0.2	0.9	180	14	0.3	294	5.6	0.35	108
RF12	45.2	6.77	0	215	80	0.1	0.3	155	4.6	0.28	206	4.7	0.44	116
RF13	72.2	6.26	3200	210	133	0.1	0.4	140	3.2	0.1	227	5.3	0.51	124

4.2 Infrastructure and energy demand

Besides the city of Rosario de la Frontera, there is also the department of Rosario de la Frontera, including two municipalities, namely the city with 26,174 inhabitants and an area of 2184 km^2, and furthermore El Potrero with 2,819 inhabitants and an area of 3218 km^2, which means that besides the city the main part of the department is rural with agricultural production of beans, soy, vegetales and tobacco as well as the largest livestock production within the province of Salta [INDEC, 2010], [Salta, 2018].
For the construction and operation of a geothermal power plant some points must be taken into account regarding the local situation such as access to the well, infrastructure for construction equipment, a corresponding demand for energy and, as far as possible, further uses of the heat to increase profitability. A brief overview of these points is given below.

Access to the well

As mentioned in section 4.1.1, the most promising site for a geothermal power plant based on previous investigations, would be in the northern part of the Balboa anticline which is roughly 3 - 5 km to the southeast of Hotel Termas. The outlets of the anticline are thereby hilly and wooded, with no major forest roads leading into the area. But the surrounding is marked by flat fields, which can be reached via the nearby Route 34. Here there would be sufficient space for the drilling work if the exact development of the reservoir is carried out using directional drilling methods.

Infrastructure

The city of Rosario de la Frontera is located at the junction of routes 9 and 34. While route 9 comes south from San Miguel de Tucumán (distance 130 km), route 34 comes southeast from Santiago del Estero (270 km). Both head north until route 9 points west to Salta (180 km). Near this turn-off, 9 km south of the town of General Güemes, are also the two largest power plants in the province of Salta (Termoandes S.A., 643 MW and Térmica Güemes S.A., 361 MW). From there a 132 kV power line leads via Rosario de la Frontera to San Miguel de Tucumán, which is a good prerequisite for connection to the power grid [CAMMESA, 2018a], [MINEM, 2016a].

Electricity demand

The electricity demand in 2016 for the entire department of Rosario de la Frontera was 39.99 GWh, distributed among 7,665 households (23.59 GWh), 812 businesses (8.96 GWh) and 128 official or public buildings (5.36 GWh) as well as 59 industrial applications (2.07 GWh).

This means an average electricity consumption of 1,379 kWh per capita per year [MINEM, 2016a].

Direct heat

The average minimum temperatures in the region of Salta fall below 10 °C between May to September [SMN,], so it is likely that there is a heating demand. This could be covered by a district heating network or the heat could be offered to the local industry (to dry tobacco for example). No information about the natural gas demand in Rosario de la Frontera could be found, but the demand for the province of Salta in 2016 was 790 Mio. m^3, of which around 27 $\%$ are used in the industry and 14 $\%$ for residential buildings. With a total of 300,082 households in the province of Salta and 3,153 industrial companies [MINEM, 2016a], that leads to an estimated demand of natural gas of 3 Mio. m^3 ($\approx$ 32 GWh) for private households in Rosario de la Frontera or almost 4 Mio. m^3 ($\approx$ 43 GWh) for the industrial companies, considering a heating value of 9300 kcal [ENARGAS, 2016].

4.3 Simulation program GeSi

At the Institute of Nuclear and Energy Technology (ger.: Institut für Kern- und Energietechnik, IKET) at the Karlsruhe Institute of Technology (KIT), a simulation program was developed to calculate organic rankine cycles with thermal water as heat source. This geothermal simulation (GeSi) program is based on a Matlab® code and uses the REFPROP fluid data provided by the National Institute of Standards and Technology (NIST) [Vetter, 2014, sect. 3.1].
It comes with a graphical user interface (GUI) where serveral modules can be selected, as example full load or partial load, with or without recuperator, course of performance or colormaps to identify optimal process parameters, which will be briefly explained within this section.

Module: Organic Rankine Cycle

This module calculates a simple ORC layout at design conditions without a recuperator and sub- or supercritical processes can be computed. First a working fluid is selected from the REFPROP fluid list and as a second step, boundary conditions as well as process parameters are specified. There are several options for defining the steam condition, such as:

- Turbine inlet temperature and pressure
- Turbine inlet pressure and saturated steam

- Turbine inlet temperature and saturated steam
- Turbine inlet pressure and turbine outlet steam content
- Turbine inlet temperature and turbine outlet steam content

Several input options can also be selected for the thermal water cycle. By default the definition of the thermal water temperature, pressure and flow rate into the heat exchanger is selected but can be switched to amount of heat transfered into the ORC or minimum permissible thermal water temperature after the heat exchanger.
For the cooling site can be selected between air or water cooling, with its temperature and relative air humidity or flow rate respectively.
In addition for the heat exchanger as well as the condenser must be given their minimal temperature difference (gradity) and pressure loss in order to calculate the unknown inlet or outlet temperatures. Finally information about the pump and turbine efficieny is required to calculate the power output and the systems real efficiency.

Module: ORC with recuperator

Hereby the layout of the ORC is extended by an internal heat exchanger (recuperator) and the input options differ in a few points from the previous module. The last two options to define the steam condition by its steam content at the turbine outlet are not available, because expanding into the two phase area would not allow an internal heat transfer due to similar temperatures at the outlets of the turbine and the pump.
For the recuperator, similar to the heat exchanger or the condenser, the gradity as well as the pressure loss must be specified. The calculation results are extended by the internal transferred heat, temperature differences at in- and outlet side of the recuperator and furthermore the thermodynamic efficiency with and without recuperator.

Module: Course of performance

This module allows the variation of one parameter (for example the pressure) of the steam condition within a desired range, while the other parameter (for example the temperature) and all other conditions remain constant. It is possible to calculate an ORC with or without recuperator and to compare these two configurations directly. The values of the power output and the efficiency are displayed as a function of the variating parameter.

Module: Colormap

Here the program starts a systematic calculation of all possible combinations of steam temperature and pressure under a defined step size within a given range. The output is given in

form of so called colormaps, where the values of power output, thermodynamic efficiency, transfered heat and flow rate are displayed as a funtion of the two parameters temperature and pressure. These diagrams allow an easy identification on how the different values depend on the parameters and to find the optimum operating condition.

Module: Partial load

All previous modules operate under the presumption of nominal capacity. In order to calculate the influence of changing thermal water conditions (temperature, flow rate, pressure) the module $Partial\ load$ offers in its submodules the same calculation possibilities as the previous modules (therefore with/without recuperator, course of performance, colormaps). The difference in these submodules to the previous is on one side the variation of the thermal water condition instead of the steam condition and on the other side the necessity to implement the efficiency curve for the turbine and the pump as a function and not as a single value. To display the pump and turbine characteristics as accurately as possible, a function as shown in equation 4.1 is given as a dependency of the partial load:

$$\frac{\eta}{\eta_{nom}} = a_0 + a_1\left(\frac{\dot{m}}{\dot{m}_{nom}}\right) + a_2\left(\frac{\dot{m}}{\dot{m}_{nom}}\right)^2 + \ldots + a_6\left(\frac{\dot{m}}{\dot{m}_{nom}}\right)^6 \tag{4.1}$$

Where a_1 to a_6 are parameters, η and $\dot{m}$ are the actual efficiency and flow rate, whereas η_{nom} and $\dot{m}_{nom}$ are the efficiency and flow rate at nominal condition respectively.

4.4 Performance model for tailored solutions

In this section calculations of a power optimized ORC plant will be presented. Besides some constant assumptions for technical installations such as the heat exchanger or the condenser, variational calculations of different parameters are performed in order to see how these affect the power plant output.
These include calculations for different thermal water temperatures within the expected range, a seasonal cycle calculation where the influence of the ambient temperature to the cooling system shall be investigated and also a partial load simulation, if the flow rate or temperature of the thermal water deviate from the design point and thus the turbine and pump efficiency drop from its optimum.
As constant assumptions for the following calculations can be considered the gradity and the pressure loss of the heat exchanger as well as the condenser. And apart from partial load calculations, the efficiency of the turbine and the feed pump are also set constant. Finally the cooling parameters are assumed on the basis of the annual averages of the Salta climate data.

With regards to state of the art technology, these values are listed in table 4.2 [Nusiaputra, 2017], [SMN,], [Song et al., 2016], [Vetter, 2014], [Zeleny et al., 2017].

Table 4.2: Boundary conditions of the nominal power calculations

ORC process		**Cooling air**	
Condensation temperature	30 °C	Inlet temperature	17 °C
Feed pump efficiency	0.7	Pressure	0.1013 MPa
Turbine efficiency	0.8	Relative humidity	73 %
Heat exchanger		**Condenser**	
Gradity	5 °C	Gradity	5 °C
Pressure loss	0.02 MPa	Pressure loss	0.02 MPa

Another important parameter for the overall power generation besides the temperature of the thermal water is its flow rate. Based on DFN simulations, [Maffucci et al. 2016] calculated the permeability to 49 mD, whereas [Invernizzi et al., 2014] measured probes with a permeability between 24.1 to 137.1 mD, with a mean value of 81.2 mD. Together with the effective thickness of around 380 m, the transmissivity can be calculated [Hölting, Coldewey, 2013, sect. 3.3.4]:

$$k_f = \frac{K \cdot \rho \cdot g}{\mu} \quad \text{and furthermore} \quad T = k_f \cdot D \tag{4.2}$$

Here, the following mean:

- k_f = Hydraulic conductivity in [m/s]
- K = Permeability in [m^2], thereby 1mD = 9.869·10^{-16} m^2
- ρ = Density of the fluid, for water: 1000 kg/m^3
- g = Gravitational constant = 9.81 m/s^2
- μ = Dynamic viscosity, for water: 10^{-3} Ns/m^2
- T = Transmissivity in [m^2/s]
- D = Thickness of the aquifer in [m]

Which leads to an average transmissivity of the aquifer of $8.8 \cdot 10^{-5}\,m^2/s$ for 24.1 mD or $5 \cdot 10^{-4}\,m^2/s$ for 137.1 mD. The graph in figure 4.5 gives a relationship between transmissivity and required pumping power for a desired flow rate. According to this, with a pumping power of around 70 kW, a flow rate between 20 to 40 l/s could be achieved for the given transmissivity and for the subsequent calculations a flow rate of 30 l/s will be assumed. If the thickness of the aquifer is multiplied by the permeability K instead of the hydraulic conductivity k_f, the transmissibility [m^3] is obtained. Transmissivity and transmissibility should have values above $5 \cdot 10^{-5}\,m^2/s$ and $5 \cdot 10^{-12}\,m^3$ respectively [Feldrappe et al., 2008, sect. 3.4].
Of the stimulation options presented in section 2.2.3, only hydraulic shearing should be used in Rosario de la Frontera to avoid contamination of the thermal springs. With this method, in Groß Schönebeck and in Landau (both in Germany) a doubling of the injectivity index was achieved. In Soultz-sous-Forêts (France), an increase of factor 4 - 5 of the injection index was reported, making the results particularly good [Bauer et al., 2014, sect. 6.3].
The technical and economic significance of such an increase will be demonstrated in sections 4.4.3 and 5.3.3.3.

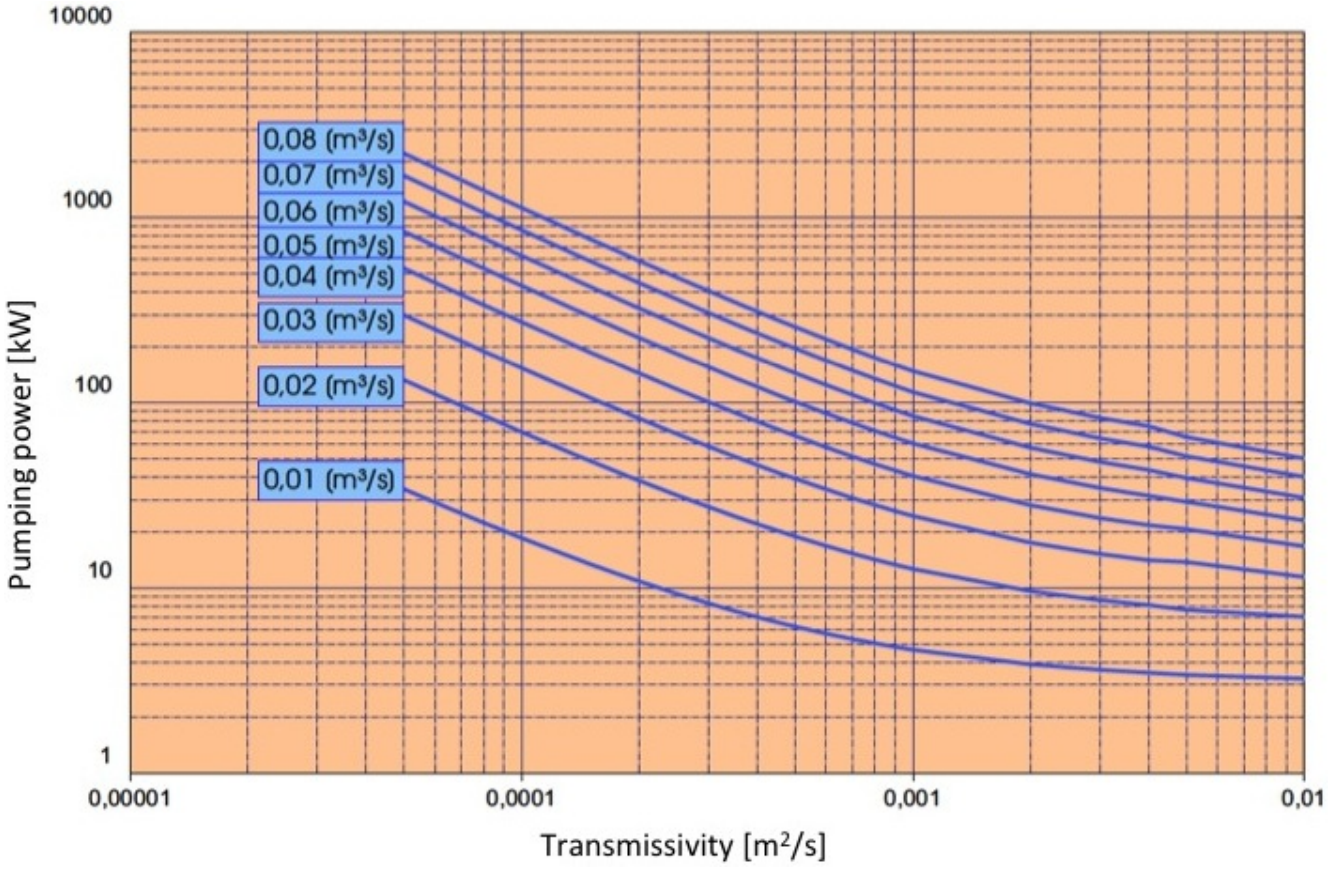

Figure 4.5: Relationship between pumping power and transmissivity [Bauer et al., 2014]

4.4.1 Simulation for different well head temperatures

With regard to the uncertainty of the well head temperature at the present time, the following four temperatures are analyzed, namely 95 °C, 105 °C, 115 °C, and 125 °C in order to gain an initial estimate of how much power output the plant will provide, in the overall and the net aspect. After a pre-selection of all fluids in the available REFPROP database the ten most promising ones regarding the power output within the analyzed temperature range were further investigated and the properties of these refrigerants are listed in table 4.3. R245fa was not among the top ten, but is listed due to its use in the two presented turnkey systems (see section 4.5). Furthermore column “Restricted” refers to the regulation of the European Union of April 2014 [EU, 2014], which successively prohibits the use of refrigerants depending on their area of application and their GWP, or as in the case of R22 and R125 are already restricted due to their ODP. Therefore, the “best performers” listed in the following subchapters were selected with special attention to the lowest possible GWP and only one fluid with highest possible performance is listed as a benchmark, independingly of its GWP.

Table 4.3: Refrigerant properties [IPCC, 2007], [EU, 2014], [REFPROP,]

	Type	Critical temperature [°C]	Critical pressure [MPa]	GWP	Restricted
Propane	HC	96.74	4.25	3.3	
Propylen	HO	91.06	4.55	2	
R22	HCFC	96.14	4.99	1810	since 2011
R32	HFC	78.10	5.78	675	as of 2022
R115	CFC	79.95	3.12	7370	since 1996
R125	HFC	66.02	3.61	3500	as of 2020
R134a	HFC	101.06	4.05	1430	as of 2022
R143a	HFC	72.7	3.76	4470	as of 2020
R218	PFC	71.87	2.64	8830	as of 2020
R1234yf	HFO	94.7	3.38	4	
R245fa	HFC	154.01	3.65	1030	as of 2022

4.4.1.1 Calculation for 95 °C

Image 4.6 displays the graphical user interface of the GeSi program for the ORC module with the calculation parameters. The termal water temperature is set to 95 °C, at a pressure of 5 bar and a flow rate as mentioned before of 30 kg/s. A gradity of 5 °C within the heat exchanger leads to a maximum possible steam temperature of 90 °C. The remaining variable parameters are the choice of the working fluid and its operating pressure.
The graphs in figure 4.7 show that each working fluid has its own optimum operating pressure, which also depends on the steam temperature. Furthermore it must be mentioned that the optimum pressure can also vary between the gross and the net power output. For example for R143a the pressure with the highest gross power is 3.8 MPa, whereas this value decrease to 3.5 MPa regarding the net power, or in the case of R125 with the highest net power at 4.2 MPa while the gross power continuously increases with higher pressures.

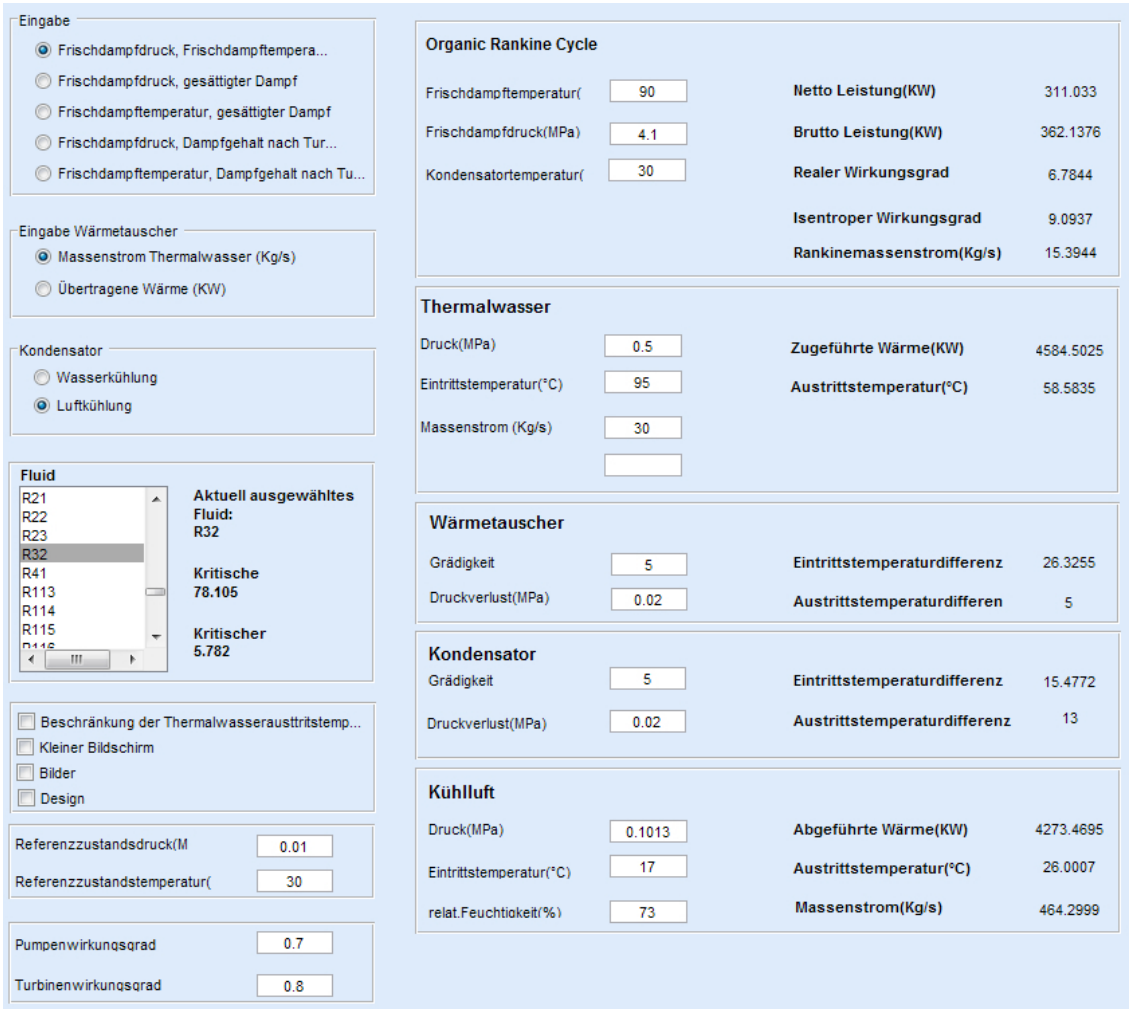

Figure 4.6: GUI of GeSi with the calculation parameters for R32 at 95 °C

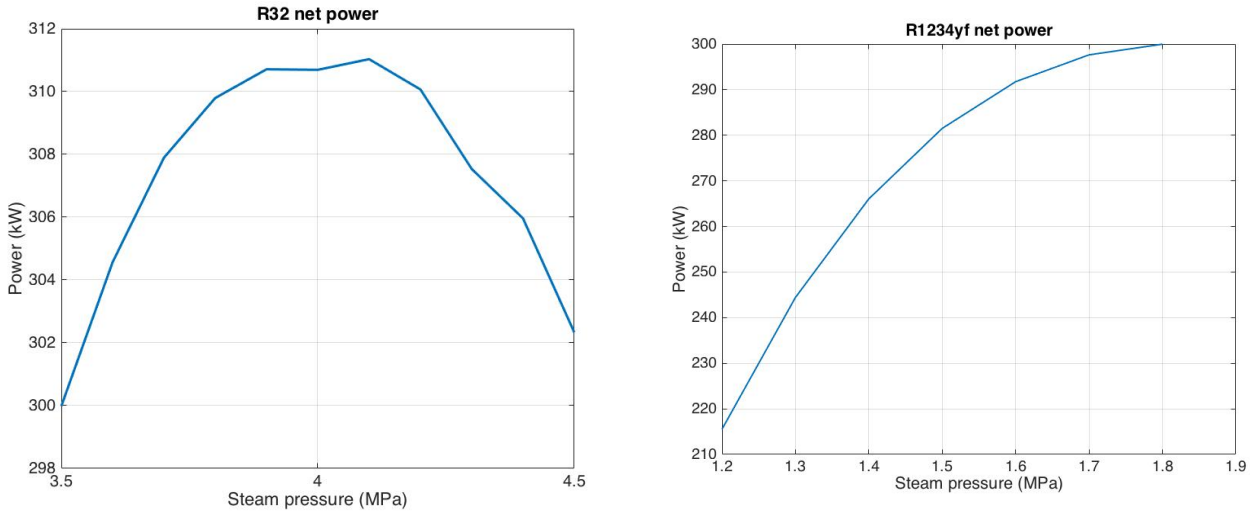

Figure 4.7: Net power curve of R32 (left) and R1234yf (right) at 95°C

Another important aspect is the optimum combination of steam temperature and pressure. From the colormap in figure 4.8 it can be seen that not always the highest steam temperature leads to the highest power output. That means, in order to reach the maximum performance the available thermal water temperature, the working fluid, the steam temperature and its pressure always have to be regarded together.

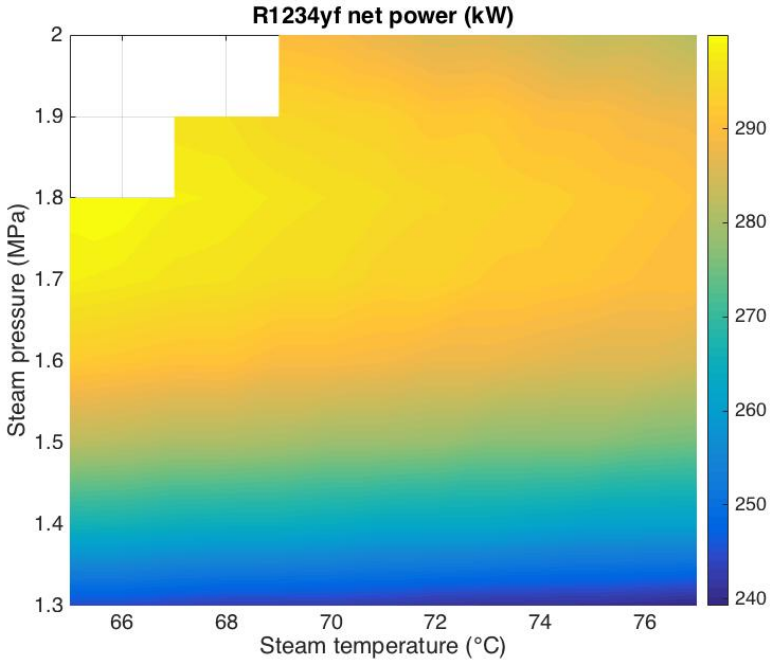

Figure 4.8: Colormap of the net power output of R1234yf at 95°C

It must be noted that for the calculation of the colormaps a minimum steam content of $x = 0.9$ at the turbine outlet was set. If pure steam is desired, or the installed turbine does not allow expansion into the two phase area, this must be changed and lower performance may result. In table 4.4 the five best performing working fluids are listed, excluding R22 and R115, as they are already restricted. The focus was placed on the highest possible net output and the corresponding values of the gross power which excludes the efficiency losses of the feed pump and the turbine, the steam temperature and pressure as well as the required flow rate of cooling air are given. The latter value is calculated by the programm in order to reach the desired condensation temperature of 30 °C and can be used to estimated the required power of the fans, as they are not part of the considered system. [Vetter, 2014] calculates the pressure loss of an air cooling system between 100 Pa to 120 Pa depending of the design of the cooling system and together with the volume flow, the hydraulic power can be calculated as:

$$P = \dot{V} \Delta p = \frac{\dot{m_{air}}}{\rho_{air}} \Delta p \tag{4.3}$$

With a pressure loss of 120 Pa and the density of air of 1.22 kg/m^3, that leads to a required fan power of roughly 10 kW per 100 kg/s mass flow rate, not taking into account any inefficiencies.

Table 4.4: Power output results for 95 °C thermal water temperature

	Gross power [kW]	Net power [kW]	Steam temperature [°C]	Steam pressure [MPa]	Cooling air flow rate [kg/s]
R218	578.4	388.9	77	2.9	725
R125	567	362.8	76	4.2	689
R32	362.1	311	90	4.1	464
R1234yf	341.4	299.9	66	1.8	466
R134a	324.6	293.3	64	1.8	470

4.4.1.2 Calculation for 105 °C

For a thermal water temperature of 105 °C the power output and the optimum operating pressure increase for all fluids compared to 95 °C. As in the previous section, the results of the calculations are listed in table 4.5. Here the difference in performance is particularly large comparing R218 as best performer to R134a, with 113.2 kW for the net power and 312.4 kW for the gross power output. This observation is therefore in line with the results of [Vetter, 2011], that a supercritical process can achieve significantly higher performance under certain conditions (see sect. 3.2.2).

Table 4.5: Power output results for 105° C thermal water temperature

	Gross power [kW]	Net power [kW]	Steam temperature [°C]	Steam pressure [MPa]	Cooling air flow rate [kg/s]
R218	774.7	526.1	89	3.5	734
R125	741.1	507.8	89	4.7	732
R32	519.6	441.2	100	4.7	560
R1234yf	494.4	429.1	69	2	616
R134a	462.3	412.9	70	2.1	576

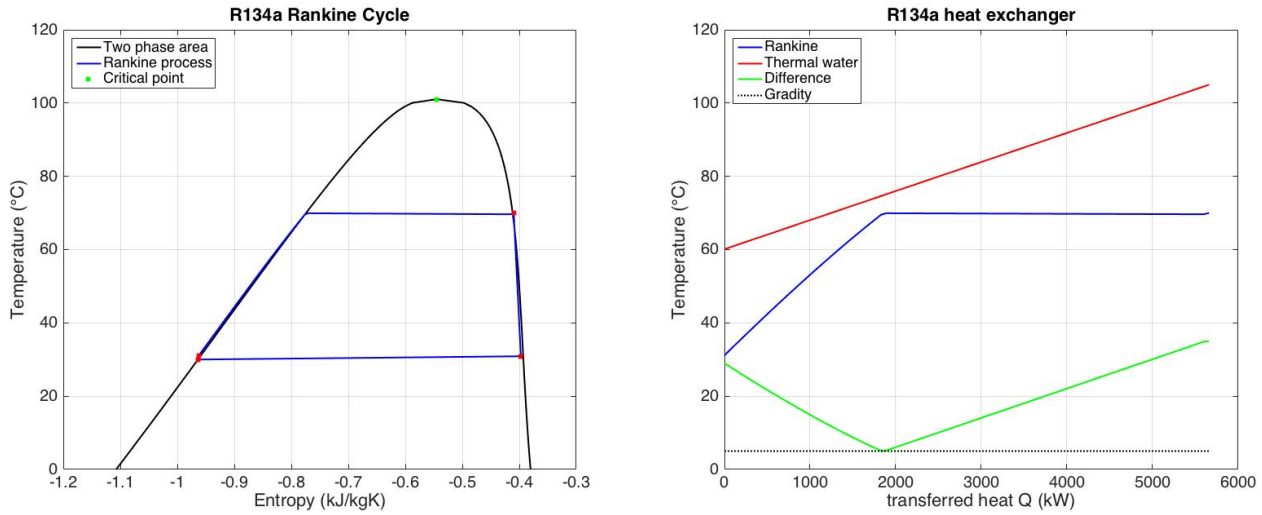

Figure 4.9: T,s - diagram (left) and heating-up curve (right) of R134a at 105° C

The T,s - diagram of R134a and the corresponding temperature curves within the heat exchanger are shown in figure 4.9 and as comparison the ones of R218 are given in figure 4.10. The subcritical process of R134a passes the two phase area, resulting in a constant temperature during the evaporation phase, whereas the supercritical process of R218 does not lead into the two phase area and therefore the temperature of the fluid increase steadingly.
This results in a consistently smaller temperature difference between the fluid and the thermal water, which makes it possible to extract more heat from it. In the case of R218 however, not the fluids temperature is raised but the associated mass flow rate is increased, which ultimately leads to higher performance.

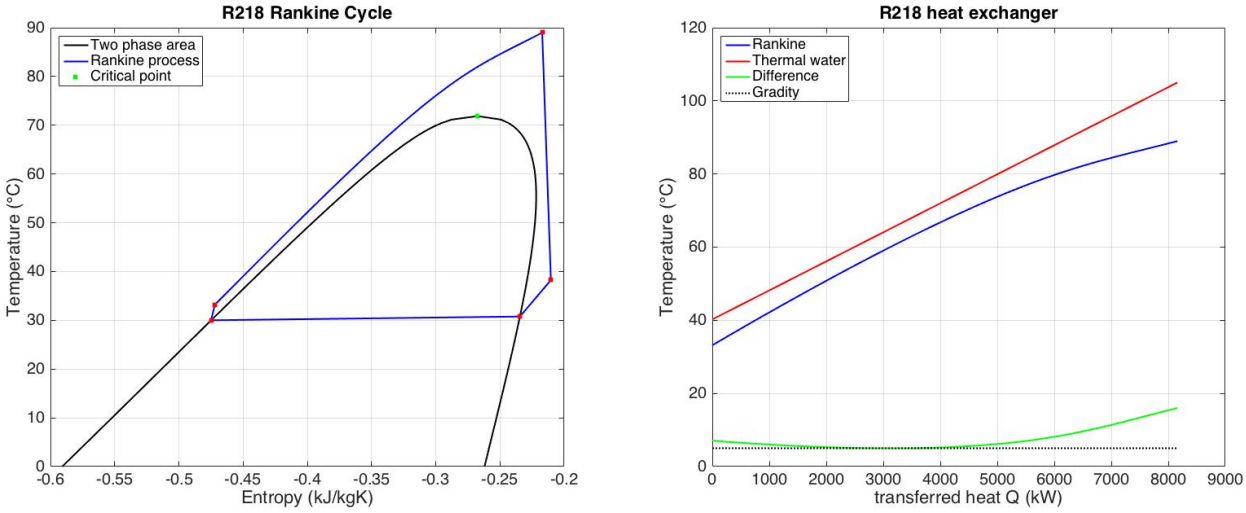

Figure 4.10: T,s - diagram (left) and heating-up curve (right) of R218 at 105 °C

4.4.1.3 Calculation for 115 °C

Table 4.6 lists the performance of the fluids for a thermal water temperature of 115 °C. It can be seen that the ranking changed for the fifth place. While R218 is still the best performer of all investigated fluids, Propylen now produces more net power than R134a. Thereby R32 remains the only fluid with its optimum power output at the maximum possible steam temperature of 110 °C, whereas all other fluids reach their optimum at lower temperatures. Furthermore a clear trend can be seen that with higher operating temperatures also the optimum pressure increases.
The graphs in figure 4.11 show the temperature of the thermal water after the heat exchanger as a function of the steam pressure. The left graph illustrates the curve for an inlet temperature

of 95 °C, and the right graph for 115 °C. The comparison shows that the outlet temperatures are almost the same for the respective steam pressure optimum (57.1 °C at 1.8 bar for 95 °C and 57.4 °C at 2.7 bar for 115 °C).
This means that for a higher thermal water temperature at the inlet a higher return temperature does not automatically occur and if further use of the thermal water is desired, for example by district heating, this circumstance must be taken into consideration.

Table 4.6: Power output results for 115° C thermal water temperature

	Gross power [kW]	Net power [kW]	Steam temperature [°C]	Steam pressure [MPa]	Cooling air flow rate [kg/s]
R218	979.5	668.1	99	4	776
R125	979	667.6	99	5.3	826
R32	751.4	618.8	110	5.8	683
R1234yf	724.1	605.1	84	2.7	716
Propylen	758.1	587.8	85	4	731

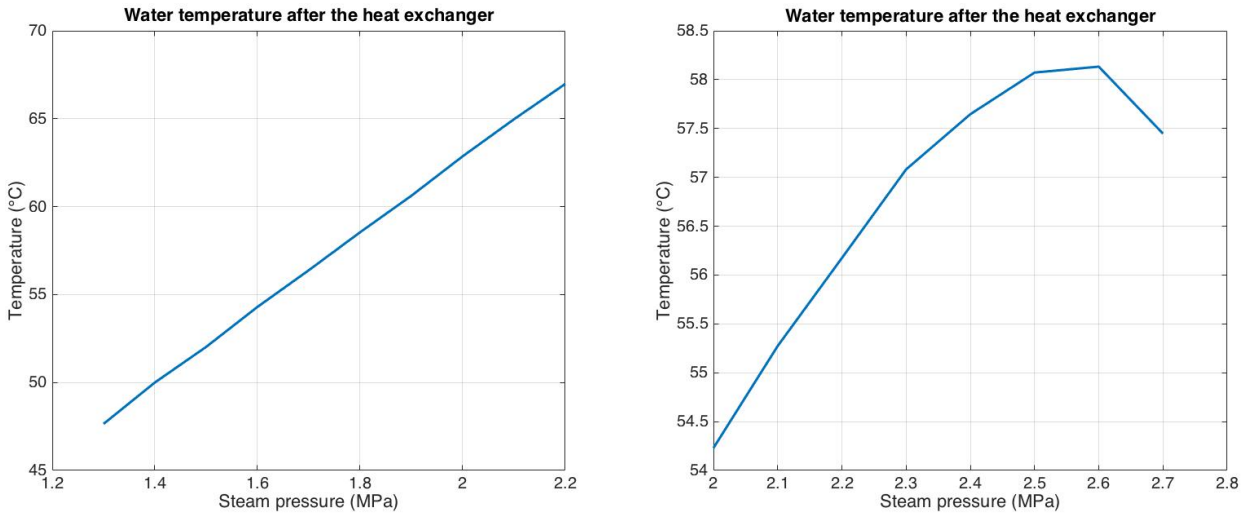

Figure 4.11: Thermal water temperature after the heat exchanger at 95° C inlet temperature (left) and 115° C (right) with R1234yf as working fluid

4.4.1.4 Calculation for 125 °C

For the highest investigated thermal water temperature, there is another change with regard to the performance of the working fluids. Although the gross and net power output further increases for all fluids comparing lower temperatures, R218 is no longer the fluid with the highest net power output, but is now in fourth place, just before Propylen (table 4.7).
As mentioned before, with higher thermal water temperatures also the optimum steam pressure increases for all fluids, and for all temperatures R32 and R125 are the fluids which require the highest pressures and R134a together with R1234yf the lowest (fig. 4.12).

Table 4.7: Power output results for 125 °C thermal water temperature

	Gross power [kW]	Net power [kW]	Steam temperature [°C]	Steam pressure [MPa]	Cooling air flow rate [kg/s]
R1234yf	1181.6	893.9	100	3.7	1039
R125	1198.6	833.9	109	5.7	875
R32	1006.4	819.8	120	6.5	814
R218	1204.5	813.2	109	4.6	818
Propylen	1077.9	802.7	98	4.8	914

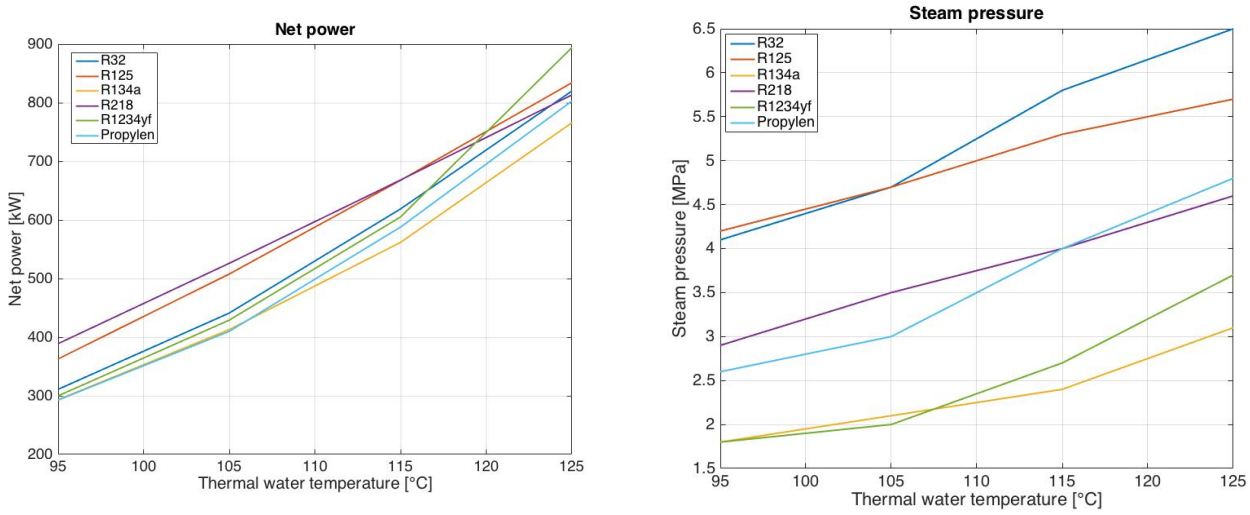

Figure 4.12: Net power curves (left) and steam pressure curves (right) of the working fluids from 95 °C to 125 °C

Although steam pressures in conventional steam power plants are around 170 to 180 bar [Strauss, 2016, sect. 7.1], pressures in ORC power plants are normally way lower, due to two reasons. On the one hand, the fluids which are used in ORC processes do not require such high pressures as the previous results show, on the other hand, higher operating pressures require thicker pipe and component wall thicknesses, which ultimately lead to higher costs. It is therefore necessary to weigh up what is finally more economical, an optimum operating pressure or reduced costs.
In figure 4.12 it can also be seen that the power curves for R125 and R218 are almost linear over the entire range and for a well head temperature between 80 to 140 °C, the net power can be estimated with good approximation as follows, with the temperature T in [°C]:

$$P_{net\,R125} = 15.66 \cdot T - 1123 \qquad \text{and} \qquad P_{net\,R218} = 14.37 \cdot T - 976.4 \tag{4.4}$$

Finally it has to be mentioned that, regarding the net power output, R143a showed similar performance as R125 for all temperature ranges with slighly lower operating pressures, but was not included in the lists due to its higher GWP.

4.4.2 Seasonal cycle calculation

Due to the fact that in the area of Rosario de la Frontera there is no river or further water source which could be used for cooling the ORC process, air cooling must be applied. Therefore the impact of changing ambient temperatures on the power plant needs to be investigated.

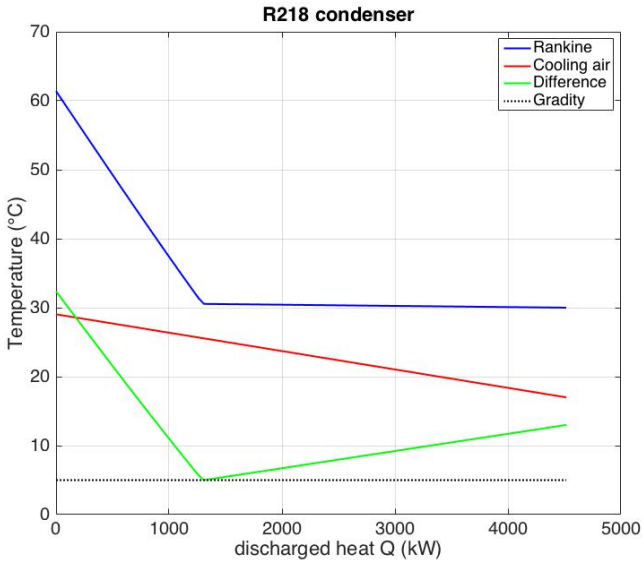

Figure 4.13: Condensation curve and cooling air temperature of R218 at 95° C

The gradity of the condenser given in table 4.2 is the minimum temperature difference between the cooling air and the working fluid within the condenser as shown in in figure 4.13. Hereby the outlet temperature difference is normally in the range between 10 °C to 15 °C and marks the difference between the ambient temperature and the condenser temperature. This value can be increased or decreased by variating the mass flow of the cooling air but can never go below the limit of the gradity, which itself depends of the quality of the condenser.
During all former calculations an ambient temperature of 17 °C, which is the annual average for Salta, and a condenser temperature of 30°C were set, resulting in an outlet temperature difference of 13 °C. In order to know how a changing ambient temperature influences the performance, July as coldest month with an average temerature of 10.1 °C is compared to December as hottest month with 21.5 °C. For this, R218 as best performer for a thermal water temperature of 95 °C and R1234yf as best performer for 125 °C thermal water temperature are investigated.
As the average temperature in December, as hottest month, is still roughly 8 °C below the average condenser temperature, and therefore above the gradity limit of 5 °C, there are two options:

- Vary the condensation temperature so that it is around 13 °C above the ambient temperature. The required cooling air mass flow remains almost constant.
- Keep the condensation temperature constant by adjusting the required cooling air mass flow.

Varying condensation temperature

As table 4.8 indicates, for a change of the condensation temperature the required cooling air flow rate is more or less constant. At the same time the power output changes due to a higher or lower difference between evaporation and condensation temperature. Since the fans only have to be designed for one operating point, they can always be operated optimally. On the other hand, the disadvantage is that the power output of the plant is higher in winter than in summer, whereas the power demand is reversed [CAMMESA, 2018b].

Table 4.8: Power output and cooling air flow rate for changing condensation temperatures for R218 and R1234yf at 95° C and 125° C

	Month	Gross power [kW]	Net power [kW]	Condenser temperature [°C]	Ambient temperature [°C]	Cooling air flow rate [kg/s]
R218	Reference	578.4	388.9	30	17	725

		Gross power [kW]	Net power [kW]	Condenser temperature [°C]	Ambient temperature [°C]	Cooling air flow rate [kg/s]
at 95 °C	July	696.5	497.5	23.6	10.1	728
	December	509.3	326.8	34	21.5	727
R218	Reference	1204.5	813.2	30	17	818
at 125 °C	July	1363.4	966.2	23.6	10.1	818
	December	1105.1	718.6	34.2	21.5	814
R1234yf	Reference	341.4	299.9	30	17	466
at 95 °C	July	419.3	373.8	23.4	10.1	466
	December	291	253	34.3	21.5	466
R1234yf	Reference	1181.6	893.9	30	17	1039
at 125 °C	July	1346.7	1065.4	23.5	10.1	1040
	December	1080	797.2	34.2	21.5	1040

Varying cooling air mass flow

The second option tries to keep the condensation temperature constant. From table 4.9 it can be seen that with a constant condensation temperature the power output also remains constant and only the mass flow rate of the cooling air has to be adjusted. The advantage of constant power generation must be achieved by oversizing the cooling system and operate it at low performance during most time of the year, as it must be designed for the highest mass flow rate required.

Table 4.9: Power outputs and cooling air flow rates for constant condensation temperature for R218 and R1234yf at 95 °C and 125 °C

	Month	Gross power [kW]	Net power [kW]	Condenser temperature [°C]	Ambient temperature [°C]	Cooling air flow rate [kg/s]
R218	Reference	578.4	388.9	30	17	725
at 95 °C	July	578.4	388.9	30	10.1	412

		Gross power [kW]	Net power [kW]	Condenser temperature [°C]	Ambient temperature [°C]	Cooling air flow rate [kg/s]
R218 at 125 °C	December	578.4	388.9	30	21.5	1515
	Reference	1204.5	813.2	30	17	818
	July	1212	813.3	30	10.1	458
	December	1212	813.3	30	21.5	1708
R1234yf at 95 °C	Reference	341.4	299.9	30	17	466
	July	341.4	299.9	30	10.1	264
	December	341.4	300.7	30	21.5	1020
R1234yf at 125 °C	Reference	1181.6	893.9	30	17	1039
	July	1181.6	893.9	30	10.1	590
	December	1181.6	893.9	30	21.5	2084

4.4.3 Partial load calculation

Many geothermal power plants around the world provide among electricity also heat, often in parallel operation, whereby the heat exchanger for the district heating network is parallel to the ORC process and either the heat extraction or the electricity production can be increased by changing the respective mass flows. If more heat is demanded and therefore the flow rate to the district heating is increased, the flow rate available for the ORC process will decrease. Due to the lower mass flow, the ORC process deviates from its design point and the efficiencies of the feed pump and the turbine change. The parameters a_0 to a_6, which are necessary for calculating the efficiency curves from equation 4.1 for the feed pump and the turbine, can be found in [Vetter, 2014, p.57]. They are listed in equation 4.5 and 4.6 as well as shown in graph 4.14 for a range from 20 % to 100 %.

$$\frac{\eta_{pump}}{\eta_{nom_{pump}}} = 0.159 + 0.008\left(\frac{\dot{m}}{\dot{m}_{nom}}\right) + 6.014\left(\frac{\dot{m}}{\dot{m}_{nom}}\right)^2 - 11.562\left(\frac{\dot{m}}{\dot{m}_{nom}}\right)^3 + 10.007\left(\frac{\dot{m}}{\dot{m}_{nom}}\right)^4 - 4.424\left(\frac{\dot{m}}{\dot{m}_{nom}}\right)^5 + 0.789\left(\frac{\dot{m}}{\dot{m}_{nom}}\right)^6 \tag{4.5}$$

$$\frac{\eta_{turb}}{\eta_{nom_{turb}}} = 0.007 + 3.182\left(\frac{\dot{m}}{\dot{m}_{nom}}\right) - 6.491\left(\frac{\dot{m}}{\dot{m}_{nom}}\right)^2 + 10.504\left(\frac{\dot{m}}{\dot{m}_{nom}}\right)^3 - 11.413\left(\frac{\dot{m}}{\dot{m}_{nom}}\right)^4 + 7.068\left(\frac{\dot{m}}{\dot{m}_{nom}}\right)^5 - 1.856\left(\frac{\dot{m}}{\dot{m}_{nom}}\right)^6 \tag{4.6}$$

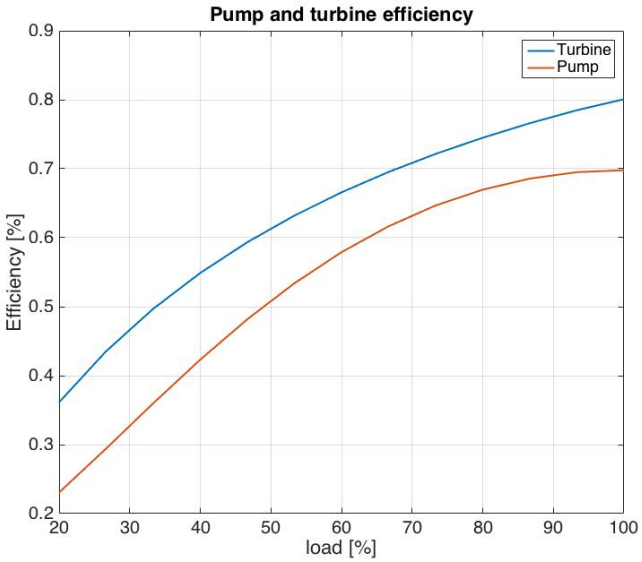

Figure 4.14: Feed pump and turbine efficiency curves

To illustrate the influence of the partial load efficiencies, figure 4.15 and 4.16 show the net power of R218, R32 and Propylen. For the first graph, the optimum parameters are set for different mass flows in order to achieve the highest possible net output for 95 °C and 125 °C, which means that for each mass flow the process operates in its design point and pump and turbine efficiency are set constant.
In contrast, the latter shows the resulting net power for different partial load situations. Here the module *Partial load* of GeSi and the parameters from equations 4.5 and 4.6 are used. Starting from a nominal mass flow of 30 kg/s (100 %) this value was reduced up to 14 kg/s (47 %).

It can be seen, that with the influence of the decreasing efficiencies of the turbine and the feed pump, the net power drops faster and that for 95 °C and 125 °C at about 50 % of the original mass flow almost no more power output is possible, whereas for a design point of 16 kg/s all fluids still produce a net power of more than 150 kW at 95 °C or more than 400 kW at 125 °C. Figure 4.15 also shows the linear course of all fluids regarding the volume flow. If therefore a different permeability is found after the first drilling, the presented results can be easily scaled. Furthermore the results are particularly interesting with regard to possible

stimulation options, since an improvement in permeability and thus an increase in mass flow will ultimately achieve a higher power yield.

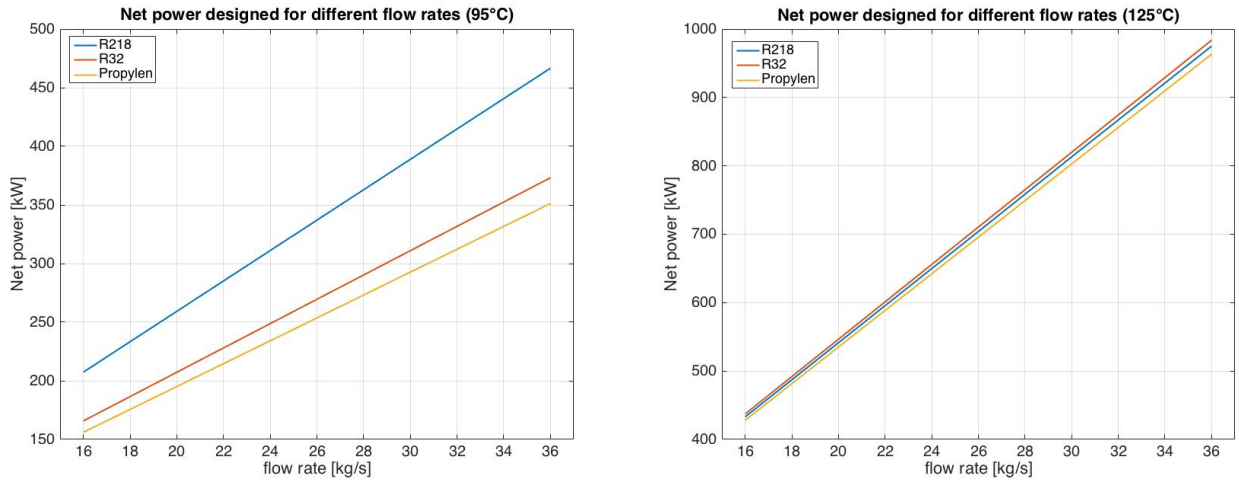

Figure 4.15: Net power output for R218, R32 and Propylen at 95°C (left) and 125°C (right) for design flow rates between 16 kg/s and 36 kg/s

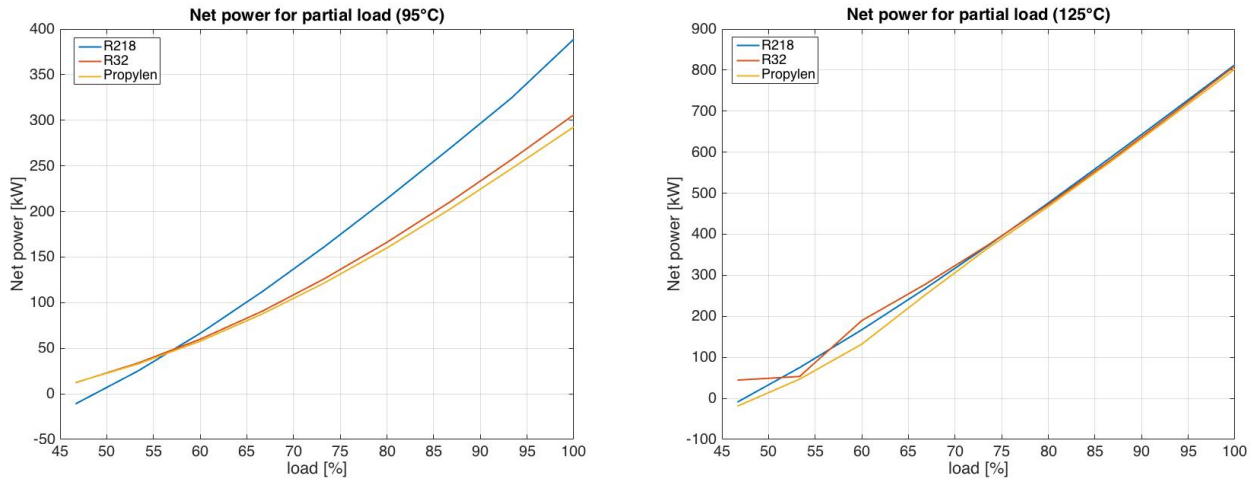

Figure 4.16: Net power output for R218, R32 and Propylen at 95°C (left) and 125°C (right) for partial loads between 47% and 100%

However, not only in the case of a competing use of the thermal water by an additional district heating use, but also over the regular operation lifetime, the available mass flow can vary. [Budisulistyo et al., 2016] proposes in his work to take the entire operation lifetime into account when it comes to the design of a geothermal power plant. This is necessary because some geothermal fields (for example Geyserardes US, Larderello-Valle Secolo IT, Wairakei

NZ) show a drop in both, reservoir temperature and mass flow over the years, which leads to strong deviations from the nominal output if the power plant was initially dimensioned too generously.

As the influence of the mass flow deviating from the design point of the power plant has already been discussed, figure 4.17 now shows the effects, if the reservoir temperature drops by 5 °C from its design condition, resulting in reduction of the net power output between 100 to 250 kW, depending on the working fluid and the original temperature.

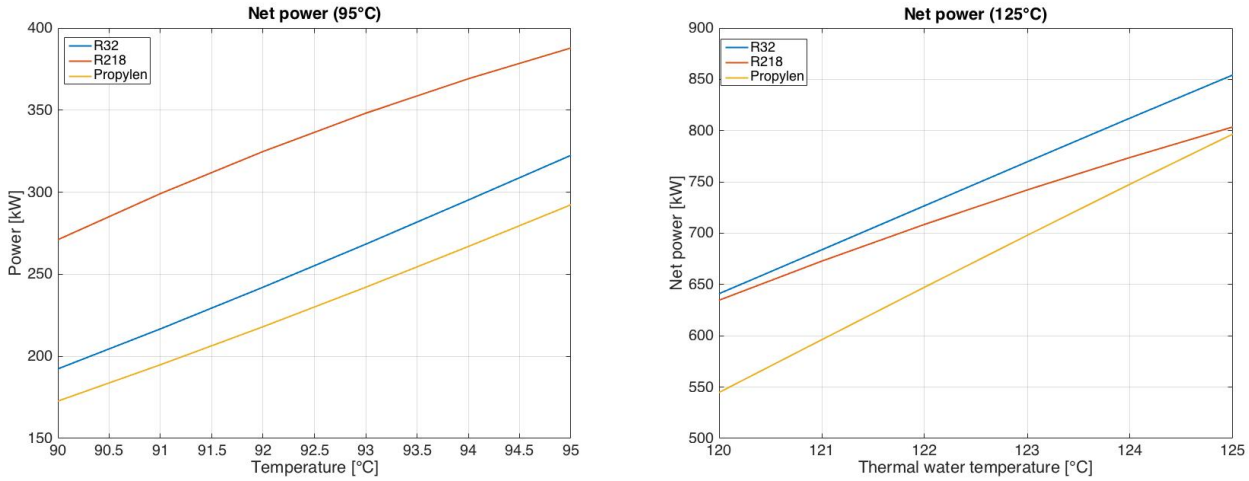

Figure 4.17: Resulting net power curves for R32, R218 and Propylen for a declining reservoir temperature by 5 °C

4.5 Performance model for turnkey solutions

While in the previous chapter the conditions and possible performances were presented on the basis of a power plant specially designed for the situation in Rosario de la Frontera, two examples of turnkey ORC systems are now to be discussed. Since these are generally designed for a wide range of applications, it is likely that their performance is lower compared to a custom-made power plant, but on the other hand they often offer economic advantages in terms of a lower purchase price and lower maintenance costs.
Regarding the boundary conditions of the two example systems, GeSi is used to calculate their performance under the assumed reservoir conditions, as described in the previous chapter.

4.5.1 Electratherm

Electratherm is an american company based in Reno, Nevada, with the focus of its products in the field of waste heat recovery, but the systems are also suitable for geothermal applications. The largest ORC system provided by the company is the *Power*$^+$ *Generator 6500* with up to 110 kW, as shown in figure 4.18 and the operating parameters are listed in table 4.10. The system can be operated with 50 Hz as well as with 60 Hz and is available as a stand-alone system or with integrated cooling system. In both cases the working fluid is R245fa, with a GWP of 1030 and is supplied without heat exchanger [Electratherm, 2018], [IPCC, 2007].

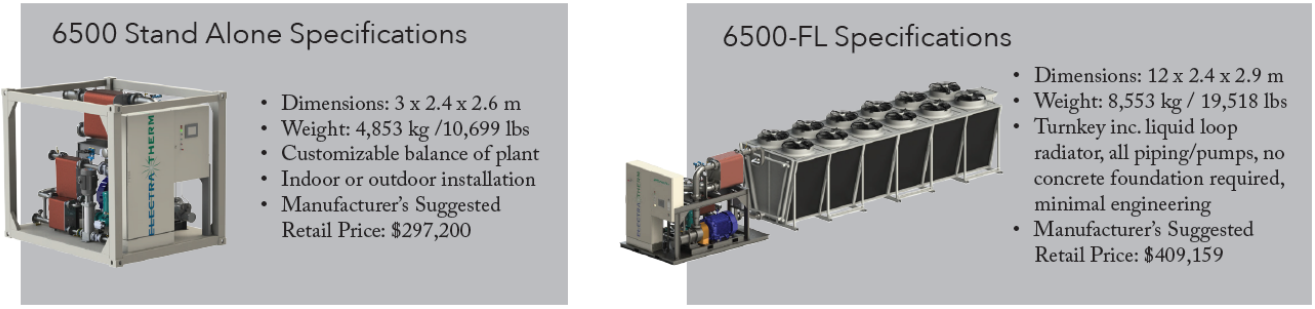

Figure 4.18: Electratherm Power$^+$ *Generator 6500 with up to 110 kW [Electratherm, 2018]*

Table 4.10: Electratherm Power$^+$ *Generator 6500 operating parameters [Electratherm, 2018]*

Thermal water input parameters		Water cooled condensation loop	
Inlet temperature [°C]	Flow rate [l/s]	Inlet temperature [°C]	Flow rate [l/s]
77 - 122	6.4 - 22.1	4 - 65	< 22.1

Nominal conditions

For the following calculations the same boundary conditions as listed in table 4.2 are assumed, but with two differences:

- The Electratherm system does not cool the working fluid directly with air but the working fluid discharges its heat to a water loop which is then cooled by air. Therefore the calculations are made for a water cooled system and with the information supplied by Electratherm, the water temperature can be expected to be around 12 °C higher than the ambient temperature, leading to a water temperature of 29 °C.

- Due to the maximum flow rate of the water loop of 22.1 l/s, the system has a limited capacity of discharging heat which results in higher condensation temperatures, depending on the thermal water inlet temperature and mass flow rate.

In figure 4.19 the T,s - diagrams for a thermal water flow rate of 22.1 l/s and temperatures of 95 °C and 122 °C are displayed. The limited flow rate of the cooling system is taken into account, leading to a minimum condensation temperature of 46.7 °C at 95 °C and 64.1 °C at 122 °C and net power outputs of 84.5 kW and 111.4 kW respectively, therefore only the highest possible thermal water temperature reach the nominal capacity of the generator.

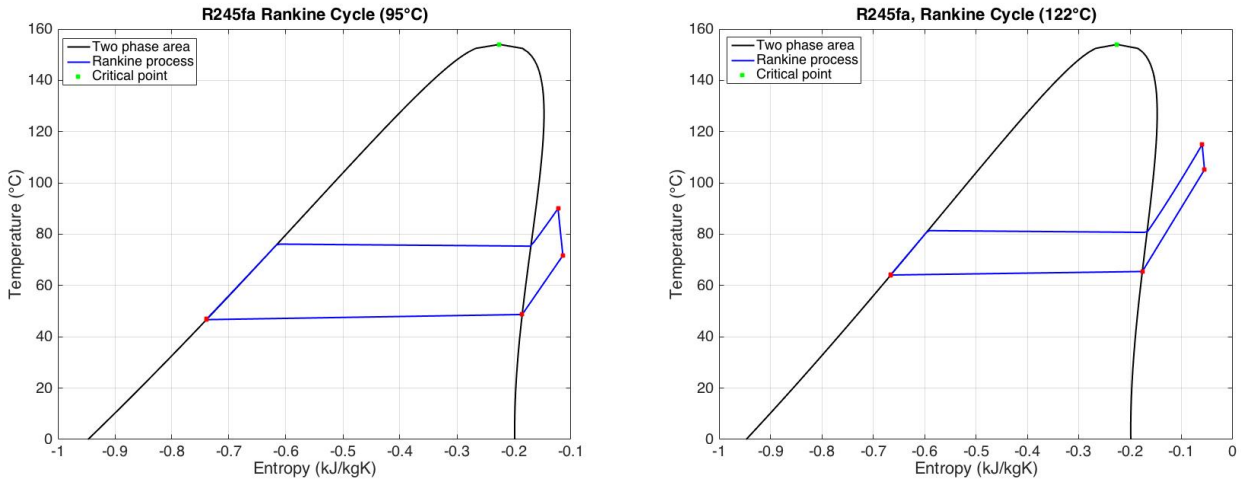

Figure 4.19: Electratherm T,s - diagram at 95 °C (left) and 122 °C (right) thermal water temperature

When the mass flow rate is reduced, the performance of the system decreases, but at the same time the condensation temperature can be reduced due to the lower heat development, which dampens the losses.
For a thermal water temperature of 95 °C but a reduced flow rate of 15 l/s the resulting net power is 68.5 kW. Thereby the condensation temperature can be reduced to 42 °C as less heat needs to be discharged from the system. If therefore two system are applied, a total net power of 137 kW can be expected.
At a thermal water temperature of 122 °C, the system produces 94.5 kW net power even for a flow rate of 7.5 l/s at a condensation temperature of 43.9 °C. Here four systems could be installed, generating a total of 378 kW by an optimal use of the thermal water mass flow of 30 l/s.

Seasonal cycle calculation

Analogous to previous seasonal cycle calculations, a comparison between July and December as the coldest and hottest month respectively, shows that the systems net power reach the output limit of 110 kW only in the cold season and for a thermal water temperature of 122 °C, assuming a flow rate as previously described of 15 l/s at 95 °C and 7.5 l/s at 122 °C (tab. 4.11).

Table 4.11: Electratherm power output and condenser temperature for the annual average as well as in July and December at 95° C and 122° C well head temperature

	Month	Gross power [kW]	Net power [kW]	Condenser temperature [°C]	Water temperature [°C]	Cooling water flow [l/s]
R245fa	Reference	71.1	68.5	42	29	22.1
at 95 °C	July	87.9	85.1	35.1	22.1	21.9
15 l/s	December	60	57.7	46.5	33.5	22
R245fa	Reference	98	94.5	43.9	29	22
at 122 °C	July	118.8	114.9	37	22.1	21.9
7.5 l/s	December	84.8	81.5	48.3	33.5	22.1

4.5.2 SUMEC

The second example for a turnkey solution is from the company SUMEC Geopower, a Switzerland based division of the SUMEC Group from China, which further is a member of the China National Machinery Industry Corporation (SINOMACH). A suitable system for the situation in Rosario de la Frontera could be the offered *PureCycle SGPTc272* (fig. 4.20) which comes in two variants.

- For a design temperature of 93 °C and a flow rate of 66.1 l/s a net power output of 191 kW is listed for a cooling water inlet temperature of 27 °C.
- The bigger system comes with a generator providing a nominal performance of 272 kW at 50 Hz, leading to a listed net power of 257 kW for 116 °C or 136 °C with flow rates of 31.1 l/s or 13.8 l/s respectively.

Similar to the *Power*$^+$ *Generator* of Electratherm, the SUMEC *PureCycle* operates with R245fa and is delivered without heat exchanger and and its design parameters are listed in table 4.12. But the two presented systems have a technical difference regarding the expander unit. Whereas the *Power*$^+$ system uses twin screw expanders, the *PureCycle* works with a radial inflow turbine [Electratherm, 2018], [SUMEC, 2018a].

Table 4.12: SUMEC PureCycle SGPTc272 design parameters [SUMEC, 2018a]

	Evaporator					
Thermal water temperature [°C]	136	136	116	116	93	93
Flow rate [l/s]	11.1	13.8	21.1	31.1	66.1	66.1
	Condenser					
Cooling water temperature [°C]	16	27	16	27	16	27
Flow rate [l/s]	57.7	61.9	57.7	61.9	70	76.9
Nominal power output [kW]	272					206

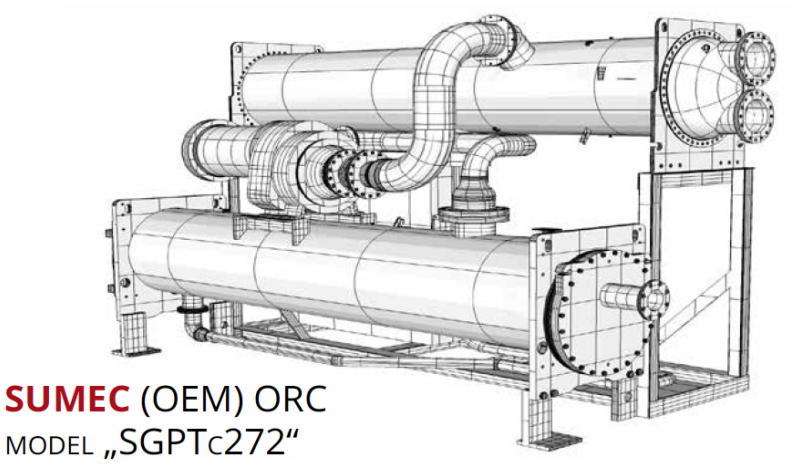

Figure 4.20: SUMEC PureCycle SGPTc272 with up to 272 kW at 50 Hz [SUMEC, 2018a]

Nominal conditions

For the performance calculations of the *PureCycle* system it is assumed that the maximum mass flow rate of the cooling water is 76.9 l/s, since the values in table 4.12 do, in general, not represent the maximum values but the design parameters. Furthermore a difference of 10 °C between the average ambient temperature and the cooling water temperature is assumed, leading to an inlet temperature of 27 °C.
Comparing figure 4.21 with figure 4.19 it can be seen, that despite the fact that both systems use the same refrigerant R245fa, due to the higher mass flow rate of the cooling loop of the *PureCycle* system, lower condensation temperatures can be reached, leading to higher performances.
For a thermal water temperature of 95 °C and a flow rate of 30 l/s, the net power is calculated to 168.4 kW at a condensation temperature of 35.6 °C and a required mass flow of the cooling water of 76.8 l/s, so that the nominal power of the system cannot be exhausted even at full mass flow.
At a well head temperature of 125 °C, the system surpass the nominal capacity by 127.2 kW, so it makes sense to use two systems, each of which is supplied with a mass flow of 15 l/s. Thereby each system can generate a net power of 245.5 kW at a condensation temperature of 37.2 °C and 76.7 l/s cooling water mass flow, resulting in a total net capacity of 491 kW.

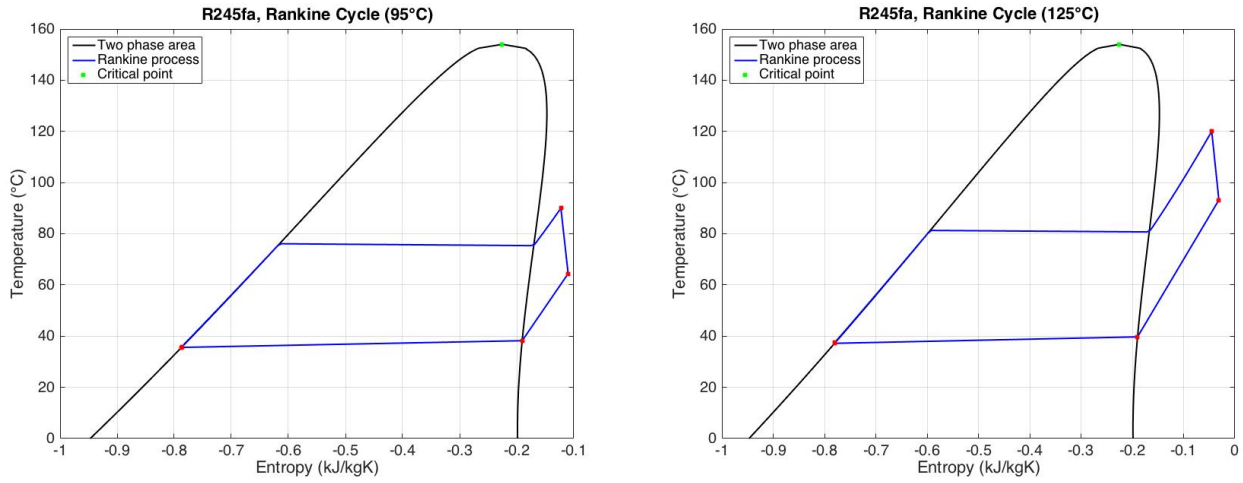

Figure 4.21: SUMEC T,s - diagram at 95 °C and 30 l/s (left) and 125 °C and 15 l/s (right)

Seasonal cycle calculation

Table 4.13 finally shows the results of the comparative calculation between different seasons and the annual average. It can be seen, that for both investigated thermal water temperatures,

only in the cold season the net capacity of 191 kW or 257 kW respectively can be reached, assuming a flow rate of 30 l/s and one system for 95 °C or 15 l/s and two systems for 125 °C thermal water temperature. Nevertheless, the power decrease at warmer conditions only deviate about 12 % to 14 % and thus offers a relatively homogeneous, average power output.

Table 4.13: SUMEC power output and condenser temperature for the annual average as well as in July and December at 95 °C and 122 °C well head temperature

	Month	Gross power [kW]	Net power [kW]	Condenser temperature [°C]	Water temperature [°C]	Cooling water flow [l/s]
R245fa	Reference	174	168.4	35.6	27	76.8
at 95 °C	July	210.6	204.5	28.4	20.1	76.6
30 l/s	December	150.4	145.1	40.3	31.5	75.8
R245fa	Reference	253.6	245.5	37.2	27	76.7
at 125 °C	July	302.1	293.4	30.1	20.1	76.6
15 l/s	December	223.5	215.8	41.8	31.5	76.7

4.6 Power output for district heating

There are generally two options to provide heat for a district heating network from a geothermal power plant:

- The heat exchanger for the district heating is parallel to the power plant, which means depending on the demand and need of electricity or heat the main thermal water stream can be lead to the power plant or the district heating network.
- The disctrict heating network is serial to the power plant, meaning that the outlet stream of the power plant is then directed to the heat exchanger of the district heating network.

The first option is suited for a well established district heating network, where the power supply is not the primarily aim, as the entire mass flow at well head temperature of the thermal water can be used for the district heating if needed. The latter is an option for a further use of the still warm thermal water but with the main objective of electricity production and shall be

presented in this section, as the main targed for a possible geothermal power plant in Rosario de la Frontera would be to generate electricity.
The heat transferred from the thermal water to the district heating network can be estimated from the heat flow, which is calculated as in equation 4.7:

$$\dot{Q} = c_p \dot{m} \Delta T \tag{4.7}$$

with the heat capacity c_p for water of 4.18 kJ/kgK, an assumed mass flow $\dot{m}$ of the thermal water of 30 l/s and the temperature difference ΔT between the inlet and outlet stream of the heat exchanger.

Table 4.14 shows the outlet temperatures of the thermal water after the heat exchanger of the power plant. It can be seen that, with the exception of R1234yf, the outlet temperatures are independent of the inlet temperatures. In addition, all values are determined for an ambient temperature of 10.1 °C, therefore in July, when the heating demand is potentially highest. For the annual mean temperature of 17 °C, all outlet temperatures are about 2 °C above the values given in the table.

Table 4.14: Thermal water outlet temperatures after the heat exchanger at 95 °C and 125 °C inlet temperature for an ambient air temperature of 10.1 °C

	Outlet temp. for 95 °C inlet	Outlet temp. for 125 °C inlet
R32	57.1	57.8
R1234yf	55	37.5
R125	40.1	39.9
R218	34.8	35

Most central heating or hot water systems in buildings are designed for temperatures of around 60 °C [Quaschning, 2015, sect. 3.2.2.2]. In order to guarantee this within the district heating network, the minimum outlet temperature of the thermal water after the power plant must be limited. This can be achieved by reducing the volume flow of the working fluid within the secondary circuit, which, however, reduces the achievable electrical power.
Table 4.15 lists the net power outputs for different working fluids if the thermal water outlet temperature is limited to 70 °C.

Table 4.15: Net power output and thermal performance at 95 °C and 125 °C inlet temperatures and limited outlet temperature of 70 °C

	Net power [kW_e] at 95 °C	Net power [kW_e] at 125 °C	Thermal power [kW_{th}]
R32	270.4	789.1	4389
R1234yf	253.3	697.2	
R125	234.7	672.7	
R218	232.6	623.5	

All fluids have a reduced performance compared to the previous calculations, but this loss can be kept small by adjusting the condensation temperature. This is possible because the reduced mass flow of the working fluid also results in less waste heat and thus the excess fan power can be used to reduce the condensation temperature.
Finally, the possible thermal power according to equation 4.6 results on the assumption that the thermal water is cooled down from 70 °C to 35 °C before it is injected back into the reservoir.

4.7 Risks and environmental impact

Binary geothermal power plants are free of CO_2 or flue gas emissions and thus do not contribute to negative effects on climate change or impair the air quality in their surroundings. Nevertheless, like any man-made facility, they represent an intervention in the natural environment, where the effects of which should be considered and, if necessary, minimised by appropriate measures. Thereby the potential effects can affect three groups:

- The environment, including the surface area as well as the underground resevoir,
- The people in the vicinity, or by resistance of the same,
- The geothermal project itself.

As mentioned in section 3.1, high material and space requirements are particularly necessary during the drilling phase. Additionally to foundation construction and soil sealing, roads must be built which are designed for the heavy loads (in Rosario de la Frontera $\approx$ 2.5 km, see sect. 4.2). On the other hand, the future power plant itself requires considerably less space than the drilling site previously laid out, so no further intervention is to be expected here.

Since some of the hot springs in Rosario de la Frontera are used for balneological purposes, and two of them are even used for drinking water (Palau mineral water, [Invernizzi et al., 2014]), great care must be taken to protect the groundwater. Furthermore, these sources are fed from the reservoir, which means that no chemicals can be used even far down in the reservoir (for example during stimulation) and also the long term behaviour should be observed, to exclude a negative interaction between the hot springs and the geothermal reservoir use.

Therefore the only option to enhance the reservoir flow rate (if desired) is either drilling more wells, or hydraulic shearing, which involves the risk of seismic activity (see sect. 2.2.3). These micro earthquakes are usually below 3 on the Richter scale [Stober, Bucher, 2014, sect. 9.3], [Xie et al., 2014] and thus have no safety-related relevance. However, this can quickly turn an original neutral or even positive attitude of the population towards the project into a negative one. Early information and good communication between all participants about the planned project, its progress, its benefits and possible negative effects are therefore central components to increase and maintain public acceptance.

5 Economic and financial analysis for different solutions

To bring a geothermal power plant online takes about five to seven years [Nathwani, Mines, 2015], [Serdjuk et al., 2013, sect. II], [Stefánsson, 2001], wereby the project is continously influenced by a variety of factors and a number of interdisciplinary experts need to work together in order to make a geothermal project a success.
Geologists, engineers and technicians, lawyers and financial experts need to interact and exchange information to find the best solution. In this chapter, therefore, a small insight into the expected costs, based on previous projects as well as the legal framework conditions in Argentina shall be given.

5.1 Regulations and support

With the signing of the climate agreement of the UN climate change conference from Paris (COP21) in 2015, Argentina has set itself the goal of reducing its emissions by 15 % till 2030. Law No. 27.191, adopted on September 23, 2015, is intended to make a contribution to this by setting the expansion target for renewable energies to 20 % by 2025 [MINEM, 2016b]. In this context, the term "renewable energies" excludes large hydroelectric power plants with an output of more than 50 MW, as they currently already contribute 29 % to the national electricity supply [CAMMESA, 2018b].
But climate protection is not the only motivation for an accelerated energy expansion. In recent years, more and more energy sources have had to be imported, including oil, gas and electricity. In 2015, net imports of energy sources were about four billion US dollars, which corresponds to approximately 7 % of all import expenditures [KPMG, 2016, p. 10].
Although installed capacity and electricity consumption have risen continuously since 2002, the first has reached its limits, especially due to a lack of investment within the last decade. At the same time, the Association of Electricity Producers (AGEERA) assumes that the expansion of the grid will also have to be driven forward massively in the coming years, and the Secretary for Energy Planning, estimates a total required investment within the energy sector of 50 billion US dollars till 2025 [MINEM, 2016c].

5.1.1 National and provincial regulations

National regulations

The main stakeholders in the argentinian electricity market are the Minsitry of Energy and Mines (MINEM), the National Electricity Regulatory Agency (ENRE) as well as the Electric Wholesale Market Management Company (CAMMESA) [MINEM, 2016b], whereas in the sector of electricity generation and transportation mainly private companies are in charge. For example, the operation of the 500 kV high-voltage lines is mainly subject to the Transener S.A. company, whereas the subsidiary Transba S.A. is responsible for around 6150 km of the medium (132/220 kV) voltage network [Behm et al., 2017, sect. 2.2.2.1].
The basic national regulation for electrical energy in Argentina is law No. 24.065 of 1992. It includes the legal framework of energy generation, transport and distribution. Furthermore it regulates the in- and export of energy as well as the tariffs and includes the establishment of a fund for electrical energy (Fondo Nacional de la Energía Eléctrica, FNEE).
Thereby the regulatory authority (ENRE) sets a quarterly upper limit for the electricity price. This so called "seasonal price" (Precio Monómico Estacional, PME) is passed on to consumers via the electricity distribution companies and accounts for approximately 27 % of the final consumer price. A further 26 % is incurred for taxes and about 47 % is added by transport and distribution [MINEM, 2017a].
The Precio Monómico (PM) further designates to the cost of electricity generation, but due to the Economic Emergency Act No. 25.561 of 2001/2002 and also the ongoing price and subsidy policy thereafter, end consumer prices are below the actual electricity generation costs, whereby the difference between these is paid by subsidies from the state budget [Behm et al., 2017], [MINEM, 2017a].

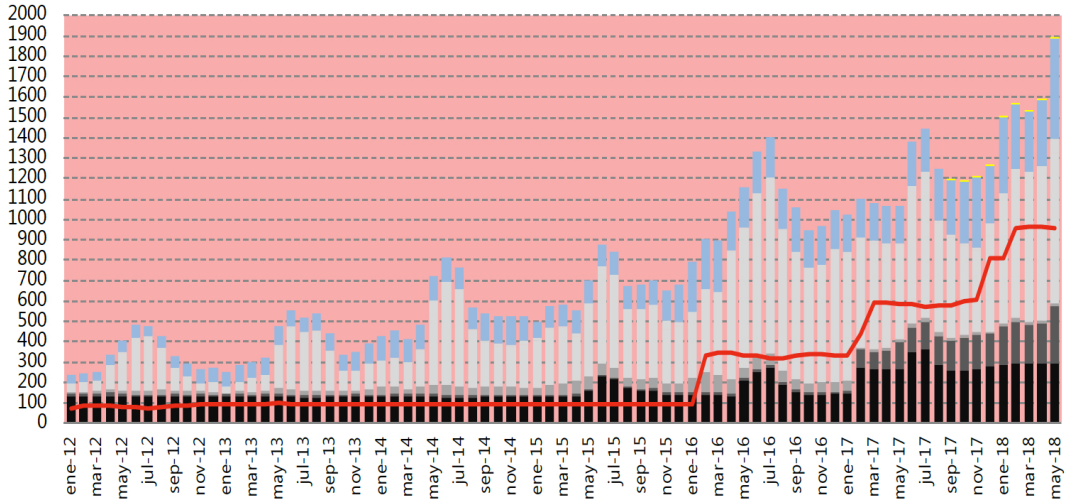

Figure 5.1: Electricity price development from 2012 to 2018 in [ARS/MWh] [CAMMESA, 2018b]

Figure 5.1 shows the development of the electricity price in Argentine Pesos (ARS) during the last years. The red line displays the seasonal price PME, the bars indicate the total average generation price, including costs for transport and distribution. The reason for the strong increase of the PME since 2016 is that the current government plans to gradually reduce support and thus return to a free market price.

In general there is free access to the Argentine energy grid for all kind of energy producer (public and private) but all grid costumer (producer and consumer) need to fullfil technical regulations. The contract between energy producer and CAMMESA regulates the conditions under which energy can be fed into the grid.
To facilitate this for small producers Juan Carlos Villalonga drafted a law which shall promote a decentralized energy generation (Fomento a la Generación Distribuida de Energía Renovable Integrada a la Red Eléctrica Pública), which was approved in September 2017 (No. 27.424). It regulates the generation and feed-in of small amounts of energy (< 30 kW) as well as an incentive for the producer, who will receive a financial support for the first five years.

Altough the law No. 25.019 (Régimen Nacional de Energía Eólica y Solar) of 1998, created a legal basis for renewable energies at an early stage and also tax benefits and feed-in tariffs were included, these kind of energies did not gain momentum. Even after the introduction of law No. 26.190 (Régimen de Fomento Nacional para el uso de Fuentes Renovables) of 2006, no improvement could be achieved.
A noticeable increase in renewable energies could only be observed with the new law No. 27.191 and the associated subsidy program. It includes the framework of establishing a renewable energy development fund (Fondo para el Desarollo de Energías Renovables, FODER) which shall enable an easier investment and also guarantees that the energy producer will get paid, if CAMMESA should be insolvent [Behm et al., 2017, sect. 3.5.1].
To further raise awareness of this kind of energies, the government under President Mauricio Macri declared 2017 to the year of the renewable energies with the decree No. 09/2017 and also the national industry agreed to invest 4 Mio. US$ in 59 projects, such as wind and solar parks, biomass and biogas plants.

Provincial regulations

The federal organization of Argentina means that the provinces can enact their own laws, which also applies to the use of renewable energies.
For Salta Province, one of these is law No. 7823 of 2014, which declares research, development, generation and usage of renewable energies as a provincial interest. In addition, it includes an investment program and has been adapted to the new national law No. 27.191.
Also in 2014, the legal framework for feeding in electrical energy from private individuals or small producers (for example households or companies) was established by law No. 7824,

which also sets the feed-in tariff for two years. Finally, the turnover of the national law No. 27.191 is regulated by the decree 1271/16 of 2016.

The distributor responsible for Salta is EDESA (Empresa Distribuidora de Electricidad de Salta S.A.) and has eight different electricity tariffs as of June 2018, depending on the purchase quantity, from small households to large consumers. For an average energy consumption of about 115 kWh per month (see section 4.2), tariff 1 results in a monthly fixed price of 46.62 ARS (1.94 US$) and an additional variable price of 2.3433 ARS/kWh (0.097 US$/kWh) [EDESA, 2018]. These prices are above nationwide average, as for example the tariffs from EDENOR (the distributor responsible for a part of Buenos Aires), are 28.43 ARS for the monthly fixed price and additionally 1.49 ARS per kWh [EDENOR, 2018].

5.1.2 Incentives

GENREN

The first project to push renewable energies on a nationwide scale was the program GENREN (Generación Eléctrica a partir de Fuentes Renovables), established in 2009. The subsidy was to have a renewable energy capacity of 1015 MW and the main objective besides saving greenhouse gas emissions was to reduce electricity and fuel imports. The contracts of the energy suppliers were concluded (in US$) with the state-owned energy utility ENARSA (Energía Argentina S.A.) and had a term of 15 years.
Due to the difficult situation and limited access to the international capital market during this period, by the end of 2014 only about 10 % of the projects had been completed or in turnover. The GENREN project is based on Law No. 26.190 of 2006, which became ineffective with the introduction of Law No. 27.191. As a result, the old supplier contracts with ENARSA as an intermediary have also been cancelled, but the possibility has been created to take them up again through new power purchase agreements (PPA) with CAMMESA. In addition, the planned but not yet implemented GENREN projects can be transferred to the RenovAr program [Behm et al., 2017, sect. 3.5.1].

PERMER

The project for renewable energies in rural markets (Proyecto de Energías Renovables en Mercados Rurales, PERMER) has the aim to provide electricity through renewable energies in the rural areas of Argentina. Due to the size of the country, a decentralised energy supply is an ideal solution to keep transmission costs and losses low and the project focus on energy supply for schools, hospitals and community centers. Hereby the purchase and installation of, for example, photovoltaic or small wind power plants, but also the associated mini grids and

possibilities of electricity storage are subsidized.
The funds for the project come from the ministry of energy and mines, which is supported by a loan from the World Bank and a grant from the global environment fund (GEF), as well as from the private sector, with an estimated total investment of 58.2 Mio. US$ [Behm et al., 2017, sect. 3.5.1].

RenovAr

The RenovAr program was launched in May 2016 and contains regulations and contractual enhancements as well as financial supports and guarantees. The latter in particular is intended to remove some investment barriers and offer investors greater security in order to prevent a failure like in the previous GENREN project.
As mentioned before, the central legal framework is the renewable energy law No. 27.191, with further regulatory decrees to regulate the energy law and/or to introduce some changes, as well as various resolutions (Res. MINEM 71/16, Res. MINEM 147/16, Res. MINEM 275/2017, ...) to open a call for tenders or set the framework for signed projects [MINEM, 2016b].
In order to promote the expansion of renewable energies while at the same moment giving time to the projects to establish and preventing destabilisation of the grid, the RenovAr program is implemented in phases. So far there have been three rounds (1, 1.5 and 2) in which 1142 MW, 1281.5 MW and 2043 MW were allocated respectively, forming a total capacity of 4466.5 MW in 147 projects (of which 4198 MW are wind and solar power) [MINEM, 2018].
The companies of these awarded projects enter into a 20 year PPA with CAMMESA. The contract includes, among other things, an agreed commissioning date on the part of the energy producer and on the part of CAMMESA to purchase the power at a guaranteed price, set in US$. In advance to the tender rounds, an upper price limit is set for the various renewable energies (for example 56.25 US$/MWh for wind power and 160 US$/MWh for biogas in Round 2) for each new bidding round. Besides that, the final awarded price for a project can be adjusted over the time by two factors, namely the annual price adjustment factor and the price incentive factor. The first occurs due to the fact, that legislation in Argentina does not allow to set contracts indexed with foreign currency, so that an annual adjustment on the such nominal bid price can be done. The latter is intended to provide an incentive to realize awarded projects in a timely manner and is established for each calender year from 2017 to 2038, starting at 1.2 and decreasing gradually to 0.8 [MINEM, 2017b].
Round 1 and 1.5 received together 170 bids with a total capacity of 8829 MW for the originally 1600 MW tendered. Since only some of the bids can be selected at a time, those with the lowest price per MWh will be selected first. In case two or more bids offer the same price, projects that also integrate the local industry are to be given preference. On the one hand,

this is intended to promote national value creation and, on the other hand, to create jobs [Behm et al., 2017, sect. 3.5.1], [MINEM, 2016b].
Besides the PPA, awarded projects also enter into the renewable energy trust fund (FODER), which is fed by MINEM, and shall provide liquidity in case CAMMESA is unable to pay in full for the electricity for 4 consecutive month or 6 non-consecutive month within any 12-month period. For all rounds an optional third level guarantee in cooperation with the international Bank for Reconstruction and Development (IBRD) was offered, where bidders could request covers for up to 500,000 US$ for up to 20 years [MINEM, 2016b], [MINEM, 2017b].
But the energy producer must also comply with its duty and there will be fixed penalties for delayed commissioning and also compensation payments if fossil fuels have to be used to substitute a reduced capacity.

5.2 Assessment of installation cost

Although each geothermal project can be considered as unique, the required steps to establish a power plant are very similar to all and can be divided into four main phases:

- Site exploration
- Well field development
- Surface installation
- Commissioning and operation

For the possible project in Rosario de la Frontera, the phases *site exploration* and *well field development* are regarded as independend costs within the following subchapter, in the meaning that these steps are independent of the surface installation, whether this would be a custom made or a turnkey solution.
The cost assessments for the phases *surface installation* and *comissioning* are described within the respective sections for a custom made as well as the turnkey solutions, since the investment costs can vary greatly, and also the profits are influenced by different power outputs.

5.2.1 Independent cost

Exploration

Even though the previous works of [Barcelona et al., 2012], [Chiodi et al., 2012, 2015], [Invernizzi et al., 2014] and [Maffucci et al. 2015, 2016], have already provided insights into

the geology and the geochemistry at Rosario de la Frontera, further actions have to be taken into account before the final decision can be made to install a geothermal power plant. Among these might be the application for an exploration permit for the land, underground investigations with active or passive seismic methods as well as the drilling of a first exploration well. The costs for exploration given in literature range from 400,000 US$ [IRENA, 2017] to up to 3 Mio. US$ [Reif, 2009] and are not only country specific, but also depend strongly on the used exploration methods. With regard to the price of different technologies, but also their accuracy or their remaining uncertainty, it is therefore necessary to weigh them against each other during the exploration phase.

Bore-wells

If the results of the exploration phase are positive and the decicion is made to install a geothermal power plant, the installation of the wells is the next big step and especially for smaller projects, this can make up to 55 % of the total investment costs [Serdjuk et al., 2013]. The expenditures for drilling usually contain service costs like drilling site preparation, the rig rent, personal and material costs which further includes the expenses for casting and cementation, as well as the required energy for operation.
The drilling costs thereby depend strongly on the geological situation and also of the required depth as figure 5.2 shows. Furthermore they depend on the desired power plant size, as for higher power output more wells are needed, but as [Stefánsson, 2001] points out, there will be a “learning curve”, so that with an increasing number of wells and therefore a better knowledge of the underground, the costs for each well will decline.

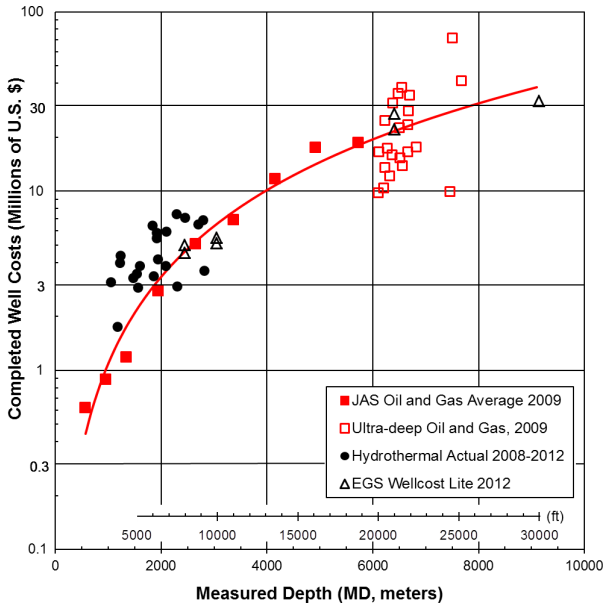

Figure 5.2: Drilling costs as a function of drilling depth [Lukawski, 2014]

According to figure 5.2 and the expected drilling depth of 2400 m to 2800 m from the information of chapter 4, drilling costs of 6 Mio. US$ per well can be expected. This number is in line with costs given in [Nathwani, Mines, 2015, p. 2], [Serdjuk et al., 2013, p. 33] and within the range of the figures given in [Stefánsson, 2001] and [Reif, 2009] where costs between 1 to 2.5 Mio. US$ per 1000 m are listed.

Other

Further expenditures which are more or less independent on the surface installation are costs for consulting (legal and economic) as well as project management, costs for risk or business liability insurances and also costs for mitigation measures which might need to be applied. Additionally electrical installations (including pumps for thermal water extraction and reinjection) and the grid connection are counted among these expenditures.
As mentioned in section 4.2 the drilling site can be moved out of the forest area by good planning. Nevertheless, mitigation measures might be necessary for example for goundwater protection. On the other hand, the costs for grid connection are likely to be low, as the 132 kV line near the city is a good precondition. In [Nathwani, Mines, 2015] the expenses for taxes and insurances are listed with 1.5 Mio. US$, whereas these costs are given with around 4 Mio. US$ in [Reif, 2009] and [Serdjuk et al., 2013]. Here further 300,000 to 500,000 US$ are expected for the grid connection and around 1 Mio. US$ for the pumps. Finally 450,000 US$ are listed in [Serdjuk et al., 2013] as costs for planning, consulting and project management for each year of construction after the exploration phase.

Table 5.1: Expected independent costs in million US dollar

	1st year	2nd year	3rd year	4th year	
Site Exploration	1				
Well field			12		
Risk insurance		2.75			
Pumps and grid connection				1.4	
Project management		0.3	0.3	0.3	
Sum	1	3.05	12.3	1.7	18.05

Table 5.1 summarize the exploration, drilling and other expected costs, presented in this subchapter. The costs for the well field are listed with 12 Mio. US$ as there will be at least two

wells required, one production and one injection well, and for the range of exploration costs as well as the expenditures for the project management, slighly lower values are assumend due to lower personal costs in Argentina than in the United States or Germany for example.

5.2.2 Tailored solution

After the drilling costs, the power plant itself is the biggest component of investment and depend upon the type (dry steam or flash plants are normally cheaper than binary power plants), the location and the plant size.
The expenditures for the binary power plant include all technical components like heat exchanger, turbine, condenser and generator, as well as pumps and piping. According to the Special Report on Renewable Energy Sources (SRREN) of the [IPCC, 2012], the average total investment costs (including binary power plant and all further expenditures like drilling) are 3,650 US$ per kW installed capacity, within a range from 2,130 to 5,200 US$ per kW, whereby the average share of the power plant regarding the total investment costs is about 32 % [IRENA, 2017], [Reif, 2009], [Serdjuk et al., 2013].
However, these figures represent the global average of 2005 and were subject to an upward trend in the past years due to increased material and engineering costs [IPCC, 2012]. And as the examples of Unterhaching and Bruchsal (both in Germany) show, they can also be highly erratic. In the first case, the total investment was 115 Mio. US$ with an installed capacity of 3.36 MW [Unterhaching, 2018], the latter has an electric power output of 0.55 MW at an investment volume of 19.6 Mio. US$ [Bruchsal, 2018], so that both come to costs of around 35,000 US$ per kW installed capacity.
Assuming the mean value between 3,650 US$ per kW given in [IPCC, 2012, sect. 4.7] and the costs of 35,000 US$ per kW from [Unterhaching, 2017] and [Bruchsal, 2018], around 6,180 US$ per kW can be expected for the power plant, taking a share of 32 % of the total investment costs.

5.2.3 Turnkey solutions

5.2.3.1 Electratherm

As from figure 4.18 it can be seen that the purchase price of the *Power*$^+$ *Generator 6500* by Electratherm, including the cooling loop is 409,159 US$. As already mentioned, this system comes without a heat exchanger between the thermal water loop and the ORC process and based on the prices listed in a report of the Fraunhofer-Institute [Althaus et al., 2012, p.52]

another 70,000 US$ can be assumed for a heat exchanger, summing up the price for one complete system to around 480.000 US$.

5.2.3.2 SUMEC

The investment cost of the SUMEC *PureCycle SGPTc272* system is listed with 820,000 US$, and similiar to the *Power*$^+$ *Generator* system from Electratherm it is delivered without a heat exchanger [SUMMEC, 2018b].
As the *PureCycle* system has a higher power performance than the *Power*$^+$, a slightly higher price for a larger dimensioned heat exchanger of 80,000 US$ is assumed, resulting in a total investment of 900,000 US$ per unit.

5.3 Investment calculation

After the two previous chapters presented the possibility and security of financing through the RenovAr funding program on the one hand and discussed the expected investment costs on the other, as well as an insight into the legal framework was given, the boundary conditions under which such a project would be economically viable are now to be demonstrated by means of an investment calculation.

5.3.1 Levelized Costs

Since the pure investment costs are unsuitable for an economic comparison between different power plants, levelized cost of energy (LCOE) are often used for this purpose. Hereby the total costs of a power plant are calculated over its lifetime and divided by the energy generated during this period. It is mathematically expressed as in equation 5.1.

$$LCOE = \frac{\sum_{i=1}^{n} \frac{I_i + M_i + F_i}{(1+r)^i}}{\sum_{i=1}^{n} \frac{E_i}{(1+r)^i}} \tag{5.1}$$

Where I_i are the investment costs in year i, M_i are the operation and maintenance (O&M) expenditures for the same year and F_i are the expenses for fuel, which in the case of a geothermal power plant are zero. E_i is the generated electricity and r is the discount rate, which ranges in [IPCC, 2012, sect. 4.7] between 3 to 10 % and n is the total lifetime of the power plant.
The LCOE is usually stated in cents/kWh and can be regarded as an average minimum price

for which the energy of a technology must be sold in order to break even over its lifetime [Varney et al., 2016].

Figure 5.3 displays the levelized cost as a funtion of the capacity factor (CF) of geothermal power plants. For the global average availability of 74.5 % in 2008, which means around 6,530 operating hours a year, the levelized cost are 7.2 US cents per kWh and it can be seen, that the capacity factor has a significant influence on the levelized cost and thus on the economic efficiency of the power plant. As in section 5.2.2, it should be noted that the LCOE given here, corresponds to the global average of 2005 and that these may vary considerably from country to country.

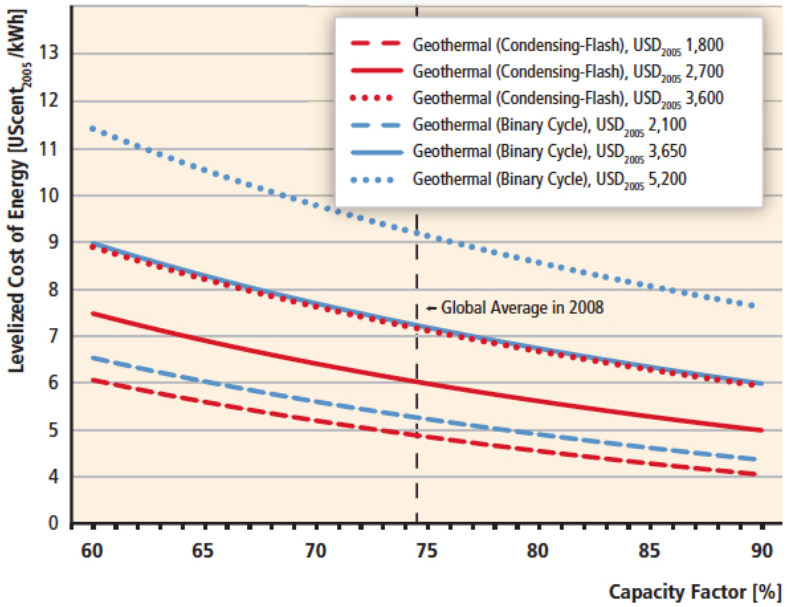

Figure 5.3: Levelized cost of energy depending on the capacity factor of the power plant [IPCC, 2012]

5.3.2 Net present value and internal rate of return

Net present value

The net present value method is a dynamic investment calculation. Hereby all payments over a certain period are summed up to the net present value (NPV), whereby future payments are discounted to the original time using a costing interest rate. This means that if a fictitious loan was repaid over this period at the selected discount rate, the net present value would be the profit that could be taken at the end of this period and should therefore always be positive for a worthwhile investment.

The NPV is calculated according to equation 5.2, where C_0 represents the net present value, R_i denote the net cash flow, which is the difference between incoming and outgoing payments, and r is the calculation discount rate [Schuster, von Collenberg, 2017, sect. 2.1.1].

$$C_0 = \sum_{i=1}^{n} \frac{R_i}{(1 + r)^i} \tag{5.2}$$

Internal rate of return

Since the results of the net present value method are strongly dependent on the chosen calculation discount rate and this might be difficult to determine, the internal rate of return (IRR) method can be applied. The IRR method is based on the NPV, but does not calculate the capital value but sets it to zero and determines which interest rate r_0 is necessary to achieve this. Thus the IRR can be calculated as in equation 5.3.

$$0 = \sum_{i=0}^{n} \frac{R_i}{(1 + r_0)^i} \tag{5.3}$$

It can be seen that in equation 5.3, the interest rate r_0 cannot easily be resolved and that a n-th degree polynomial must be resolved in order to determine it. Alternatively, an approximation solution can be obtained by a graphical method. The net present value is plotted as a function of the interest rate r_0, whose value can be read off at the zero point of the net present value curve [Schuster, von Collenberg, 2017, sect. 3.1].

5.3.3 Costs of the different variants

5.3.3.1 Tailored solution at 95 °C

The highest power output result from section 4.4.1.1, for a thermal water resource of 95 °C is around 389 kW and together with the expected investment costs of 6,180 US$/kW from section 5.2.2, the expenditures for the power plant will be 2,404,020 US$.

The last point missing for the investment calculation are the expenditures for operation and maintenance. Like the costs for the power plant, these depend strongly on the type and size of the plant, but also on the thermal water conditions, as frequent precipitation increases maintenance costs. There is also a relatively wide range for these costs in the literature. In [IPCC, 2012, sect. 4.7] approximately 25 US$/MWh are assumed, whereas in [Reif, 2009] costs of about 47 US$/MWh are listed. And [Varney et al., 2016] uses O&M costs in the order of 20 to 30 % of the LCOE as a basis of his calculations.

Due to the fact that the LCOE cannot be calculated without knowing the O&M costs, these can at least be estimated in Figure 5.3. From the average total investment costs of 19,325 US$/kW from section 5.2.2, it can be assumed that the LCOE will also be almost four times higher than the curve for 5,200 US$/kW as the upper limit given in [IPCC, 2012], leading to LCOE of 36 cents/kWh or around 90 US$/MWh for the O&M costs.
That finally leads to an O&M cost range of 25 to 90 US$/MWh and for further calculations a value of 50 US$/MWh will be assumed.

On the basis of all these considerations, the LCOE, the NVP and the IRR can now be calculated. The results for the net present value and the internal rate of return calculations are shown in figure 5.4 as graphs. It can be seen, that at a discount rate of 3 % an electricity sales price of 479 US$/MWh needs to be reached in order to get a positiv net present value and therefore to break even. Other way round, for a theoretical guaranteed sales price of 400 US$/MWh, the internal rate of return would be as low as 0.45 %.

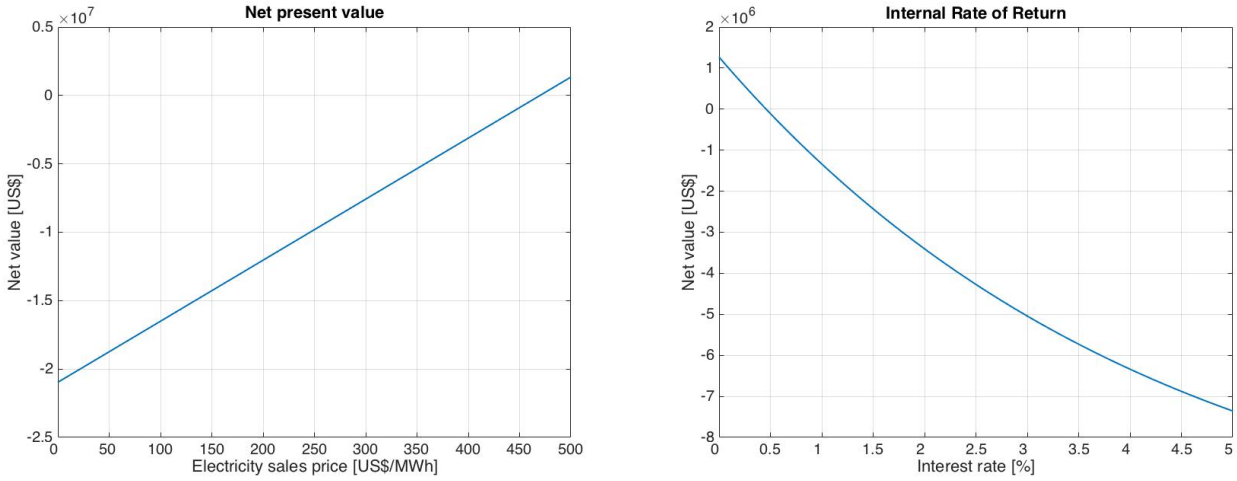

Figure 5.4: Net present value (left) and internal rate of return (right) curves for a power plant at 95 °C

5.3.3.2 Tailored solution at 125 °C

With the same financial assumptions as of the previous chapters, but with the power output results from section 4.4.1.4, indicating a maximum net power output of around 894 kW, it leads to an investment of 5,524,920 US$ for the power plant. Another 332,840 US$ have to be expected as operation and maintenance costs per year, assuming a capacity factor of 85 %. Other consumers that reduce the net output, such as the cooling system, are not explicitly

considered in the cost calculations, since on the one hand a possible subsidy is higher than the market electricity price and it is therefore more economical to sell all electricity and to purchase all own requirements again and on the other hand these own requirements are already included in the O&M expenditures. Furthermore a five year construction period and a lifetime of 25 years are assumed. But as a possible PPA contract under the RenovAr program would only last for 20 years, a sales price of 15 US cents/kWh is assumed after that period, based on nowadays average electricity costs of 7 US cents/kWh with an annual increase of 4 %.

The two graphs in figure 5.5 show the results of the NVP and the IRR for a thermal water temperature of 125 °C. From the IRR curve on the right it can be seen, that in order to be economic for a guaranteed sales price of 250 US$/MWh (160 US$/MWh was the highest so far in RenovAr rounds 1 and 1.5), the interest rate would be very low (1.8 %).

The NPV curve on the left indicates, that for a discount rate of 3 % an average sales price of 263 US$/MWh must be reached in order to break even.

It should be mentioned, that the LCOE and a possible guaranteed price from the PPA are not identical if the lifetime of the power plant is longer than the PPA contract, then the LCOE correspond to a mixed value between the guaranteed price from the PPA and the real market price after 20 years.

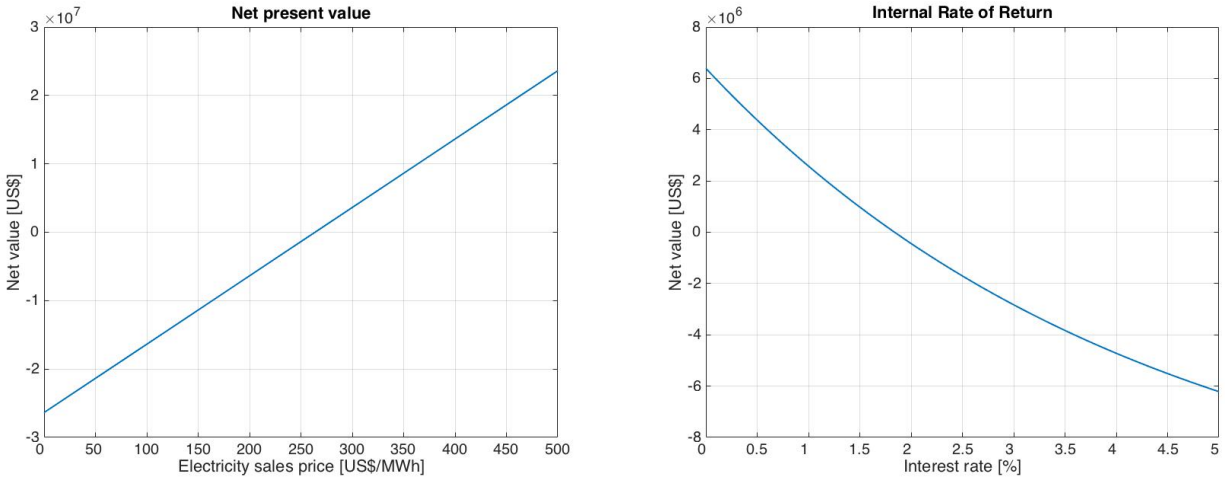

Figure 5.5: Net present value (left) and internal rate of return (right) curves for a power plant at 125° C

5.3.3.3 Tailored solution with increased flow rate

There are basically two ways to increase the volume flow of the thermal water. One method is to create several wells, whereby the sum of the volume flows finally leads to the desired result. The alternative to this is a successful stimulation of the reservoir rock, so that one bore is sufficient to achieve a high volume flow.
If further drilling is undertaken to increase productivity, the economic situation also changes. In [Stefánsson, 2001] the drilling costs in a known field are indicated between 10 to 15 % lower than in an unknown area. Assuming this, drilling costs per well will result at approximately 5.25 Mio US$, for a field with three or more wells drilled.
Assuming that all wells meet the previously considered mass flow rate of 30 l/s and with the results from section 4.4.3, that the power output is linearly related to the mass flow, it means that by doubling the number of production wells, also the power output can be doubled.
In the case of 125 °C thermal water temperature and four production wells and further two reinjection wells, it would lead to a maximum net power of 3576 kW. Under the same cost assumptions as in the previous sections but regarding on the one hand the higher investment costs for drilling but on the other hand higher revenues through increased electricity production, the LCOE drop to 18.3 US cents/kWh, and the resulting interest rate for a guaranteed price of 200 US$/MWh would be slightly over 3.5 % (fig. 5.6).
If the number of wells and thus the production capacity is further increased, the LCOE fall asymptotically to just under 17 US cents/kWh.

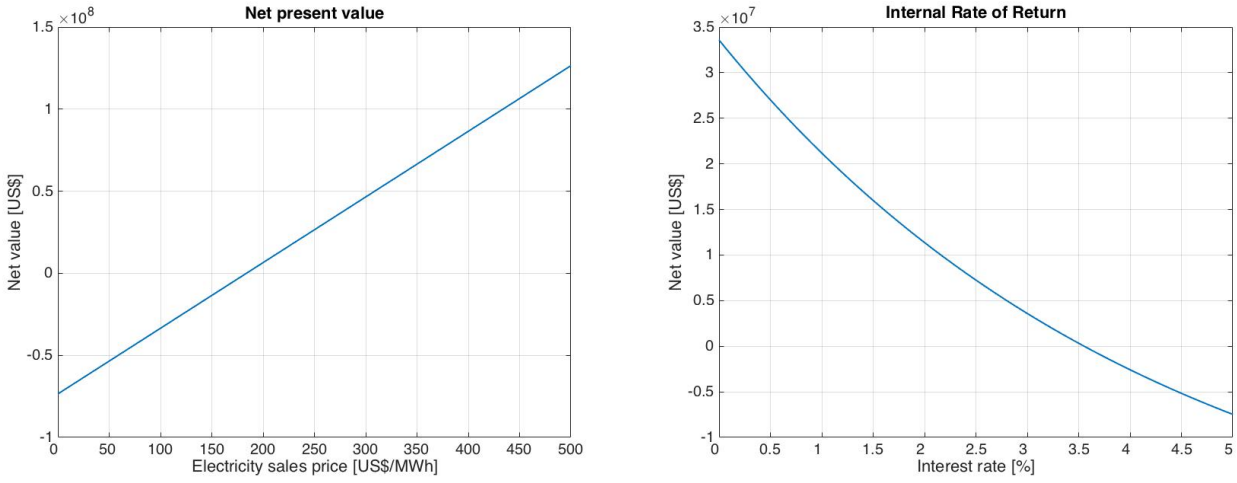

Figure 5.6: Net present value at a discount rate of 3 % (left) and internal rate of return for a guaranteed price of 200 US$/MWh (right) for a power plant fed by six wells at 125 °C

Alternatively, hydraulic shearing can be used to improve the flow rate and thus the power plant performance. Even if no chemicals or other expensive aids are used, the time required and the enormously high water consumption of 12,000 - 30,000 m^3 on average increase the costs. Therefore, a further 250,000 US$ is estimated for the subsequent calculation at the original drilling cost of 6 Mio. US$ per well. Assuming that stimulation can double the flow rate, taking into account the above-mentioned additional costs as well as the higher energy yield, this would lead to LCOE of 18.2 US cents/kWh at 125 °C well head temperature and 3 % discount rate.
It should be taken into account here that similarly low LCOE can be achieved as when drilling several holes, however already with a doubling of the power and not with a quadrupling thanks to the lower investment costs.

This circumstance can also be seen at a well head temperature of 95 °C, which makes LCOE of 29.3 US cents/kWh possible if stimulation is successful with doubling the flow rate. In contrast, with a fourfold increase in performance with the aid of six wells, the LCOE would be 29.5 US cents/kWh.

5.3.3.4 Turnkey solution: Electratherm

The company gives a range of the approximated costs for operation and maintenance with 1 to 1.5 US cents/kWh, so the average of 12.5 US$/MWh is assumed for the following calculations. Additionally the expenditures for project management are reduced by one third to 200.000 US$ per year as there is no need for project management in the field of the power plant and a plant in average has a share of one third of the total investment costs.

95 °C well head temperature

In the case of a thermal water temperature of 95 °C the average net power output for two units as from section 4.5.1 can be expected to 137 kW, leading to specific investment costs of 7007 US$/kW for the power plant.
The capacity factor is set from previous 85 % to 95 % as there are two units operating, providing some sort of back-up and it is unlikely that both systems will fail simutaneously. With the O&M costs as well as the project management costs as mentioned above and all further expenditures for exploration and drilling are assumed equal to previous sections, the levelized costs of energy sum up to 1.18 US$/kWh at a discount rate of 3 %.
Even for a guaranteed sales price of around 940 US$/MWh, the interal rate of return would still be below 1 %, making this option absolutely unfeasible.

122 °C well head temperature

For the highest supported thermal water temperature of the system of 122 °C, the net power output for four systems is 378 kW at investment costs for these in total of 1.92 Mio US$. This results into specific investment costs of about 5080 US$/kW.
Figure 5.7 shows the NPV curve at a discount rate of 3 % and the IRR curve for an electricity guaranteed price of 420 US$/MWh. The design lifetime of the *Power*$^+$ *Generator 6500* is given by Electratherm with 20 years. Due to the shorter lifetime and lower performance than the comparable tailored solution, the LCOE is as high as 45.8 US cents/kWh.

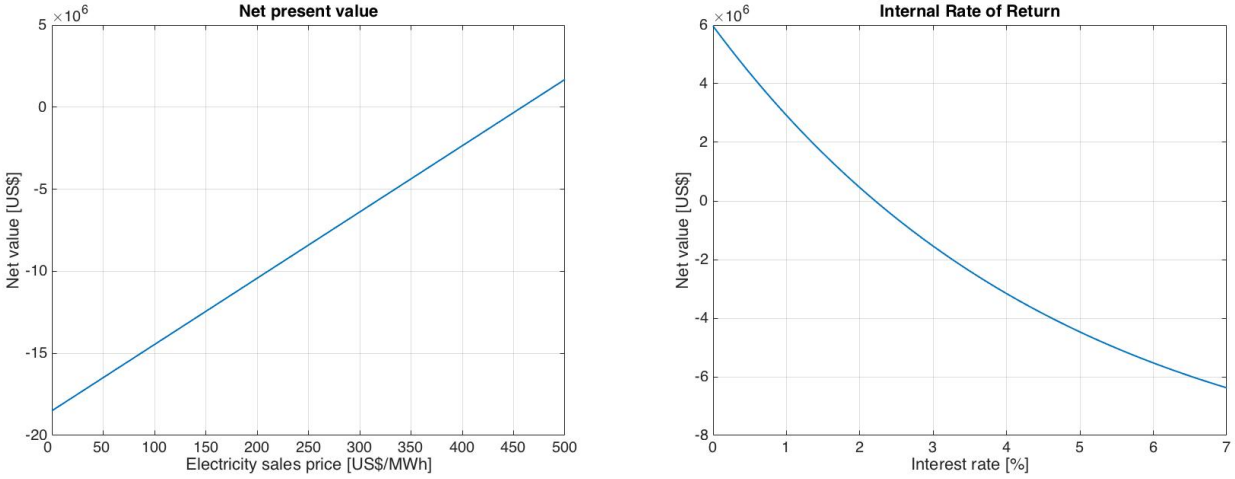

Figure 5.7: Electratherm net present value at a discount rate of 3 % (left) and internal rate of return for a sales price of 420 US$/MWh (right) at 122 °C

Under the condition that instead of one production and one injection well are drilled, but as mentioned before six wells in total are established at an average price of 5.25 Mio. US$, a total of 16 *Power*$^+$ *Generator* systems could be installed producing 1512 kW. Now the low O&M costs of 12.5 US$/MWh and the high CF of 95 % lead to LCOE of 26.5 US cents/kWh at a discount rate of 3 %, even though the power output is remarkably lower compared to a custom made solution.
Assuming in contrast a successful stimulation and thus a doubling of the flow rate, the LCOE would be 26.1 US cents/kWh.

5.3.3.5 Turnkey solution: SUMEC

Besides the investment costs of the *PureCycle* system, no further information about operation and maintenance costs could be found, so that the upper limit of the price range provided by Electratherm of 1.5 US cents/kWh are assumed. And similar to the *Power*$^+$ *Generator*, 200,000 US$ per year of installation work are calculated for project management expenditures.

95 °C well head temperature

At the lower end of the investigated well head temperatures, one *PureCycle* unit can provide in average 168 kW net power at a thermal water mass flow rate of 30 l/s. Taking the investment costs of 900,000 US$ into account, this leads to specific costs of 5357 US$/kW. Since there is only one unit in operation a capacity factor of 85 % is assumed and the design lifetime again is given with 20 years. Resulting in levelized costs of energy of 1.07 US$/kWh and therefore slightly lower than the beforementioned Electratherm option but still uneconomical.

125 °C well head temperature

For a thermal water temperature of 125 °C, two units can be applied as described in section 4.5.2, which leads to a redundant system and thus a higher capacity factor of 95 % is assumed. With a combined net power generation of 491 kW and investment expenditures of 1.8 Mio. US$ the specific costs result to 3665 US$/kW.
Thereby the LCOE are 35.6 US cents/kWh at a discount rate of 3 %, or if a PPA could guarantee a purchase price of 300 US$/MWh for the entire lifetime of the power unit, the internal rate of return would be only 1.4 %.

For the *PureCycle* system accounts the same as for the two previous solutions, namely a drop of the LCOE by higher output performance, which is either reached by more production wells or by stimulation. Again for four production wells and eight generators in total, the LCOE drop to 20.7 US cents/kWh at a discount rate of 3 % and an assumed CF of 95 %, whereas for the stimulation option the LCOE result in 20.4 US cents/kWh.

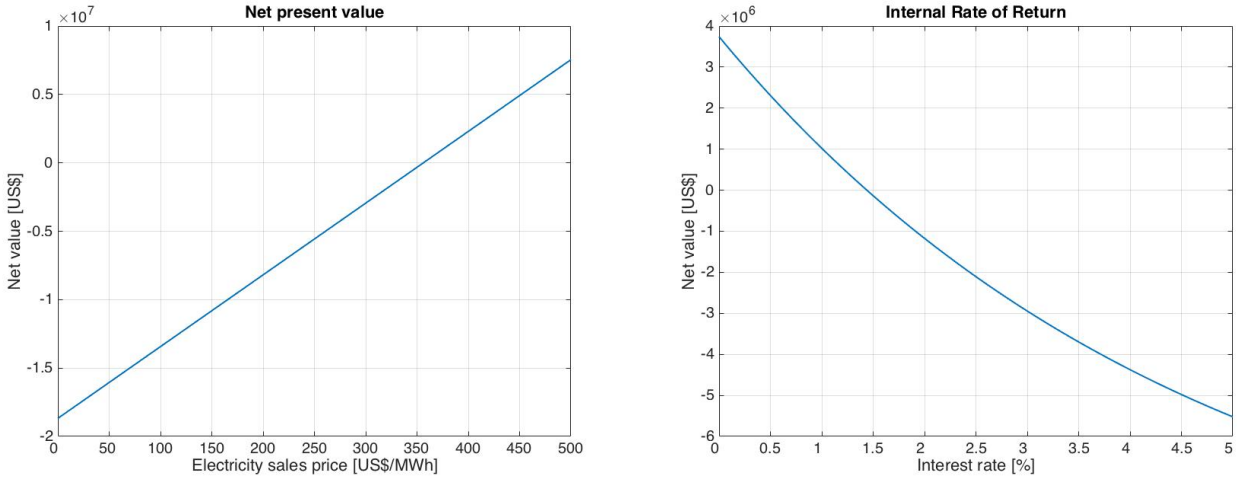

Figure 5.8: SUMEC net present value at a discount rate of 3 % (left) and internal rate of return for a sales price of 300 US$/MWh (right) at 125 °C

5.3.4 District heating

The primary objective of this tesis is a general feasibility study for a geothermal ORC power plant. Nevertheless, this section will briefly discuss the possibility of supplying district heating in addition to electricity production, with a rough estimate of the economic effects, as on the one hand the exact heat demand in Rosario de la Frontera is unknown, and on the other hand there is a lack of experience with district heating networks in Argentina.
An important part of the worldwide primary energy demand is in the form of heat. Since low temperatures below 80 °C are sufficient for many applications such as room heating or hot water generation, a supply from geothermal sources makes sense. This is also illustrated in table 2.1, where the share of geothermal heat generation exceeds its electricity generation by far.

Table 4.15 shows the net power outputs if the thermal water outlet temperature is set to 70 °C. On this assumption and assuming a four-month heating period per year, this results in an average power plant output of 337 kW at 95 °C thermal water temperature when R218 is used, and 828 kW at 125 °C for R1234yf as working fluid.
This would increase the LCOE at the low temperature by 3 cents to 50.9 US cents/kWh and at 125 °C from 26.3 to 26.5 US cents/kWh, if all other parameters remain unchanged.

In addition, there are additional costs for the district heating network, which are given in [Clausen, 2012, sect. 2.2] with approximately 150 US$/m pipe length. Furthermore, pumps and heat exchangers are needed on both the power plant side and at the customer's site, as

well as a back-up heating system for possible failures of the thermal water flow or as support if there is an extraordinary heating demand.
Even if a possible district heating network is not installed for private households but would only concentrate on larger companies and therefore would not have to be finely distributed, potential customers are still close to the city and about 12 km of route must be taken into account.

Therefore the total investment is estimated at 2.9 Mio.US$, of which 500,000 US$ for heat exchangers and pumps and 600,000 US$ for back-up heating are assumed, which is in line with numbers found in [EnergiNetDK, 2012, sect. 5.17] and [Soysal et al., sect. 3.1]. A big advantage of a district heating network with regard to its economy are the low O&M costs of 1 US$/MWh on average.Including distribution losses of 15 % and a discount rate of 3 %, this leads to LCOE of 17.3 US$/MWh, or slightly above 1.7 US cents/kWh.

If this price is low enough to ensure profitability depends on the one hand on whether enough customers can be won to use all the possible heat and on the other hand on the future development of the gas price, which is currently 4.37 ARS/m^3 for this region [GASNOR, 2018], which corresponds to about 1.68 US cents/kWh.

6 Evaluation of the work

The calculations carried out in the context of this work, both in the technical area with regard to the power plant performance as well as in the economic sense when determining the levelized costs of energy, are subject to a certain degree of uncertainty due to various factors. In this chapter, these factors and their effects on a possible project in Rosario de la Frontera will be examined in more detail.

6.1 Technical assumptions

Technical assumptions include the calculations presented in chapter 4. These are based, on the one hand, on the results of investigations by third parties and, on the other hand, on self made assumptions based on previous studies or already realized projects. Thereby the following points must be particularly taken into account, as they have a considerable influence on the power calculations:

- **Reservoir temperature:** As the calculations show, the temperature of the reservoir not only affects the maximum achievable power, but also the choice of the optimum working fluid. The geological investigations carried out so far determine the temperature by means of so called geothermometers. These are suitable for obtaining an estimated magnitude, but are also subject to uncertainty and in order to minimize this, the four different temperatures were examined. Besides the main reservoir, the temperature of the shallower aquifer cannot yet be determined and the way in which it mixes with the rising water of the deeper aquifer has not yet been sufficiently clarified.

- **Permeability:** Permeability and porosity data refer to direct measurements of the rock which outcrops in the southern reservoir area and to DFN modeling. The resulting transmissivity and the volume flow used for the calculations were assumed to be rather conservative, also taking into account a still acceptable pump capacity. Since there is a linear relationship between mass flow and power output, no separate calculations were made for this. However, reliable statements for the permeability and the temperature can only be made after the drilling work and pump tests have been completed.

- **Ambient temperature:** Since there is no river in Rosario de la Frontera that is suitable for cooling a power plant, air cooling must be used. It became apparent that fluctuating outside temperatures have a considerable influence either on the power plant output or on the cooling requirement. However, these must only be taken into account in the detailed planning of the power plant, as all other parameters are also known at this point in time. For an initial estimation of the power plant output, as it is the aim of this work, these extreme values have negligible effects.
- **Efficiency:** Turbine and feed pump efficiency have been determined according to the current state of the art. Furthermore, a constant efficiency for the feed pump and the turbine of the two considered systems was assumed for the calculations of the turnkey solutions. However, these values may deviate from a realized solution, with the corresponding effects leading to a changed net performance.
- **Simulation:** Since the simulation program GeSi is a model of real systems and includes simplifications to reduce complexity, the results are only an approximation. However, [Vetter, 2014, sect. 3.2.2] compared this program with an approved commercial program. Thereby the resulting deviations for all modules were less than 0.2 $\%$, which guarantees error free and accurate operation of GeSi.

6.2 Economic assumptions

Assumptions also had to be made for the economic calculations in chapter 5, and besides the obvious variation in performance data of the power plant the following points also need to be considered:

- **Investment costs:** With the exception of the two turnkey ORC modules presented, the investment costs are a major uncertainty factor. As described in chapter 5.2.2, these costs can deviate extremely from each other and depend on various factors. Therefore, only an attempt could be made to estimate the expected costs as accurately as possible on the basis of a large number of different data and studies. The costs of exploration and drilling are particularly important, as it is often only possible to determine whether the expected conditions of the reservoir are fulfilled once the drilling has been completed.
- **Operation and Maintenance:** In addition to operating costs, the capacity factor of the power plant plays an important role. It is influenced by planned maintenance work as well as malfunctions, whereby the latter cannot be predicted. The combination of dissolved substances in the thermal water and the materials used for piping is also important for smooth operation and a long service life. However, all these points can only be estimated at present time, which means that data from existing plants must also be used here.

7 Summary and prospects

7.1 Conclusion

According to the task a first feasibility study for a possible geothermal power plant in Rosario de la Frontera was carried out. To this end, the expected performance was initially determined under various boundary conditions. With the subsequent consideration of the expected investment and operating costs, the levelized costs of energy could thus be determined as an important basis for comparison with other technologies. In summary, the following findings can therefore be derived:

- Rosario de la Frontera offers good conditions in terms of size and infrastructure for the construction and operation of a geothermal power plant. On the one hand, there is a sufficiently high demand for electricity and heat in the vicinity of a possible power plant and, on the other hand, important parts of the infrastructure, such as power lines and main roads, are largely present.

- The reservoir is highly likely to have temperatures between 100 °C to 130 °C, but the permeability is widely varying, which does not allow a reliable statement on the expected volume flow. Here, hydraulic shearing to increase the volume flow and thus ultimately the economic efficiency could become an important factor.

- The geochemical investigation of the hot springs shows a generally low content of TDS, which is likely to result in low deposits during operation of the plant. However, in some cases high concentrations of chloride [Cl^-] and sulphate [SO_4^{2-}] occur, which can have a highly corrosive effect.

- The calculated net power for an annual mean temperature of 17 °C and a volume flow of 30 l/s, ranges from 293.3 kW using R134a at a well head temperature of 95 °C to 893.9 kW for R1234yf as working fluid and a water temperature of 125 °C. Furthermore, the net power output of the investigated working fluids and temperatures is linearly dependent on the volume flow, so no further consideration has been given to that point, except for the economic efficiency calculations.

- With the exception of 125 °C thermal water temperature, R218 offers the highest possible performance. However, this cannot be recommended due to its high GWP of 8830 and should therefore tend to use R32 or R1234yf in view of possible climate impacts. If heat extraction is also desired and the outlet temperature of the heat exchanger is thus to be limited, R218 will also show the greatest drop in performance (-23.4 % and -40.1 %).
- The two presented ORC modules from the companies Electratherm and SUMEC have low investment costs in absolute terms, but the costs per kW and the electricity generation costs are mostly higher compared to a costom made design due to the low achievable output. An important advantage, however, is the redundancy when using several systems, which can contribute to a higher capacity factor.
- Exploration, drilling and project management costs were estimated at approximately 18 Mio. US$. In addition, another 0.9 - 5.5 Mio US$ were calculated, depending on the selected power plant option. However, factors such as capacity factor and net output are more important for economic efficiency over the entire service life, as they have a particular influence on electricity generation costs.
- For a thermal water temperature of 95 °C and a volume flow of 30 l/s, all three options are uneconomical. Even if the mass flow doubles, the LCOE for the tailored solution, as the cheapest option, is 293 US$/MWh. Only at a well head temperature of 125 °C and an increased volume flow, either by stimulation or through several wells, the LCOE can be reduced to values between 182 to 261 US$/MWh. This is still high compared to other energy sources, but would be within a realistic range for funding through the RenovAr program.
- Assuming a sufficient demand, a district heating network in Rosario de la Frontera could be interesting. If the outlet temperature of the thermal water is limited to 70 °C, the power plant output will decrease, but up to 4.3 MW of heat can be provided. With 1.7 US cents/kWh, the calculated LCOE is only slightly above the current gas price but independent of future market developments and could therefore compensate the high electricity generation costs of the power plant.
- With Law No. 27.191 and the resulting RenovAr program, the government has created a good basis for promoting renewable energies. With regard to a possible project in Rosario de la Frontera, Round 3, which is planned for the second half of 2019 is particularly interesting. There it is planned to include geothermal energy projects for the first time and thus also establishes guaranteed prices for a power purchase agreement. This makes it clearer to estimate whether the electricity generation costs presented here will be within a competitive range.

7.2 Prospects

The results of this study show that a geothermal power plant in Rosario de la Frontera can be realized at least technically. Whether economical operation is also possible depends on the real geological conditions on the one hand and on the price of a guaranteed feed-in tariff on the other. For the latter, more advanced projects such as Copahue or Tuzgle can provide a basis and the knowledge gained there can be transferred to the decision makers of the RenovAr program as well as to other geothermal projects within Argentina.

In the specific case of Rosario de la Frontera, more detailed preliminary explorations, such as 2D or 3D seismic reflections in combination with gravimetric or further geoelectric methods, should be carried out in order to obtain more accurate data of the reservoir. These allow a more precise definition of a drilling site and also provide a more reliable basis for a preliminary design of the power plant. Furthermore, a study can be carried out to determine the exact heat demand in the surrounding area, as the construction of a district heating network can be attractive if there is sufficient demand.

As the energy transition continues, geothermal energy can become an important element, as it is independent of further resources and is able not only to produce electricity but also to provide heat. These advantages are offset by the high discovery risk and high investment costs. Therefore, an increased research activity in the field of geophysical investigations is necessary for a successful expansion of geothermal energy and incentives for financing must be created and adapted in order to push the sector.

Bibliography

[ADI-NQN, 2014] Agencia de Inversionen del Neuquén (ADI-NQN). (August 2014). *Programa de Desarrollo de Energías Renovables.* Seminario: Hacio un Futuro Energético Sustentable

[Althaus et al., 2012] Althaus, W., Grob, J., Stahl, E. (2012). *Kombiniertes Mini-ORC- und Emissionsminderungskonzept für Biomassefeuerungen bis 1 MW_{th}.* Berlin: Fraunhofer-Institut für Umwelt-, Sicherheits- und Energietechink (UMSICHT)

[Amatyakul et al., 2016] Amatyakul, P., Boonchaisuk, S., Rung-Arunwan, T., Vachiratienchai, C., Wood, S.H., Pirarai, K., Fuangswasdi, A., Siripunvaraporn, W. (2017). *Exploring the shallow geothermal fluid reservoir of Fang geothermal system, Thailand via 3-D magnetotelluric survey.* Bankok: Department of Physics

[Aneke et al., 2011] Aneke, M., Agnew, B., Underwood, C. (2011). *Performance analysis of the Chena binary geothermal power plant.* Newcastle: Northumbria University

[Armijo et al., 2015] Armijo, R., Lacassin, R., Courdurier-Curveur, A., Carrizo, D. (2015). *Coupled tectonic evolution of Andean orogeny and global climate.* Paris: Université Paris Diderot

[Barcelona et al., 2012] Barcelona, H., Favetto, A., Peri, V.G., Pomposiello, C., Ungarelli, C. (2011). *The potential of audimagnetotellurics in the study of geothermal fields: A case study from the northern segment of the La Candelaria Range, northwestern Argentina.* Buenos Aires: Universidad de Buenos Aires

[Bauer et al., 2014] Bauer, M., Freeden, W., Jacobi, H., Neu, T. (2014). *Handbuch Tiefe Geothermie.* Berlin Heidelberg: Springer Spektrum

[Behm et al., 2017] Behm, T., Camacho, D., Garff, D., Keim, C., Myrda, D., Ortiz, O. (2017). *Zielmarktanalyse Argentinien 2017.* Buenos Aires: Deutsch-Argentinische Industrie- und Handelskammer

[Bertani, 2015] Bertani, R. (2015). *Geothermal Power Generation in the World 2010-2014 Update Report.* Melbourne: Proceedings World Geothermal Congress

[Bona, Coviello, 2016] Bona, P., Coviello, M.F. (2016). *Valoración y gobernanza de los proyectos geotérmicos en América del Sur.* Santiago: Naciones Unidas (CEPAL)

[Bonyadi et al., 2017] Bonyadi, N., Johnson, E., Baker, D. (2017). *Techonoeconomic and exergy analysis of a solar geothermal hybrid electric power plant using a novel combined cycle.* Ankara: Middle East Technical University

[Bruchsal, 2018] Informationsportal Tiefe Geothermie (ITG). (2018). *Projekt Bruchsal.* `www.tiefegeothermie.de/projekte/bruchsal`

[Budisulistyo et al., 2016] Budisulistyo, D., Wong, C.S., Krumdieck, S. (2016). *Lifetime design strategy for binary geothermal plants considering degradation of geothermal resource productivity.* Christchurch: University of Canterbury

[CAMMESA, 2018a] Compañia Administradora del Mercado Mayorista Electricó S.A. (CAMMESA). (2018). *Esquema geografico de sistema interconectado.* `http://portalweb.cammesa.com/memnet1/Pages/descargas.aspx`

[CAMMESA, 2018b] Compañia Administradora del Mercado Mayorista Electricó S.A. (CAMMESA). (May 2018). *Informe Mensual, Principales Variables del Mes.* `http://portalweb.cammesa.com/MEMNet1/Informe%20Mensual/Informe%20Mensual.pdf`

[CanGEA, 2014] Canadian Geothermal Energy Association (CanGEA). (2014). *Direct Utilization of Geothermal Energy: Suitable Applications and Opportunities for Canada.* Alberta

[Cardemil et al., 2016] Cardemil, J.M., Cortés, F., Díaz, A., Escobar, R. (2016). *Thermodynamic evaluation of solar-geothermal hybrid power plants in northern Chile.* Santiago: Universidad Diego Portales

[Childers et al., 2017] Childer, I.M., Endres, M., Burns, C., Garcia, B.J. Liu, J., Wietsma, T.W., Bonneville, A., Moore, J., Leavy, I.I., Zhong, L., Schaef, H.T., Wang, H.F., Fernandez, C.A. (2017). *Novel highly dispersible, thermally stable core/shell proppants for geothermal applications.* Richland: Pacific Northwest National Laboratory

[Chiodi et al., 2012] Chidi, A.L., Báez, W., Viramonte, J.G., Tassi, F., Maffucci, R., di Paolo, L. (2012). *Características geoquímicas e isotópicas de los fluidos hidrotermales del sistema geotérmico de Rosario de la Frontera, Sierra de la Candelaria, Salta, Argentina.* Salta: Universidad Nacional de Salta

[Chiodi et al., 2015] Chiodi A.L., Tassi, F., Báez, W., Maffucci, R., Invernizzi, C., Giordano, G., Corrado, S., Bicocchi, G., Vaselli, O., Viramonte, J.G., Pierantoni, P.P. (2015). *New*

geochemical and isotopic insights to evaluate the geothermal resource of the hydrothermal system of Rosario de la Frontera (Salta, northern Argentina). Salta: Universidad Nacional de Salta

[Chiodini et al., 2014] Chiodini, G., Liccioli, C., Vaselli, O., Calabrese, S., Tassi, F., Caliro, S., Caselli, A., Agusto, M., D'Alessandro, W. (2014). *The Domuyo volcanic system: An enormous geothermal resource in Argentine Patagonia.* Napoli: Istituto Nazionale di Geofisica e Vulcanologia sezione di Napoli

[Clausen, 2012] Clausen, J. (2012). *Kosten und Marktpotenziale ländlicher Wärmenetze.* Hannover: Borderstep Institut für Innovation und Nachhaltigkeit gGmbH

[Clauser, 2009] Clasuer, C., Heinloth, K. (ed.) (2009). *Geothermal Energy.* Group VIII: Advanced Materials and Technologies, Vol. 3: Energy Technologies, Subvol. C: Renewable Energies. Berlin Heidelberg: Springer Verlag

[Cohen et al., 2017] Cohen, K.M., Finney, S.C., Gibbard, P.L., Fan, J.X. (2017). *The ICS International Chronostratigraphic Chart. Episodes 36: 199-204.* `http://www.stratigraphy.org/ICSchart/ChronostratChart2017-02.pdf`

[Crutzen, Stoermer, 2000] Crutzen, P.J., Stoermer, E.F. (2000). *The "Anthropocene".* International Geosphere-Biosphere Programme (IGBP): Global Change News Letter

[DiPippo, 2015] DiPippo, R. (2015). *Geothermal Power Plants: Principles, Applications, Case Studies and Environmental Impact.* Elsevier Science & Technology

[EDENOR, 2018] Empresa Distribuidora y Comercializadora Norte S.A. (EDENOR). (Febrero 2018). *Cuadro Tarifario.* `www.edenor.com.ar`

[EDESA, 2018] Empresa Distribuidora de Electricidad de Salta S.A. (EDESA). (Junio 2018). *Cuadro Tarifario.* `www.edesa.com.ar`

[Electratherm, 2018] Electratherm. (2018). *Power+ Generator 6500 Specification Sheet.* `www.electratherm.com/products/product-brochures/`

[ENARGAS, 2016] Ente Nacional Regulador del Gas (ENARGAS). (2016). *Informe Energas: Datos Operativos de Gas Natural, Gas Entregado por Tipo de Servicio y Provincia, y por Tipo de Usario.* `www.energas.gob.ar`

[EnergiNetDK, 2012] EnergiNet.dk, Danish Energy Agency (2012). *Technology Data for Energy Plants: Individual Heating Plants and Energy Transport.* Danish Energy Agency

[EU, 2014] The European Parliament and The Council of the European Union (2014). *Regulation No 517/2014 on fluorinated greenhouse gases and repealing Regulation (EC) No 842/2006.* Official Journal of the European Union

[Feldrappe et al., 2008] Feldrappe, H., Fritsche, H.G., Fritzer, T., Göthel, M., Huckriede, H., Kracht, M., Obst, K., Pasternak, M., Pester, S., Rappsilber, I., Schellschmidt, R., Schulz, R., Stober, I., Storz, R., Thomson, C., Walter, T., Wirth, W., Wolf, P., Wrede, V. (2008). *Nutzung der geothermischen Energie aus dem tiefen Untergrund (Tiefe Geothermie).* Bund-Länder-Ausschuss "Bodenforschung": Personenkreis Tiefe Geothermie

[Frisch et al., 2011] Frisch, W., Meschede, M., Blakey, R.C. (2011). *Plate Tectonics: Continental Drift and Mountain Building.* Berlin Heidelberg: Springer Verlag

[GASNOR, 2018] GASNOR, (April 2018). *Régimen Tarifario.* www.gasnor.com

[Ghasemi et al., 2014] Ghasemi, H., Sheu, E., Tizzanini, A., Paci, M., Mitsos, A. (2014). *Hybrid solar-geothermal power generation: Optimal retrofitting.* Cambridge: Massachusetts Institute of Technology

[Gubinelli, 2017] Gubinelli, G. (2017). *Energía geotérmica, la próxima energía renovable que tiene en la mira el Gobierno nacional.* Energía Estratégica. www.energiaestrategica.com/energia-geotermica-la-proxima-renovable-la-mira-gobierno-nacional/

[Heinonen et al., 2016] Heinonen, S., Karjalainen, J., Helle, A., Nisula, S. (2016). *Argentinian Energy Landscapes: Case Study of the Neo-Carbon Energy Project.* Helsinki: Finland Futures Research Centre

[Hildyard, 2010] Hildyard, R. (2010). *Earth Structure* https://www.leeds.ac.uk/ruskinrocks/Geology%20pictures%20and%20files/internal%20earth%20structure.jpg

[Hirose et al., 2017] Hirose, K., Morard, G., Sinmyo, R., Umemoto, K., Hernlund, J., Helffrich, G., Labrosse, S. (2017). *Crystallization of silicon dioxide and compositional evolution of the Earth's core.* Tokyo: Tokyo Institute of Technology

[Hölting, Coldewey, 2013] Hölting, B., Coldewey, W.G. (2013). *Hydrogeologie: Einführung in die Allgemeine und Angewandte Hydrogeologie.* Berlin Heidelberg: Springer Spektrum

[IEA, 2017] International Energy Agency (IEA). (2017). *Key World Energy Statistics.* www.iea.org

[IEA, 2018] International Energy Agency (IEA). (2018). *Geothermal 2017 Annual Report, Draft for release.* IEA Geothermal: Wairakei Research Centre

[INDEC, 2010] Instituto Nacional de Estadística y Censos de Argentina (INDEC). (2010). *Censo Nacional de Población, Hogares y Viviendas.* www.indec.gob.ar

[Invernizzi et al., 2014] Invernizzi, C., Piertantoni, P.P., Chiodi, A.L., Maffuci, R., Corrado, S., Báez, W. Tassi, F., Giordano, G., Viramonte, J. (2014). *Preliminary assessment of the geothermal potential of Rosario de la Frontera area (Salta, NW Argentina): Insight from hydro-geological, hydro-geochemical and structural investigations.* Camerino: Università degli Studi di Camerino

[IPCC, 2007] Intergovernmental Panel on Climate Change (IPCC). (2007). *Fourth Assessment Report.* Working Group I: The Physical Science Basis, Chapter 2.10.2 Direct Global Warmig Potentials

[IPCC, 2012] Intergovernmental Panel on Climate Change (IPCC). (2012). *Renewable Energy Sources and Climate Change Mitigation.* Special Report of the Intergovernmental Panel on Climate Change, Working Group III.

[IRENA, 2017] International Renewable Energy Agency (IRENA). (2017). *Geothermal Power: Technology Brief.* Abu Dhabi

[ITAG, 2013] ITAG Tiefbohr GmbH (2013). *ITAG Drilling & Workover.* https://itag-celle.de/wp-content/uploads/2018/01/gesamtinfo_RIG_01.pdf

[KPMG, 2016] KPMG sociedad civil argentina (2016). *Desarrollo de energías renovables: Contexto latinoamericano y el caso argentino.* www.kpmg.com.ar

[Litasov, Shatskiy, 2015] Litasov, K.D., Shatskiy, A.F. (2015). *Composition of the Earth's core: A review.* Novosibirsk: Sobolev Institute of Geology and Mineralogy

[Lukawski, 2014] Lukawski, M. (2014). *Using Supercritical Fluids for Thermal Energy Storage, Drilling Cost Analysis, and Design of a Hybrid Geothermal-Biomass Energy System.* Cornell University. www.jeff-tester.cbe.cornell.edu/research/maciej_lukawski_research.html

[Lund, Boyd, 2015] Lund, J.W., Boyd, T.L. (2015). *Direct utilization of geothermal energy 2015 worldwide review.* Klamath Falls: Oregon Institute of Technology

[Maffucci et al., 2015] Maffucci, R., Bigi, S., Corrado, S., Chiodi A.L., Di Paolo, L., Giordano, G., Invernizzi, C. (2015). *Quality assessment of reservoirs by means of outcrop data and "discrete fracture network" models: The case history of Rosario de la Frontera (NW Argentina) geothermal system.* Roma: Università Roma Tre

[Maffucci et al. 2016] Maffucci, R., Corrado, S., Aldega, L., Bigi, S., Chiodi, A.L., Di Paolo, L., Giordano, G., Invernizzi, C. (2016). *Cap rock efficiency of geothermal systems in fold-and-thrust belts: Evidence from paleo-thermal and structural analyses in Rosario de La Frontera geothermal area (NW Argentina).* Roma: Università Roma Tre

[MINEM, 2016a] Ministerio de Energía y Minería (MINEM). (2016). *Informe Estadístico del Sector Eléctrico.* www.energia.gob.ar

[MINEM, 2016b] Ministerio de Energía y Minería (MINEM). (2016). *Energías Renovables en Argentina: Informe a Diciembre de 2016.* Subsecretaría de Energías Renovables

[MINEM, 2016c] Ministerio de Energía y Minería (MINEM). (2016). *Argentina-Energy for growth.* La Jolla: Secretaría Planeamiento Energético. For The Institute of the Americans

[MINEM, 2017a] Ministerio de Energía y Minería (MINEM). (May 2017). *Normalización del Precio Mayorista de la Electricidad en el país y Revisión Tarifaria Integral de Transporte y Distribución AMBA.*

[MINEM, 2017b] Ministerio de Energía y Minería (MINEM). (August 2017). *Programa RenovAr Ronda 2: Convocatoria Abierta Nacional e Internacional en el Marco de la Resolución MEyM N° 275/2017.*

[MINEM, 2018] Ministerio de Energía y Minería (MINEM). (2018). *Adjudicaciones del Programa RenovAr.* https://public.tableau.com/profile/datosenergia#!/vizhome/AdjudicacionesRenovARMINEMArgentina/AdjudicacionesRenovArArgentina

[Mlcak, Mirolli, 2002] Mlcak, H., Mirolli, M. (2002). *Notes from the North: a Report on the Debut Year of the 2 MW Kalina Cycle Geothermal Power Plant in Húsavík, Iceland.* Húsavík: Power Engineers Inc.

[Nakao et al., 2015] Nakao, Y., Kaieda, H., Mugikura, Y., Iwatsubo, T., Ichi, M., Watanabe, Y. (2015). *Development of Hybrid Geothermal Power Plants Combined with other Thermal Energy Sources.* Melbourne: Proceedings World Geothermal Congress

[Nathwani, Mines, 2015] Nathwano, J., Mines, G. (2015). *Cost Contributors to Geothermal Power Generation.* Melbourne: Proceedings World Geothermal Congress

[Neukirchen, 2011] Neukirchen, F. (2011). *Bewergte Bergwelt: Gebirge und wie sie entstehen.* Heidelberg: Springer Akademischer Verlag

[NREL, 2011] National Renewable Energy Laboratory (NREL). (2011). *Geopressured Geothermal Resource and Recoverable Energy Estimate for the Wilcox and Frio Formations, Texas.* San Diego: Geothermal Resource Council Annual Meeting

[Nusiaputra, 2017] Nusiaputra, Y.Y. (2017). *Coupled Hydraulic, Thermal and Chemical Simulations for Geothermal Installations.* Karlsruhe: Karlsruher Institut für Technologie (KIT)

[OTB,] Open text book (OTB). *A model of convection within Earth's mantle.* https://opentextbc.ca/geology/wp-content/uploads/sites/110/2015/08/convection-within-the-Earth%E2%80%99s-mantle.png

[Pesce, 2015] Pesce, A.H. (2015). *Argentina Country Update.* Melbourne: Proceedings World Geothermal Congress

[Quaschning, 2015] Quaschning, V. (2015). *Regenerative Energiesysteme: Technologie - Berechnung - Simulation.* 9. Auflage, München: Hanser Verlag

[Raksaskulwong, 2015] Raksaskulwong, M. (2015). *Update on Geothermal Utilizations in Thailand.* Melbourne: Proceedings World Geothermal Congress

[Razzano, Cei, 2015] Razzano, F., Cei, M. (2015). *Geothermal Power Generation in Italy 2010-2014 Update Report.* Melbourne: Proceedings World Geothermal Congress

[REFPROP,] Reference Fluid Thermodynamic and Transport Properties Database (REFPROP). As implemented in the GeSi Program

[Reich, 2015] Reich, M. (2015). *Auf der Jagd im Untergrund: Mit Hightech auf der Suche nach Öl, Gas und Erdwärme.* 2. Auflage, Berlin Heidelberg: Springer Spektrum

[Reif, 2009] Reif, T. (2009). *Wirtschaftlichkeit von Geothermieprojekten.* München: Bundesverband Geothermie e.V. Workshop: "Finanzierung von Geothermie-Projekten"

[Salta, 2018] Portal Informativo de Salta (2018). http://www.portaldesalta.gov.ar/rosdelafront.htm

[Sanner, 2005] Sanner, B. (2005). *Synergie nutzen - Geothermie in Kombination mit anderen Erneuerbaren (und sonstigen) Energien.* http://ubeg.de/Lit/2005%20Sanner%20synergien%20dgk%202005.pdf

[Schuster, von Collenberg, 2017] Schuster, T., von Collenberg, L.R. (2017). *Investitionsrechnung: Kapitalwert, Zinsfuß, Annuität, Amortisation.* Berlin: Springer Gabler

[Seggiaro et al., 1995] Seggiaro, R., Aguilera, N., Gallardo, E., Ferreti, J. (1995). *Structure and geothermal potential of the Rosario de la Frontera thermal area,* Florence: World Geothermal Congress

[Serdjuk et al., 2013] Serdjuk, M., Dumas, P., Angelino, L., Tryggvadóttir, L. (2013). *Geothermal Investment Guide.* Geoelec www.geoelec.eu

[SMN,] Servicio Meterológico Nacional (SMN) *Estadísticas Climáticas Normales.* https://www.smn.gob.ar/descarga-de-datos

[Song et al., 2016] Song, J., Gu, C.W., Ren, X. (2016). *Influence of the radial-inflow turbine efficiency prediction on the design and analysis of the Organic Rankine Cycle (ORC) system.* Beijing: Tsinghua University

[Soysal et al.,] Soysal, E.R., Sneum, D.M., Skytte, K., Olsen, O.J., Sandberg, E. *Electric Boilers in District Heating Systems: A Comparative Study of the Scandinavian market conditions.* DTU Management Engineering and NMBU Ecology and Natural Resource Management

[Stefánsson, 2001] Stefánsson, V. (2001). *Investment cost for geothermal power plants.* Reykjavík: National Energy Authority

[Stober, Bucher, 2014] Stober, I., Bucher, K. (20014). *Geothermie.* 2. Auflage, Berlin Heidelberg: Springer Spektrum

[Strauss, 2016] Strauss, K. (2016). *Kraftwerkstechnik: zur Nutzung fossiler, nuklearer und regenerativer Energiequellen.* 7. Auflage, Berlin Heidelberg: Springer Vieweg

[SUMEC, 2018a] SUMEC GeoPower (2018). *Geothermal ORC Turbines, Residual Heat.* http://www.sumecgeopower.com/resources/f/4/18/General%20SGP%206.6.pdf

[SUMEC, 2018b] SUMEC GeoPower (2018). *Electricity from heat: Revolution in heat utilization, New ORC & VCRC technology.* http://www.sumecgeopower.com/resources/f/4/18/SGP%20tech%20mix.2.5_EN.pdf

[Sutra et al., 2017] Sutra, E., Spada, M., Burgherr, P. (2017). *Chemicals usage in stimulation processes for shale gas and deep geothermal systems: A comprehensive review and comparison.* Villingen: Paul Scherrer Institut

[Unterhaching, 2018] Geothermie Unterhaching GmbH & Co KG. (Juli 2018). *Daten & Fakten: Geothermie Unterhaching.* www.geothermie-unterhaching.de/cms/geothermie/web.nsf/id/pa_daten_Fakten.html

[Varney et al., 2016] Varney, J., Zarrouk, S.J., Bean, N., Bendall, B. (2016). *Performance measures in geothermal power developments.* Adelaide: University of Adelaide

[Vetter, 2011] Vetter, C. (2011). *Parameterstudie zur Simulation von Niedertemperatur-Kreisprozessen.* Karlsruhe: Karlsruher Institut für Technologie (KIT) Scientific Publishing

[Vetter, 2014] Vetter, C. (2014). *Thermodynamische Auslegung und transiente Simulation eines überkritischen Organic Rankine Cycles für einen leistungsoptimierten Betrieb.* Karlsruhe: Karlsruher Institut für Technologie (KIT)

[Wasabi, 2011] Wasabi Energy Limited (2011). *Wasabi Energy Limited subsidiary acquires Húsavík Kalina Cycle Geothermal Power Plant in Iceland.* Melbourne: ASX Announcement

[Xie et al., 2014] Xie, L., Min, K.B., Song, Y. (2014). *Observations of hydraulic stimulations in seven enhanced geothermal system projects.* Seoul: Seoul National University

[Younger, 2015] Younger, P.L. (2015). *Geothermal Energy: Delivering on the Global Potential.* Basel: MDPI AG

[Zahoransky, 2015] Zahoransky, R. (2015). *Energietechnik: Systeme zur Energieumwandlung. Kompaktwissen für Studium und Beruf.* 7. Auflage, Wiesbaden: Springer Vieweg

[Zeleny et al., 2017] Zeleny, Z., Vodicka, V., Novotny, V., Mascuch, J. (2017). *Gear pump for low power output ORC - an efficiency analysis.* Milano: IV International Seminar on ORC Power Systems

Appendix

Conversions

1 mD	≡	$9.86{\cdot}10^{-16}$ m^2	1 m^2	≡	$1.013{\cdot}10^{15}$ mD
1 kcal	≡	0.0011 kWh	1 kWh	≡	859.8 kcal
1 kJ	≡	0.00027 kWh	1 kWh	≡	3600 kJ
1 US$^{(I)}$	≡	24 ARS	1 ARS	≡	0.041 US$
1 m^3 gas$^{(II)}$	≡	10.8 kWh	1 kWh	≡	0.092 m^3

$^{(I)}$ as in may 2018
$^{(II)}$ for a heating value of 9300 kcal [ENARGAS, 2016]

Metric prefixes

Symbol	Name	Value	
E	Exa	10^{18}	1,000,000,000,000,000,000
P	Peta	10^{15}	1,000,000,000,000,000
T	Tera	10^{12}	1,000,000,000,000
G	Giga	10^{9}	1,000,000,000
M	Mega	10^{6}	1,000,000
k	Kilo	10^{3}	1,000
-	-	10^{0}	1
m	milli	10^{-3}	0.001
μ	micro	10^{-6}	0.000,001

Climate table Salta

	Jan	Feb	Mar	Apr	May	Jun
average Temperature [°C]	21.4	20.3	19.5	16.6	13.1	10.6
maximum Temp. [°C]	27.4	26.4	25.2	22.7	20.3	19.6
minimum Temp. [°C]	16.6	15.7	15.3	11.9	7.6	4.1
Humidity [%]	78.2	81.0	83.7	82.9	80.5	75.5

	Jul	Aug	Sep	Oct	Nov	Dec
average Temp. [°C]	10.1	12.7	15.1	19.1	20.5	21.5
min. Temp. [°C]	20.0	22.3	23.9	26.8	27.5	28.0
max. Temp. [°C]	2.9	4.9	7.3	11.8	14.1	15.9
Humidity [%]	69.1	62.8	58.2	61.2	67.1	73.1

Anual adjustment factor and incentive factor

Production year	1	2	3	4	5	6	7	8	9	10
Adjustment factor	1.01	1.03	1.05	1.07	1.08	1.10	1.12	1.14	1.16	1.18
Production year	11	12	13	14	15	16	17	18	19	20
Adjustment factor	1.20	1.22	1.24	1.26	1.28	1.31	1.33	1.35	1.37	1.40

Calender year	2018	2019	2020	2021	2022	2023	2024	2025	2026	2027
Incentive factor	1.20	1.15	1.15	1.15	1.15	1.10	1.10	1.10	1.05	1.05
Calender year	2028	2029	2030	2031	2032	2033	2034	2035	2036	2037
Incentive factor	1.05	1.00	1.00	1.00	1.00	1.00	0.90	0.90	0.90	0.80

Results for Propylen

Well head temp. [°C]	Gross power [kW]	Net power [kW]	Steam temperature [°C]	Steam pressure [°C]	LCOE [US cents/kWh] for 30 l/s	LCOE [US cents/kWh] for 60 l/s
95	337.9	292.7	82	2.6	60.5	35.8
105	483.6	409.9	83	3	45.9	28.3
115	758.1	587.8	85	4	35.0	22.7
125	1077.9	802.7	98	4.8	28.2	19.2

Results for R32

Well head temp. [°C]	Gross power [kW]	Net power [kW]	Steam temperature [°C]	Steam pressure [°C]	LCOE [US cents/kWh] for 30 l/s	LCOE [US cents/kWh] for 60 l/s
95	362.1	311	90	4.1	57.5	34.2
105	519.6	441.2	100	4.7	43.4	27.0
115	751.4	618.8	110	5.8	33.7	22.0
125	1006.4	819.8	120	6.5	27.8	19.0

Results for R125

Well head temp. [°C]	Gross power [kW]	Net power [kW]	Steam temperature [°C]	Steam pressure [°C]	LCOE [US cents/kWh] for 30 l/s	LCOE [US cents/kWh] for 60 l/s
95	567	362.8	76	4.2	50.6	30.7
105	741.1	507.8	89	4.7	39.0	24.7
115	979	667.6	99	5.3	32.0	21.1
125	1198.6	833.9	109	5.7	27.5	18.9

Results for R134a

Well head temp. [°C]	Gross power [kW]	Net power [kW]	Steam temperature [°C]	Steam pressure [°C]	LCOE [US cents/kWh] for 30 l/s	LCOE [US cents/kWh] for 60 l/s
95	324.6	293.3	64	1.8	60.4	35.7
105	462.3	412.9	70	2.1	45.7	28.2
115	636.1	561.7	76	2.4	36.2	23.3
125	894.3	765.7	88	3.1	29.1	19.7

Results for R143a

Well head temp. [°C]	Gross power [kW]	Net power [kW]	Steam temperature [°C]	Steam pressure [°C]	LCOE [US cents/kWh] for 30 l/s	LCOE [US cents/kWh] for 60 l/s
95	468	336.7	76	3.8	53.8	32.4
105	718	496.4	85	4.4	39.6	25.1
115	921.3	663	98	4.9	32.1	21.2
125	1191.8	852.2	108	5.5	27.1	18.7

Results for R218

Well head temp. [°C]	Gross power [kW]	Net power [kW]	Steam temperature [°C]	Steam pressure [°C]	LCOE [US cents/kWh] for 30 l/s	LCOE [US cents/kWh] for 60 l/s
95	578.4	388.9	77	2.9	47.9	29.3
105	774.7	526.1	89	3.5	37.9	24.2
115	979.5	668.1	99	4	31.9	21.1
125	1204.5	813.2	109	4.6	28.0	19.1

Results for R1234yf

Well head temp. [°C]	Gross power [kW]	Net power [kW]	Steam temperature [°C]	Steam pressure [°C]	LCOE [US cents/kWh] for 30 l/s	LCOE [US cents/kWh] for 60 l/s
95	341.4	299.9	66	1.8	59.2	35.2
105	494.4	429.1	69	2	44.3	27.5
115	724.1	605.1	84	2.7	34.3	22.3
125	1181.6	893.9	100	3.7	26.3	18.2

Results for Electratherm $Power^{+}\ Generator\ 6500$ *with R245fa*

Well head temp. [°C]	Gross power [kW]	Net power [kW]	Steam temperature [°C]	Steam pressure [°C]	LCOE [US cents/kWh] for 30 l/s	LCOE [US cents/kWh] for 60 l/s
95	142.2$^{(II)}$	137	90	0.7	118.5	64.3
105	231.6$^{(III)}$	223.5	100	0.7	75.0	41.6
115	282.6$^{(III)}$	272.4	110	0.7	61.6	34.3
122	392$^{(IV)}$	378	115	0.8	45.8	26.1

Results for SUMEC $PureCycle\ SGPTc272$ *with R245fa*

Well head temp. [°C]	Gross power [kW]	Net power [kW]	Steam temperature [°C]	Steam pressure [°C]	LCOE [US cents/kWh] for 30 l/s	LCOE [US cents/kWh] for 60 l/s
95	174$^{(I)}$	168.4	90	0.7	107.8	58.5
105	260.7$^{(I)}$	252.1	100	0.7	72.5	39.5
115	399.2$^{(II)}$	387.2	110	0.7	44.7	25.5
125	507.2$^{(II)}$	491	120	0.8	35.6	20.4

$^{(I)}$ applying one system with 30 l/s
$^{(II)}$ applying two systems with 15 l/s each
$^{(III)}$ applying three systems with 10 l/s each
$^{(IV)}$ applying four systems with 7.5 l/s each